Fermilab Experimental
Proposal 488
Spokesperson: Irwin A. Pless
Massachusetts Institute of
Technology
Laboratory of Nuclear Science
575 Technology Square, Rm. 408
Cambridge, Massachusetts 02139
Telephone: (617) 253-6081

PROPOSAL FOR A STUDY OF HEAVY PARTICLE PRODUCTION AND DYNAMICS NEAR X = 0 AND THE DEPENDENCE ON INCIDENT QUANTUM NUMBERS

D. Brick, M. Heller, A. M. Shapiro, M. Widgoff
Brown University, Providence, Rhode Island 02912

R. Burnstein, C. Fu, H. Rubin
Illinois Institute of Technology, Chicago, Illinois 60616

E. D. Alyea, Jr.
Indiana University, Bloomington, Indiana 47401

B. Barnett, C.-Y. Chien, P. Lucas, A. Pevsner, R. Zdanis
Johns Hopkins University, Baltimore, Maryland 21218

J. Brau, J. Grunhaus, E. S. Hafen, R. I. Hulsizer, U. Karshon,
V. Kistiakowsky, P. Miller, A. Napier, I. A. Pless, J. P. Silverman,
R. K. Yamamoto
Massachusetts Institute of Technology, Cambridge, Massachusetts 02139

H. O. Cohn
Oak Ridge National Laboratory, Oak Ridge, Tennessee 37830

B. Denby, P. Jacques, T. C. Ou, R. J. Plano, T. L. Watts
Rutgers University, New Brunswick, New Jersey 08903

E. B. Brucker, E. Koller, P. Stamer, S. Taylor
Stevens Institute of Technology, Hoboken, New Jersey 07030

C. R. Sun
SUNY, Albany, New York 12222

W. M. Bugg, G. Condo, T. Handler, E. Hart
University of Tennessee, Knoxville, Tennessee 37916

H. Kraybill, D. Ljung, T. Ludlam, H. D. Taft
Yale University, New Haven, Connecticut 06520

126 pgs.

May 6, 1976

Abstract:

We propose a study of the production of heavy particles (Λ^0, K^0, K^+, K^-, p, $\bar{p}$) with a tagged positive 300 GeV/c beam incident on the Fermilab hybrid spectrometer. We propose both a positive and negative exposure. We wish to achieve a positive beam composition $p/\pi^+/K^+$ ratio of 6/3/1 and a negative beam composition of $\bar{p}/\pi^-$ of 1/4. We propose 1.5×10^6 positive beam pictures and 1.0×10^6 negative beam pictures. We would use the downstream particle identifier to be chosen by the 7-8 May 1976 workshop. The major objective of the experiment is to study the role heavy particles play in multiparticle production processes at Fermilab energies. This process would be studied as a function of the projectile particle under identical experimental conditions. This will be the first time such complete data will be available. In addition to this new data, the experiment will yield a major increase in statistics over earlier, more conventional studies. If it required a lower beam momentum to achieve the desired particle ratio, we would perform the experiment at that lower beam momentum.

INTRODUCTION

We propose to further our experimental investigation of p-p, π^+-p, and K^+-p interactions at Fermilab energies (E299). This experiment will be an improvement over our initial studies in four ways. First, it will include the use of a downstream particle identifier; second, it will be done at twice the incident momentum (300 GeV/c compared to 150 GeV/c; third, it will include a $\bar{p}$ study; and finally, it will have about three times the statistics (2.5×10^6 pictures versus 9.0×10^5 pictures). The major thrust of this experiment is to study the role heavy particles (Λ^0, K^0, K^+, K^-, p, $\bar{p}$) play in multiparticle production at Fermilab energies.

We plan to use the Fermilab hybrid spectrometer equipped with a downstream particle identifier. The choice of identifier will depend on the workshop that will be held on this topic 7-8 May 1976. However, the basic characteristics of such an identifier are known and are discussed in the section, "Beam and Experimental Apparatus". We request 1.5×10^6 pictures with a positive beam and 1.0×10^6 pictures with a negative beam. The positive beam will be a tagged mixture of $p/\pi^+/K^+$ with a ratio of 6/3/1 while the negative beam will be a mixture of $\bar{p}/\pi^-$ with ratio 1/4.

We will compare the similarities and differences of the interactions induced by the different projectiles. Since most particles are produced near X = 0 we have chosen the parameters of the experiment so as to optimize particle identification near X = 0.

The physics topics include single particle distributions, multiplicity studies, and correlation studies, all of which are of obvious interest with respect to the production of heavy particles. In addition, we will engage in more speculative searches; a search for a possibly new phenomenon where both projectile and target end up at X = 0; a search for new particles that decay into one or more heavy particles and

several pions; a study of four-constraint physics; and if statistics permits, a study of pairs of identical heavy particles to compare with the Bosé-like behavior seen in identical pion pairs.

This will be the first comprehensive study of the production mechanism of heavy particles. Although there is some data on Λ^0 and K^0 multiparticle production at these energies, there are no complete distributions for $K^{\pm}$, p, and $\bar{p}$ production.

PHYSICS JUSTIFICATION

The primary interest in this experiment is to study the characteristics of heavy particle production (Λ^0, K^0, $K^{\pm}$p, $\bar{p}$) and their dependence on quantum number at 300 GeV/c. While there is some limited data available on the production of Λ^0 and K^0 particles, there is no complete data available on the others. Since most of the particles are created at X close to zero, it is desirable to access as close as possible to this region. Only those particles that have laboratory momentum greater than 5 GeV/c leave the bubble chamber magnet within a sufficiently small exit angle so as to be captured by a reasonably sized downstream particle identifier. Also, particle identification at momenta less than 5 GeV/c presents particular technical difficulties (see appendices A, B, and C).

These considerations, plus the fact that 300 GeV/c is a relatively unexplored energy region, led to this choice of beam momentum. This is discussed more completely in the section "Beam and Experimental Apparatus." We expect a $p/\pi^+/K^+$ yield ratio of 6/3/1 and a $\bar{p}/\pi^-$ yield ratio of 1/4. With our requested number of pictures, 1.5×10^6 positive and 1.0×10^6 negative beam, we expect to do a moderately high statistics study of proton π^- and π^+ interactions and a reasonable study of K^+, $\bar{p}$ interactions. *This experiment will have the unique advantage of studying* p, π^+, K^+, π^-, and $\bar{p}$ interactions under identical experimental conditions.

The physics topics we will explore are:

1) Single particle inclusive distributions - K^+, K^-, p, $\bar{p}$ productions as a function of X and Y will be measured. This will be the first complete data of this kind at these energies. It is important to determine whether the production of these particles follows either the projectile or the target or whether production simply peaks around X = 0. The behavior of the production of those particles upon changing the incident particle should shed some light on the differences between protons, positive pions, and positive kaons. We will, of course, also study the K^0 and Λ^0 distributions. Where in the rapidity chain the heavy particles tend to lie is an interesting question. Over what range of rapidity are the produced heavy particles affected by the incident particle? Comparison of $K^{\pm} K^{\mp}$, $K^{\pm} \Lambda^0$, $K^{\pm} K^0$ production for different incident beam particles will allow a search for a strangeness = 0 plateau. A similar study for a charge = 0 plateau for incident π^- yielded the surprising fact that at these energies such a plateau does not exist. (ref. 1)

2) Associated multiplicities - Are the heavy particles produced with charged multiplicities characteristic of all events or are they created in higher charged multiplicity interactions? Do the multiplicity distributions depend on the nature of the incident particle? The data from this experiment will help answer these questions and will shed light on the fundamental interaction process.

3) Correlations - Correlations between pairs of charged particles in rapidity have yielded much of the information leading to our current understanding of the nature of multiparticle production, and the observed short-range correlations among pions have stimulated great interest in the concept of local quantum number conservation near Y = 0 (ref. 2). Specific identification of $K^{\pm}$ and $p^{\pm}$ with good efficiency in the central region will greatly extend the correlation information and allow a study of baryon number and strangeness compensation in addition to that of electric charge. Any events that contain a produced proton-antiproton pair should yield information on this production process. If statistics permits one can look for like particle effects

that have been seen between like pion pairs by looking at K^+K^+, K^-K^-, and K^+K^- pairs. In addition, one can include pairs of pions with the kaons and look at four particle correlations, again providing there are enough events.

4) Both projectile and target stop in the center-of-mass - There appears to be some experimental evidence from the ISR that a cross section approaching one millibarn exists for a process where both incident protons stop in the center-of-mass (M. Jacob - private communication). What is of great interest, and for which there are no data, is the number and distribution of the associated charged particles (presumably mostly pions). There are two speculations about the origin of this phenomena. The first is that the two protons stop due to a mutually catastrophic bremsstrahlung of pions. This would manifest itself by the emission of two large jets of pions, forward and backward. The second speculation is that the protons stop due to a coherent central collision of the fundamental constituents (quarks, partons), and this type of reaction might yield an isotropic distribution of pions. Establishing that the ISR result is real and measuring the distribution of the outgoing charged particles would be the discovery of a totally new phenomenon which should shed light on elementary hadronic properties. While it will be easy to identify the stopped (in the center-of-mass) p-p, $\bar{p}$-p, and K^+-p pair, one will only be certain of the stopped proton in the $\pi^{\pm}$-p experiments.

5) Resonance production - The capability for kaon identification in the central region will allow a detailed study of K* and ϕ meson (as well as ρ, Δ, and y*) production for each of the incident channels examined in this experiment.

A comparison with lower-energy data of particle production from the decay of 2-body resonances, for several different beam particles, is of great interest. Further, we expect that the kinematic distribution of resonances will be more sensitive to the nature of reaction mechanisms in high multiplicity events than is the distribution of their decay products.

In addition, the examination of strange particles produced in association with the ϕ meson may provide important tests of the quark model (Zweig rule).

6) New particle search - The ability to analyze multiparticle final states and identify $K^{\pm}$ mesons should allow this experiment to search for new particles (charm?) which might decay into a charged kaon and several pions. This will open an area for such a search not yet explored by counter techniques.

7) Four-constraint physics - It has been demonstrated that it is straightforward to analyze four-constraint events with the assistance of the downstream pwc information. This experiment should yield several thousand such events and would give a good survey of this type of physics. It should be emphasized that having the downstream particle identifier will go a long way toward removing the usual π-p, K-π, and K-p ambiguities.

8) $\bar{p}p$ Annihilation - It would be of great interest to measure the total $\bar{p}p$ annihilation cross section. An attempt will be made to do so in this experiment in spite of the major difficulties involved in estimating the cross section for $\bar{p}p \rightarrow \bar{n}n + X$. While this cross section can be estimated in principle by assuming factorization and applying this assumption to measurements of the channels $\bar{p}p \rightarrow \bar{n}p + X$, $\bar{p}p \rightarrow \bar{p}n + X$, and $\bar{p}p \rightarrow \bar{p}p + X$, meaningful results can only be obtained if the factorization assumption is reliable to considerably better than 5%. This is because the interesting difference $\sigma_T(\bar{p}p) - \sigma_T(pp)$ is expected to be of the order of 2mbn (3), which is 5% of either cross section and the correction for $\bar{n}n$ production must be known considerably better than the difference itself. It is obvious that inefficiencies in measuring any of the three cross sections will reduce the reliability of the estimate of the annihilation cross section. It is clearly important, however, to establish the measurable cross sections as accurately as possible.

BEAM AND EXPERIMENTAL APPARATUS

In Appendices A and B it is shown that for either Čerenkov counters or relativistic rise detectors (isis), it is very difficult to separate K mesons from protons below a momentum of about 5 GeV/c. Appendix C describes the relevant kinematics as a function of incident particle momentum. In order for a significant number of pions and kaons near X = 0 to have a laboratory momentum of greater than 5 GeV/c, a laboratory momentum of 300 GeV/c or greater is desirable. As the 7-8 May workshop will undoubtedly show, the smaller the aperture of a Čerenkov counter or isis device, the cheaper it is. Hence, 300 GeV/c is to be preferred to a lower energy, say 100 GeV/c, since particles of interest will not only be at an optimum momentum in the laboratory to be identified but these particles will come out in a narrower forward cone.

For this experiment either an isis type device or an equivalent segmented differential Čerenkov counter similar to the SLAC counter would be suitable. The choice will presumably be made at the workshop. In addition to the downstream particle identifier, the experiment would need the necessary drift chambers (or proportional wire chambers) to cover the solid angle of the identifier and furnish the necessary momentum resolution. If an isis device is chosen, one can use the forward gamma ray detector in this experiment. However, if a segmented Čerenkov counter is chosen, the mass of that device precludes use of such a detector.

We would hope to achieve a $p/\pi^+/K^+$ ratio of 6/3/1 and a $\bar{p}/\pi^-$ ratio of 1/4. We have achieved such a positive ratio at 150 GeV/c using an incident beam of 300 GeV/c. With an incident beam of 400 GeV/c and an improved absorber technique, preliminary studies indicate that the desired positive ratio is achievable at 300 GeV/c. Theoretical studies indicate that one should be able to achieve the desired negative ratio. Beam tests will have to be made to determine the actual beam composition. One would need several weeks of beam time for this measurement. If these tests indicate a lower beam momentum is required to obtain the desired ratios, we would run the experiment at the lower momentum.

Since one needs a $\Delta p/p$ of about 10% to effectively use an isis type device, this limits the useful outgoing particle momentum to about 100 GeV/c. However, as can be seen in Appendix B, this device becomes marginal at higher momentum and hence this momentum resolution restriction is not important. For particles above 100 GeV/c we will classify them as the projectile particle. This will result in some misclassification but from our experience with E-154 this should result in less than a 5% statistical error. Similar comments are valid for the Čerenkov counter system. However, the available momentum band for this device is rather limited as compared to an isis type device.

We are requesting 1.5×10^6 pictures with a positive beam and 1.0×10^6 pictures with a negative beam with 8 tracks per picture. This should yield a 4-event per microbarn experiment for each charge.

SUMMARY

We request a 1.5×10^6 positive picture exposure and a 1.0×10^6 negative picture exposure in the Fermilab hybrid spectrometer. We request a tagged positive incident beam with a momentum of 300 GeV/c and with a $p/\pi^+/K^+$ ratio of 6/3/1 and a $\bar{p}/\pi^-$ ratio of 1/4. We believe that with primary proton momentum of 400 GeV/c and improved enrichment techniques the desired beams could be achieved.

We would wish to use the downstream particle identifier selected by the 7-8 May workshop on this topic augmented by the appropriate drift chambers and proportional wire planes. Either a segmented Čerenkov counter system or an isis type device would be suitable. If an isis type system is chosen, we would wish to include the forward gamma ray detector in the spectrometer.

The major thrust of the experiment is the study of the production properties of the heavy particles (Λ^0, K^0, K^+, K^-, p, $\bar{p}$) in high energy collisions. The 300 GeV/c beam is chosen to optimize the study of the central region near X = 0. The experiment would yield 4 events per microbarn for each charge.

We would need several weeks of beam time to both tune the beam and calibrate the downstream particle identifier. If these tests indicate that a lower momentum is required to achieve the desired particle ratios, we would run the experiment at that lower momentum.

References

1) "Evidence for Charged Cluster Emission in 147 GeV/c π^-p Collisions," D. Fong et al., Phys. Lett. 61B(1976) 99.

2) "Local quantum-number compensation in multiple production," C. Quigg, Phys. Rev. D12(1975) 834.

3) "Total Cross Sections of p and $\bar{p}$ on Protons and Deuterons between 50 and 200 GeV/c," A. S. Carroll et al., Phys. Rev. Lett. 33(1974) 928.

Appendix A: Čerenkov Counter System

Figure A-1 gives the momentary thresholds for π, K, and p for emission of Čerenkov radiation as a function of η ($\eta = n - 1$, where n is the index of refraction). The upper end of this range, $\eta = 60 \times 10^{-4}$, corresponds to the index of refraction of isobutane at 4 atmospheres pressure and is the limit of presently attainable indices of refraction in substances that can be used in a Čerenkov detector. * Thus, it is not presently possible to identify K-mesons below 5 GeV/c. Also shown in fig. A-1 are the momenta for π, K, and p at which the number of photoelectrons, N_e, produced in a 3 meter Čerenkov counter is 90% of the maximum value, $(N_e)_{Max}$. Finally, fig. A-1 gives $(N_e)_{Max}$ and also the maximum Čerenkov angle, $(\theta_c)_{Max}$, again as functions of η. N_e and $(N_e)_{Max}$ are calculated from the SLAC measurement of 12 photoelectrons/meter/atmosphere.

Since isobutane is combustible a preliminary choice of freon-12 at 4 atmospheres was made. Figure A-2 gives the number of photoelectrons produced as a function of particle momentum. K-mesons could be identified from 5.7 GeV/c ($N_e = 16$) to about 12 GeV. Fig. A-3 shows the percentage of misidentified K mesons** as a function of momentum if the K to π ratio is 1/10.

Since the SLAC rapid cycling bubble chamber hybrid system Čerenkov detector has been used successfully in the momentum range, it will be used as a basis of discussion, fig. A-4. This is segmented into ten light collection units and has been successfully operated in a pulse height mode. This device must be placed after all proportional wire counters or drift chambers necessary to the momentum measurement and is not compatible with the photon detector. Auxiliary devices which are necessary to its use are a 1m x 2m drift chamber in front of the entrance

---

* A silica gel detector is being studied as a possible device with larger η.

** This is the sum of the K's identified as π's and π's identified as K's relative to the true number of K mesons.

window and a ten section scintillation counter hodoscope, matched to the mirror dimensions, behind the mirrors.

This counter may be placed with the mirror plane at 9 meters and still permit an adequate momentum measurement. At 150 GeV/c the acceptance for particles leaving the bubble chamber will be 72% , and at 300 GeV/c, 95%. Table A-I gives the percentage of spatially resolved particles from each of three momentum ranges (i. e. particles for which the Čerenkov light spot falls on a mirror where no other Čerenkov light is incident). Thus, although the acceptance is good at 300 GeV/c, the spatial resolution is low. Since there will be a scintillation counter hodoscope behind the Čerenkov counter and a drift chamber in front, it will be possible to identify those mirrors receiving light from more than one particle and to determine whether the pulseheight corresponds to two π's, two K's, or a π and a K. The uncertainties in this will of course be greater than those for the identification of a single particle.

If this Čerenkov device were placed at a greater distance then the resolution problem is improved. For example, if it were placed at 12 meters, then the resolution characteristics would be approximately those given in Table A-I for 150 GeV/c.

Table A-I

Percentage of Spatially Resolved Particles as a Function of Beam Momentum (p_{Beam}) on Particle Momentum (p)

	p_{Beam} = 150 GeV/c	300 GeV/c
$p < 5$ GeV/c	54%	35%
$5 \leq p \leq 10$	47%	22%
$10 < p$	24%	16%

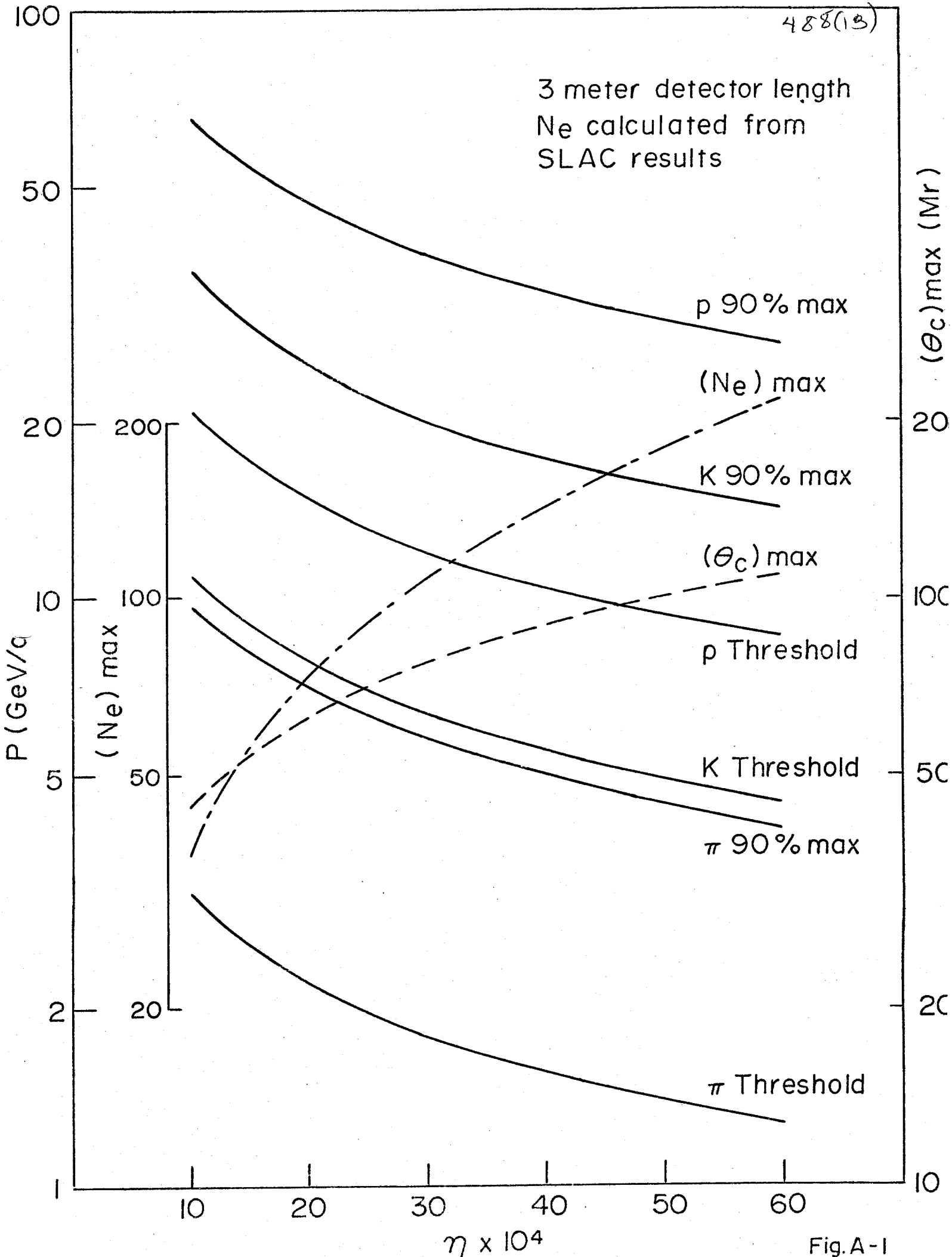
3 meter detector length
Ne calculated from
SLAC results
p 90% max
(Ne) max
K 90% max
(θc) max
p Threshold
K Threshold
π 90% max
π Threshold
P (GeV/c
(Ne) max
(θc) max (Mr
100
50
20
10
5
2
1
200
100
50
20
100
50
20
10
10
20
30
40
50
60
η x 10⁴

Fig. A-1

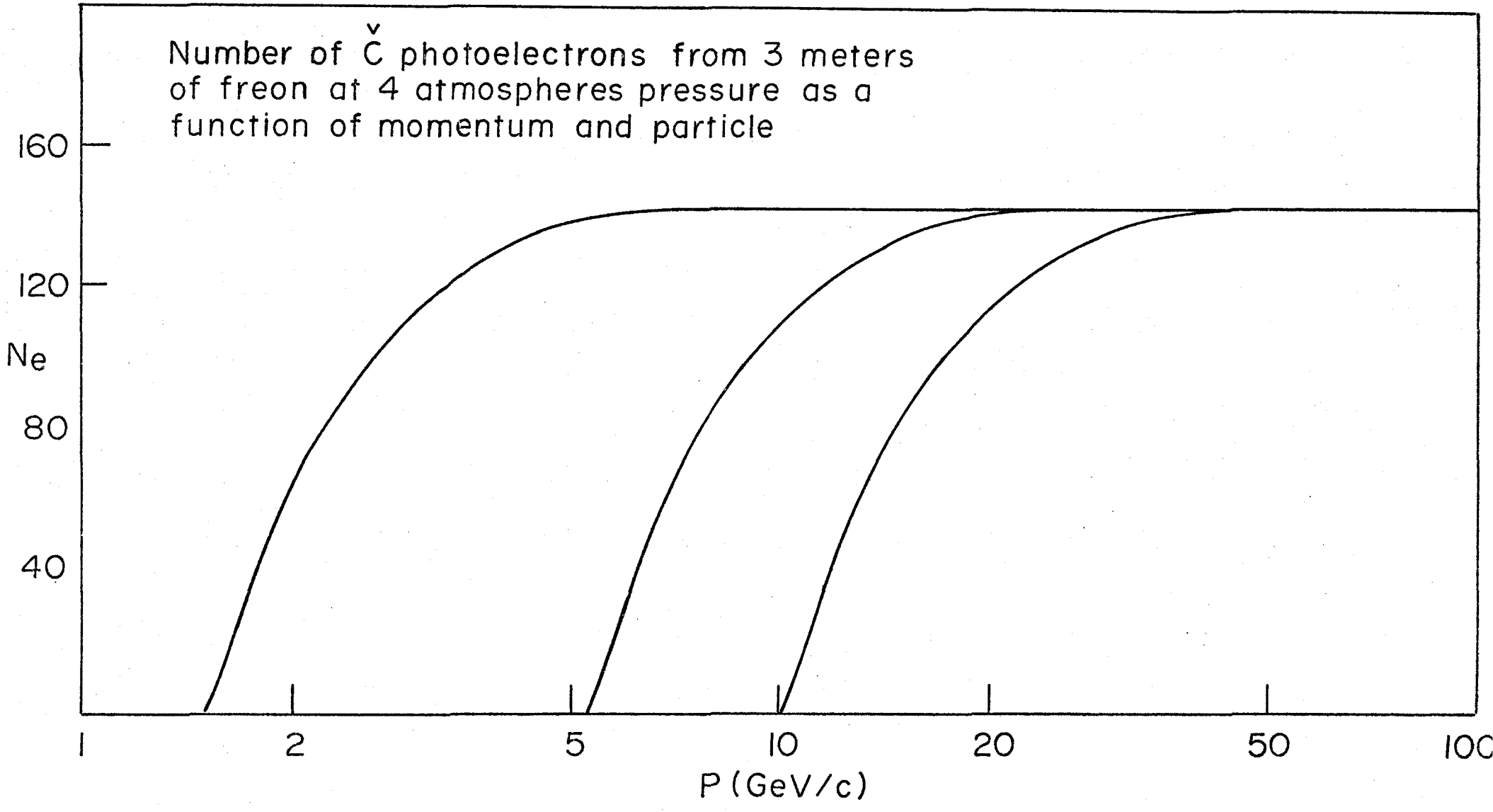
Number of Č photoelectrons from 3 meters of freon at 4 atmospheres pressure as a function of momentum and particle
160
120
Ne
80
40
1
2
5
10
20
50
100
P (GeV/c)

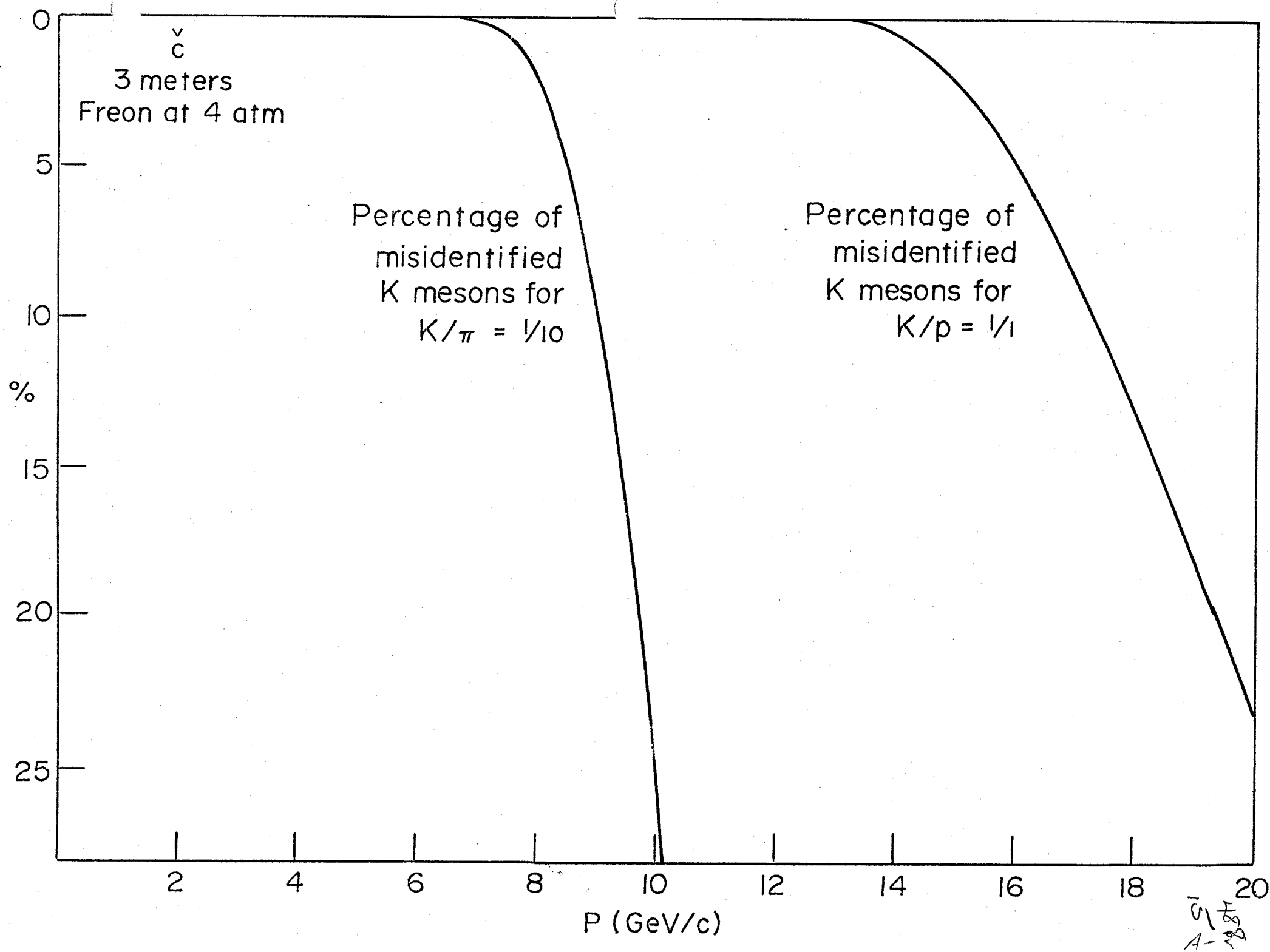
0
5
10
15
20
25
%
v/c
3 meters
Freon at 4 atm
Percentage of misidentified K mesons for K/π = 1/10
Percentage of misidentified K mesons for K/p = 1/1
2
4
6
8
10
12
14
16
18
20
P (GeV/c)

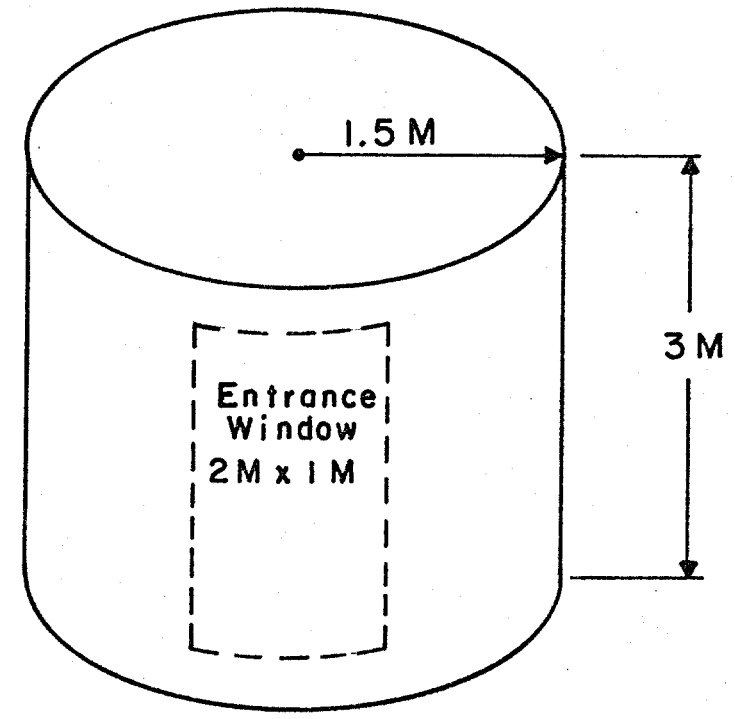

SLAC
Cherenkov
Detector

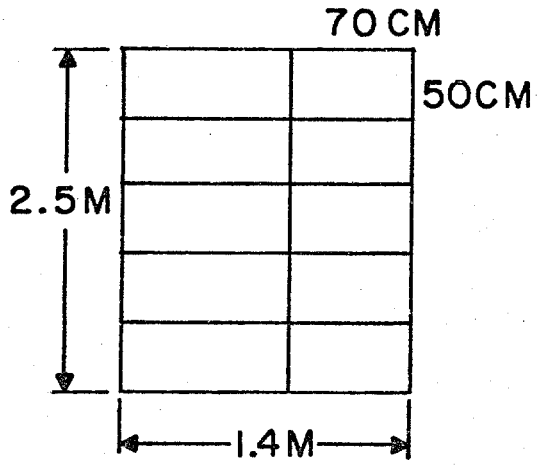

Mirror Matrix

Figure A-4

Appendix B: ISIS System

Fig. B-1 gives a suggested layout for incorporating three 1m x 1m x 1m modules of an ISIS type relativistic rise detector in the 30-inch bubble chamber hybrid system. There would be a total of 198 wires with a spacing of 1.5 cm. For a filling of 80% A- 20% CO_2 this would be anticipated to result in a resolution of 8% full width at half maximum (see attached description of ISIS).

The acceptance of this device will be 74% for an incident beam energy of 150 GeV/c and 96% for 300 GeV/c. Approximately 8% and 17% of the particles will not be spatially resolved at 150 GeV/c and 300 GeV/c, respectively.

Fig. B-2 gives the ionization as a function of p/MC. Fig. B-3 shows the percentage of K-mesons which with 8% resolution would be misidentified* as a function of momentum, assuming the ratio, $\pi/K/p = 10/1/1$. In the region from 5 to 25 GeV/c there would be a better than 70% correct identification of K-mesons since Kp and Kπ confusion would not occur simultaneously.

---

* This percentage is the sum of K's identified as π's or p's plus the π's or p's identified as K's relative to the true number of K's.

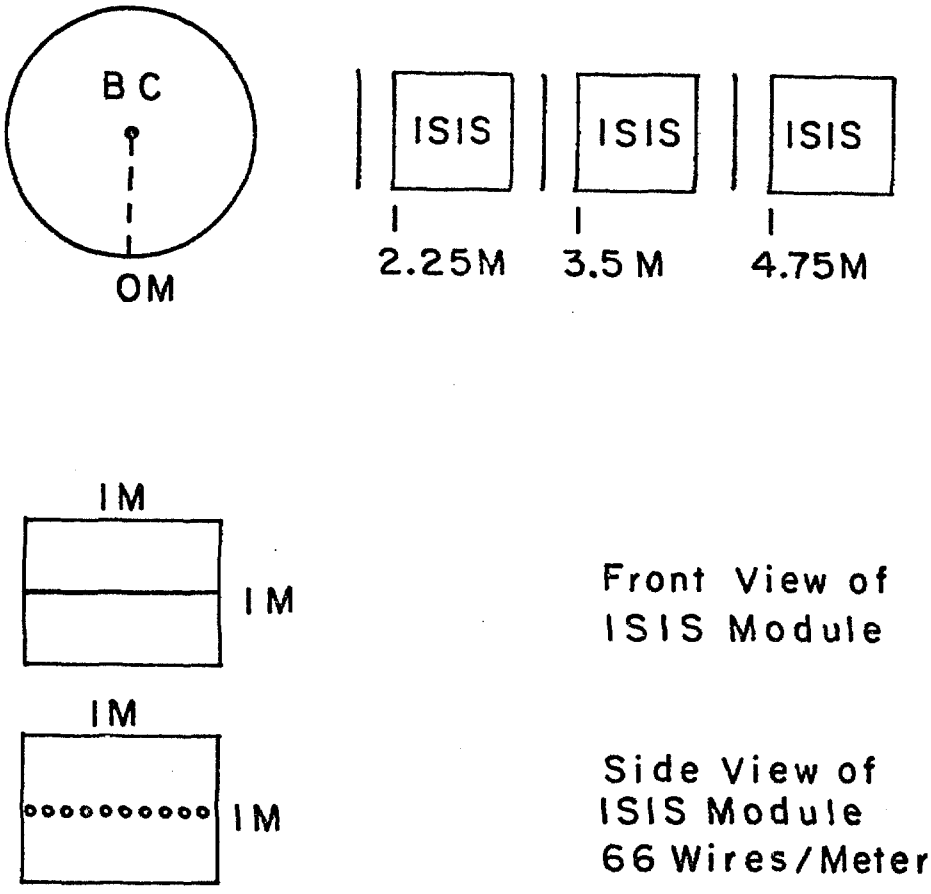
BC
OM
ISIS
ISIS
ISIS
2.25M
3.5 M
4.75M
IM
IM
Front View of
ISIS Module
IM
IM
Side View of
ISIS Module
66 Wires/Meter

Figure B-1

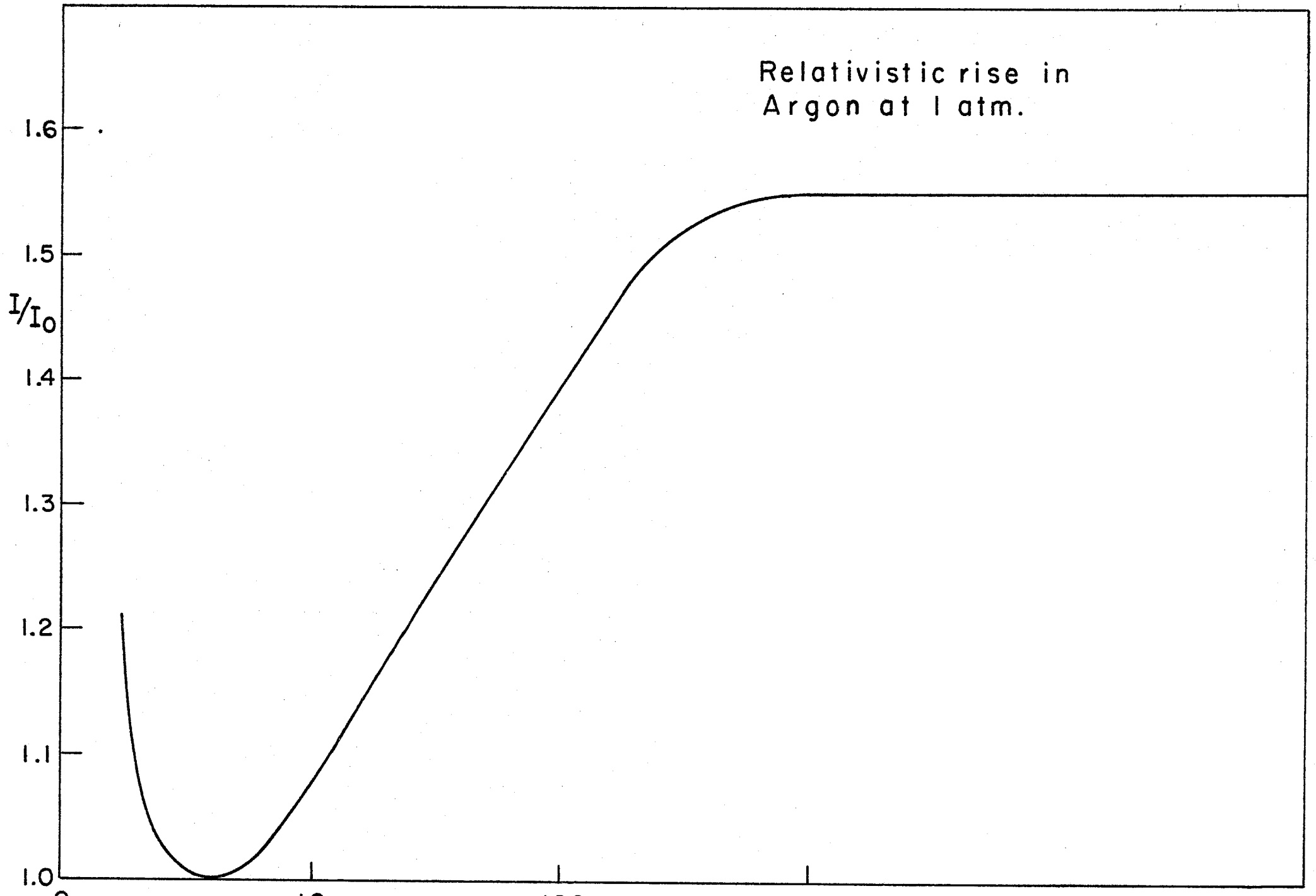

Figure B-2

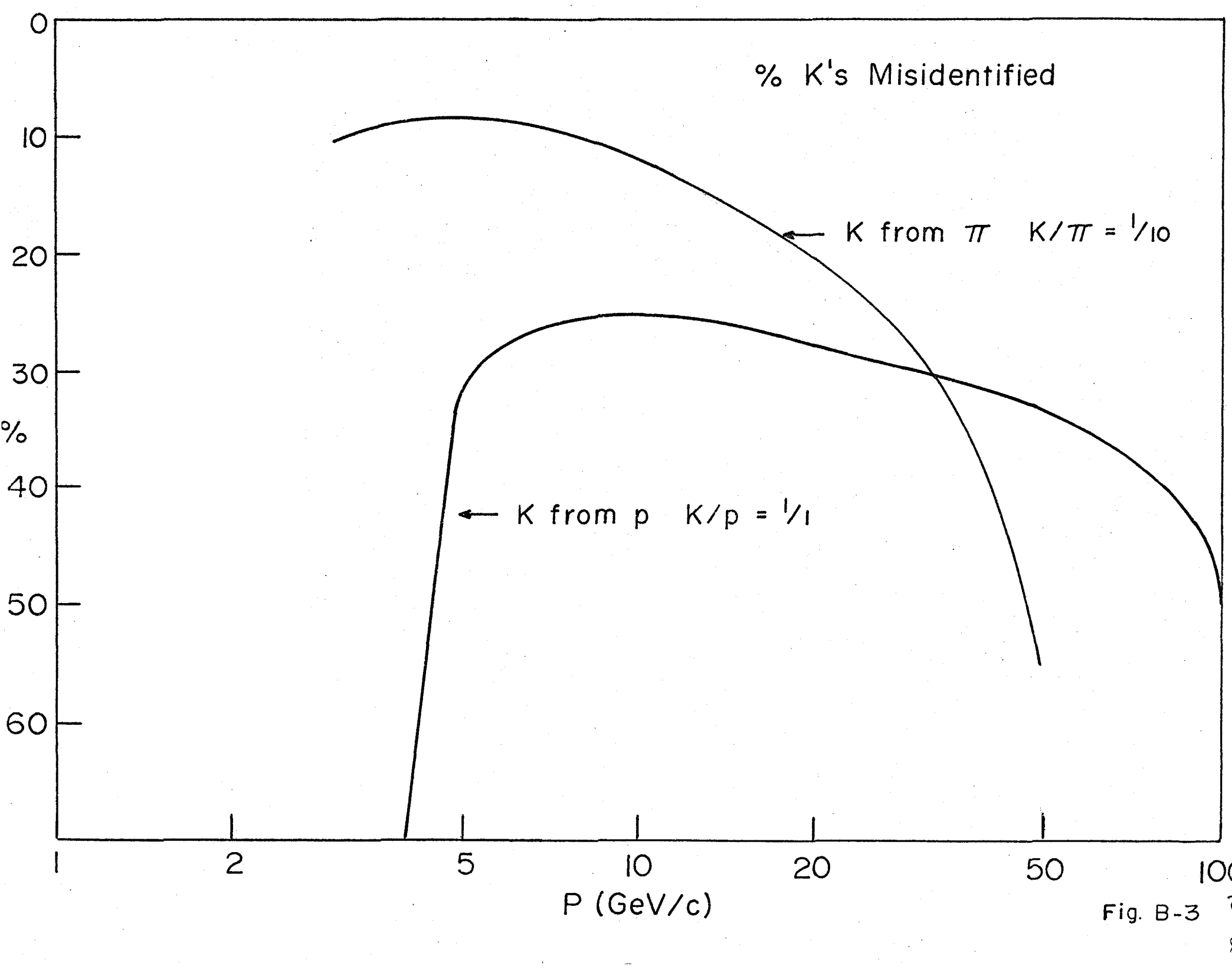
% K's Misidentified
K from π K/π = 1/10
K from p K/p = 1/1
0
10
20
30
%
40
50
60
1
2
5
10
20
50
100
P (GeV/c)

Fig. B-3

Appendix C: Kinematics

Fig. C-1 gives the laboratory momentum, p, and angle, θ, for K's and p's which have center of mass momenta, p' = 0.0, 0.1, 0.2, and 0.3 GeV/c for an incident beam momentum of 100 GeV/c. Fig. C-2 gives the same curves for an incident beam momentum of 300 GeV/c. At 100 GeV/c most of the K-mesons have a laboratory momentum below 5 GeV/c and therefore will not be identified by either downstream particle identifier discussed.

Another way of looking at the kinematical situation is to consider the rapidity in the center of mass Y_{cm}. Fig. C-3 shows the rapidity in the center of mass as a function of p_{lab} for incident momentum 100 GeV/c. Each line represents a particular particle (π, K, p) and a specific transverse momentum ($p_T = 0$, $p_T = 0.6$). Note that for $p_{lab} > 5$ GeV/c, Y_{cm} is greater than 0 for most particles of interest. However, as can be seen in fig. C-4, the situation is much improved and for $p_{lab} > 5$ GeV/c most of the region $Y_{cm} > -1$ is accessible.

The conclusion one can draw is that in order to span $Y_{cm} = 0$, one has to be at a p_{lab} significantly greater than 100 GeV/c with 300 GeV/c our choice.

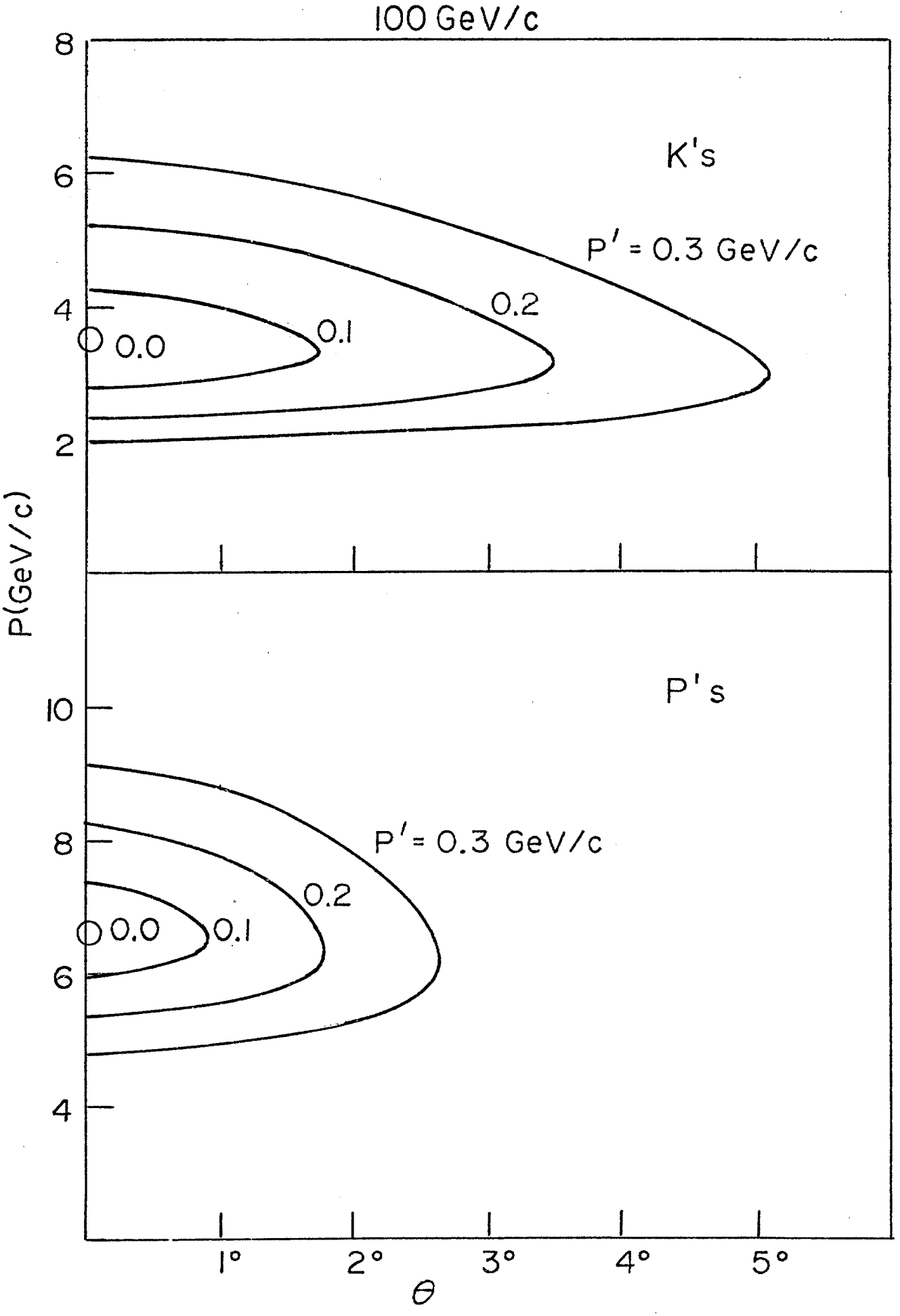
100 GeV/c
K's
P' = 0.3 GeV/c
0.0
0.1
0.2
P's
P' = 0.3 GeV/c
0.0
0.1
0.2
P(GeV/c)
θ
1°
2°
3°
4°
5°
2
4
6
8
10

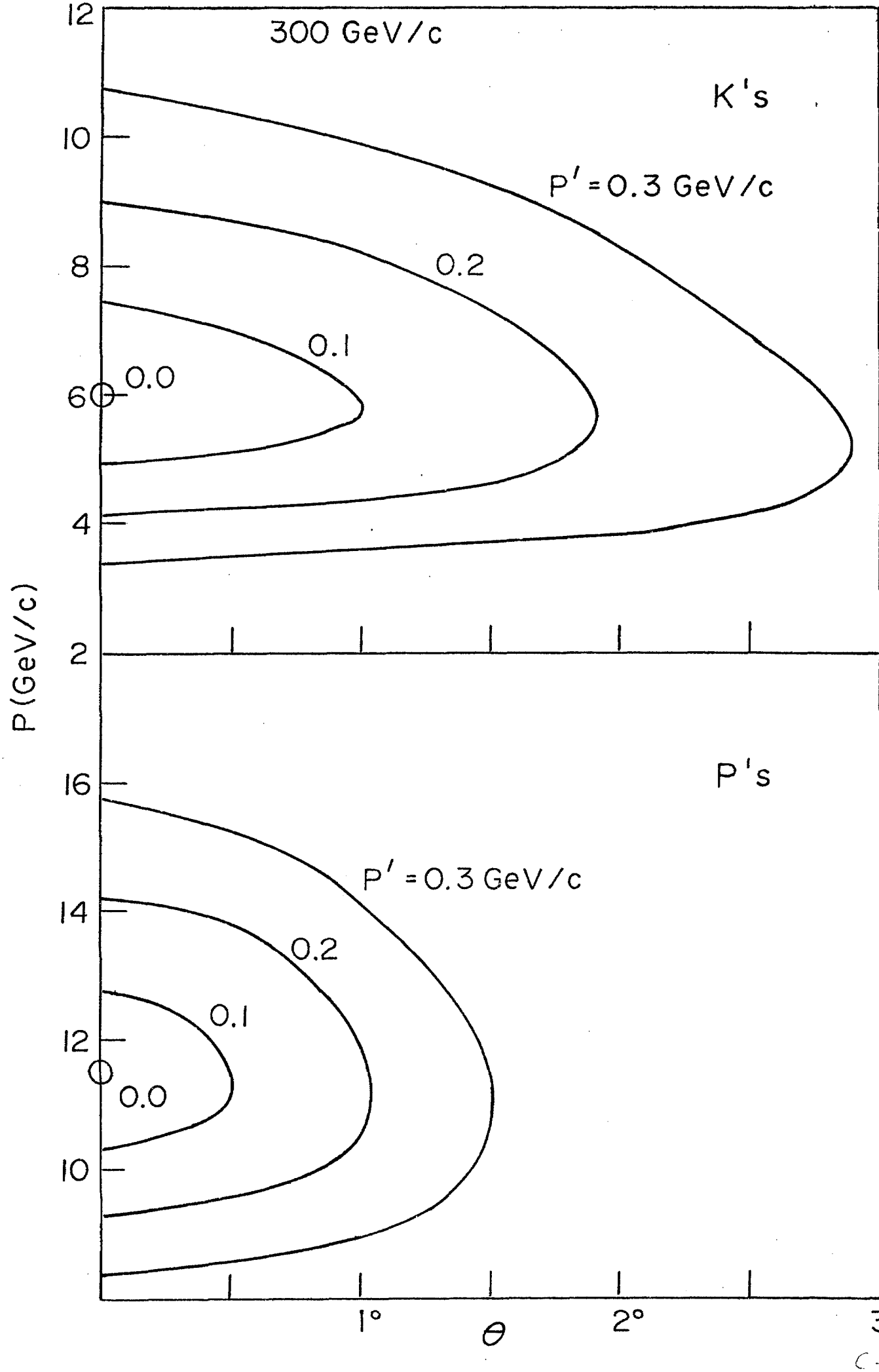
300 GeV/c
K's
P' = 0.3 GeV/c
0.2
0.1
0.0
P (GeV/c)
12
10
8
6
4
2
P's
P' = 0.3 GeV/c
0.2
0.1
0.0
16
14
12
10
1°
2°
3°
θ

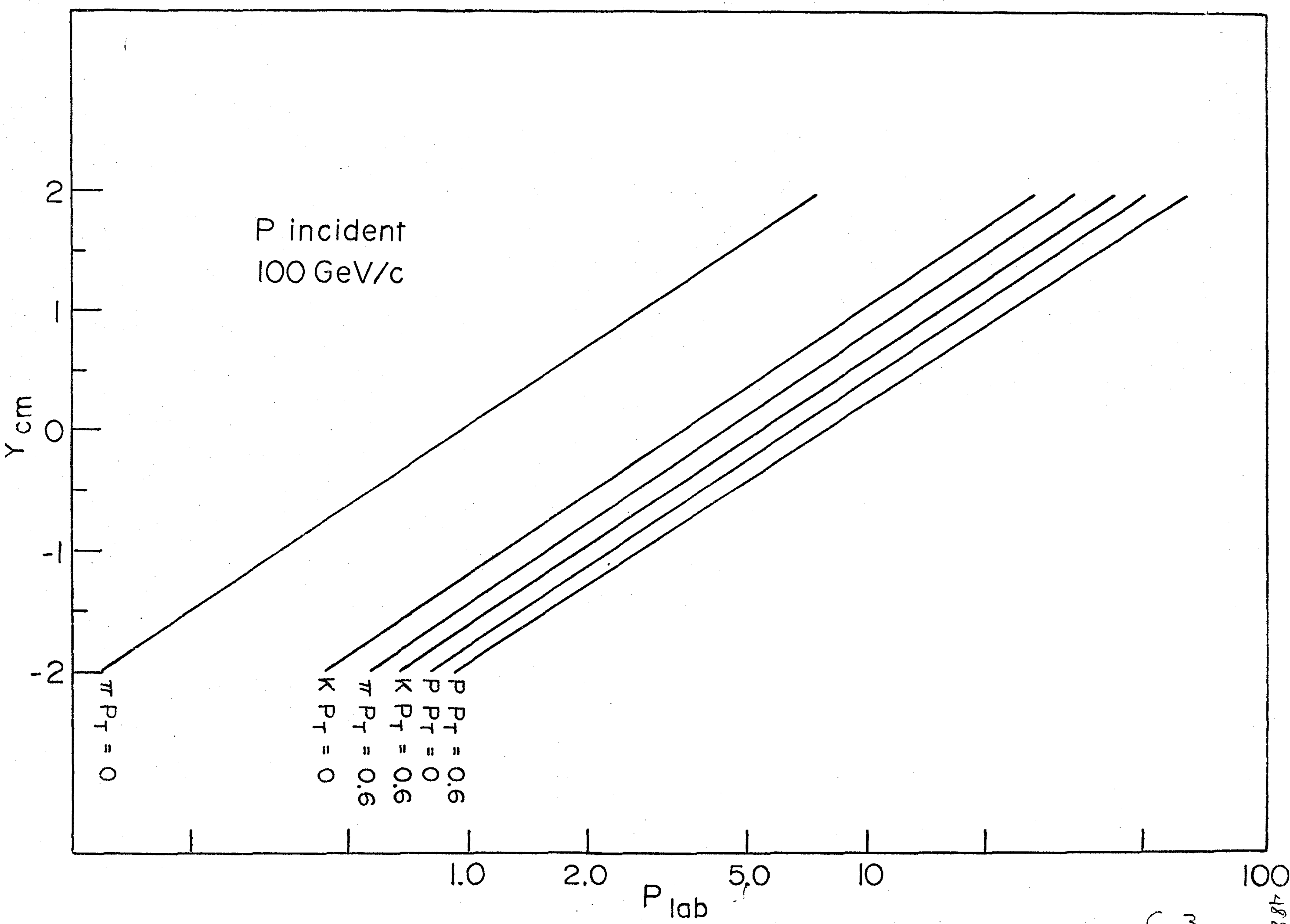

P incident
100 GeV/c
Y cm
2
1
0
-1
-2
π P T = 0
K P T = 0
π P T = 0.6
K P T = 0.6
P P T = 0
P P T = 0.6
1.0
2.0
5.0
10
100
P lab

C, 3

488-24

C, 4

100
10
5.0
2.0
1.0
P_{lab}
P P = 0.6
P P_T = 0
K P_T = 0.6
π P_T = 0.6
K P_T = 0
π P_T = 0
P incident
300 GeV/c
2
1
0
-1
-2
Y_{cm}

Appendices D - H cover the relevant knowledge and experimental tests of an ISIS device. The conclusion of these appendices is that relativistic rise devices in general and an ISIS-type device in particular should work as calculated.

CERN/D.Ph.II/RCBC 75-3
15 May 1975 LM/mk

COMPARISON OF ISIS AND A 5-STAGE MULTICELL CERENKOV COUNTER

W. Allison and A. Poppleton

We have compared the performance of ISIS and the 5 stage multicell Cerenkov counters proposed by B. French*). We have used 6 prong and 12 prong events from a 200 GeV/c π^-p experiment in the 30" NAL chamber. The table shows that the momentum ranges over which different classes of mass separation are possible are comparable in the two cases.

The main difference comes when considering the multitrack resclution in high multiplicity events. The table shows that whereas the losses in ISIS for 6 prong events are less than 7%, the loss in the Cerenkov system varies from 10-38% per track. These losses can be expected to be systematic with respect to low effective masses. For 12 prong events the ISIS losses are still less than 12%, while the Cerenkov loss ranges from 25-60%. This would be serious for any analysis involving track pairs etc. The figures are not inconsistent with the results of a naive calculation shown in fig. 1 which shows the multitrack efficiency as a function of multiplicity on the assumption of equal occupation probability for each cell.

Other considerations such as cost (∿ factor 3?), and length (5m rather than 12m) favour ISIS. The ability to provide prompt signals from a Cerenkov is not useful in a high multiplicity situation in general because of the pattern recognition problem-in the region beyond the spectrometer magnet there could be a case for such an ability. A Cerenkov to fulfill this requirement could be relatively small.

*) We have crudely optimized their system to the RCBC configuration retaining the same counter lengths and numbers of cells (20 per counter). Further details will be given in a more complete note now being prepared.

Type of Identification ***	Momentum range (GeV/c)	6-prongs (394 events) Flux in * momentum range %	Flux Identified %	Multitrack efficiency %	12-prongs (80 events) Flux in * momentum range %	Flux identified %	Multitrack efficiency %	
(1) K from π (< 10%) contam	2.6 → 56	70	62	89	76	56	74	Č
	3.0 → 39	60	56	97	67	60	92	ISIS
(2) K from π (< 1%) contam	4.4 → 37	49	36	74	54	30	56	Č
	4.5 → 25	40	39	97	46	42	92	ISIS
(3) p from π (< 10%) contam	2.6 → 106	78	70	90	80	60	76	Č
	3.0 → 100	74	69	96	75	67	91	ISIS
(4) p from π (< 1%) contam	4.4 → 70	60	47	78	62	37	60	Č
	3.0 → 60	68	63	96	73	65	91	ISIS
(5) K from p (*)	10 → 106	44	32	73	39	19	49	Č
	12 → 70	35	33	93	32	28	88	ISIS
(6) K definite ((2) and (5))	10 → 37	28	17	62	29	11	39	Č
	12 → 25	16	15	95	17	15	89	ISIS
(7) p definite ((4) and (5))	10 → 70	39	27	69	37	16	45	Č
	12 → 60	33	31	93	31	28	88	ISIS

* ISIS K/p separation at 90% purity, Č gives 100% purity with 99% efficiency.

** Data from 205 GeV $\pi^- p$ DST, fluxes normalised to tracks escaping vertex magnet M1.

*** π/K/p fluxes of 10/1/1 assumed

Idealised efficiency of multitrack resolution by cerenkov

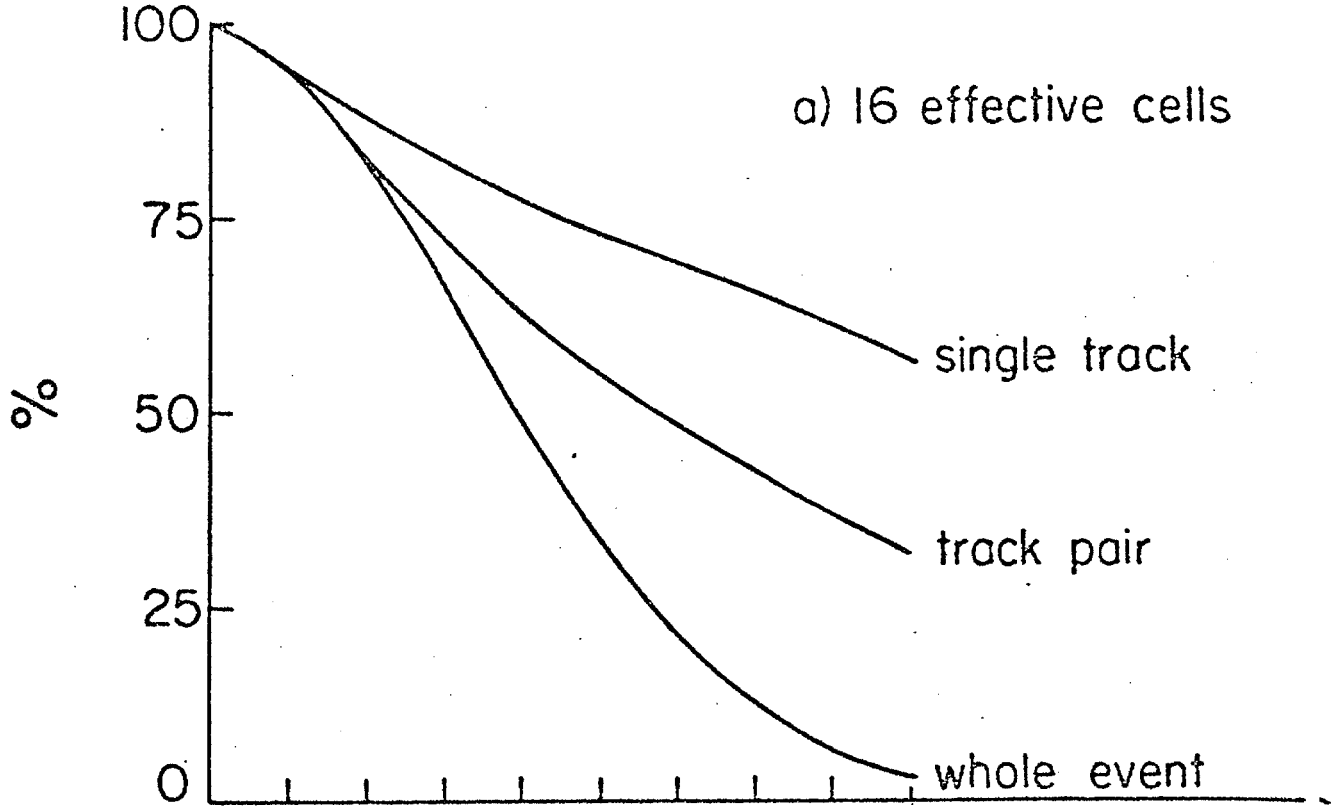

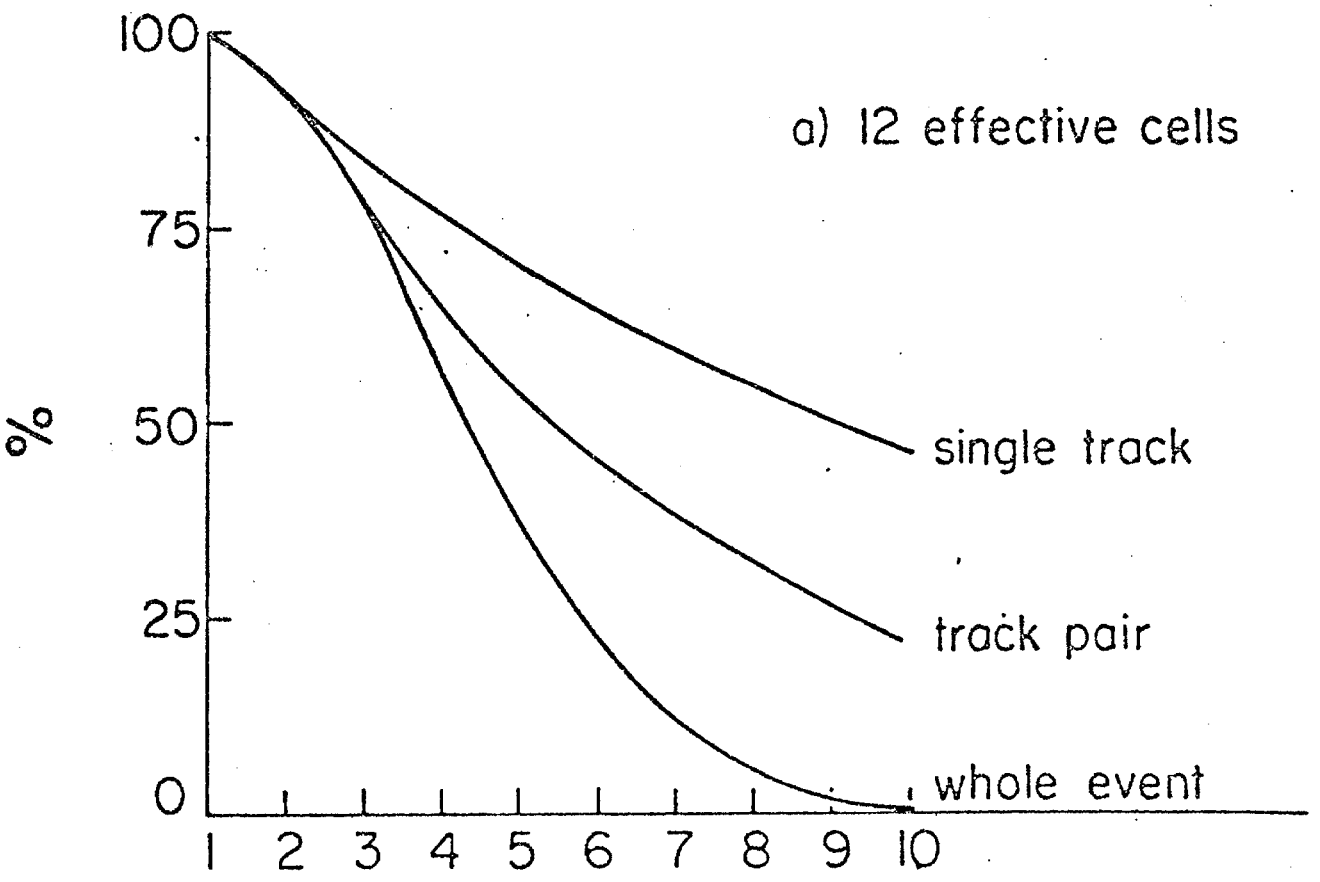

CLEAR INSTRUMENTS AND METHODS 119 (1974) 499–507; © NORTH-HOLLAND PUBLISHING CO.

THE IDENTIFICATION OF SECONDARY PARTICLES BY IONISATION SAMPLING (ISIS)

W. W. M. ALLISON, C. B. BROOKS, J. N. BUNCH, J. H. COBB, J. L. LLOYD and R. W. PLEMING

Nuclear Physics Laboratory, Oxford, England

Received 16 April 1974

A large volume multi-wire proportional chamber employing drift paths of up to 2 m in an unconventional geometry is described. This device will distinguish between kaons, pions and protons for all secondaries from 5 GeV/c to over 100 GeV/c and will obtain over 300 transverse position measurements on each track to an accuracy of approximately 2 mm. Results from experiments on a prototype in a test beam are given and a possible design for use with a rapid cycling bubble chamber at the CERN-SPS or NAL accelerators is discussed.

1. Introduction

The simultaneous identification of several secondary particles from interactions at SPS energies is a difficult problem. The most ambitious Cherenkov counters can only provide a limited number of cells, while transition-radiation detectors are efficient only for electrons unless the momenta are in the range of several hundred GeV/c [1]. As a result, effort has been directed towards the use of the relativistic rise of ionisation loss (dE/dx) in gases at atmospheric pressure[2,3]). This rise is due to the effect of the relativistic expansion of the transverse electric field of a particle[4]). Fig. 1 shows the ionisation loss for π, K and protons as a function of momentum; the difference is 10% or more over the range from 5 GeV/c to about 100 GeV/c. Above 100 GeV/c the curves begin to reach a plateau due to the polarisation of the medium screening the electric field at large impact parameters (the "density effect")[4]).

Unfortunately fluctuations in individual energy-loss measurements ("Landau fluctuations") are very large. Fig. 2 shows a spectrum of such measurements for 3 GeV/c pions in 1.5 cm of argon[1]). Further, the long tail is such that, if losses in thicker samples of gas are measured, the width of the spectrum is only slowly reduced – it is still some 50% for a thickness of 50 cm. Only be measuring many samples on each track may

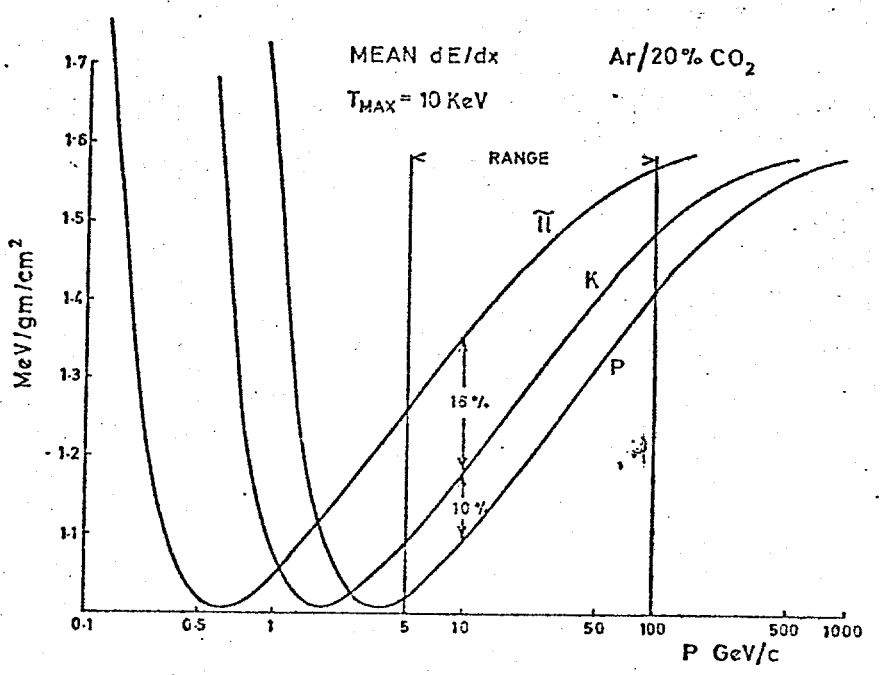

Fig. 1. The ionisation loss in argon + 20% CO_2 at atmospheric pressure for π, K and p based on the formula of Sternheimer and Peierls[13]).

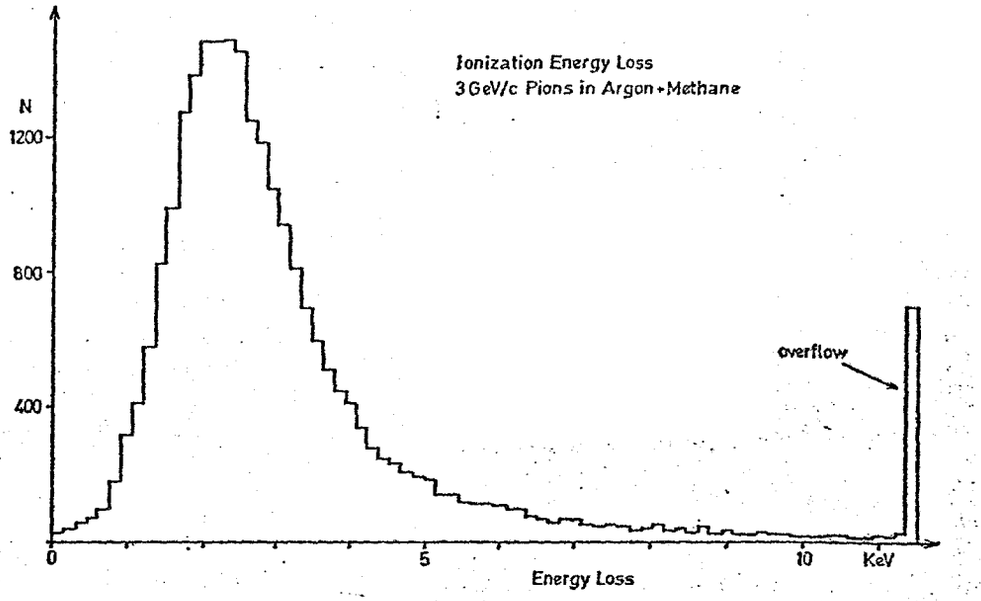

Fig. 2. The observed ionisation-loss distribution for 3 GeV/*c* pions in 1.5 cm of argon/7% methane in a conventional MW (from ref. 1).

the required resolution of a few percent be achieved. In fact considerably more than 100 samples from five or more meters of gas are required. At the same time we require the ability to handle a number of tracks simultaneously, spread in both angle and position so that a device of the widest acceptance is needed.

In a recent paper[3]) Lehraus and co-workers proposed a device 2 m wide × 60 cm high in which each of 128 sampling layers consisted of 32 proportional chamber "cells", making 4096 channels. In this paper we disc a different technique for collecting the ionisat samples which allows an order of magnitud "cells", an order of magnitude less channels, c with improvements in acceptance, efficiency, calibratio and cost.

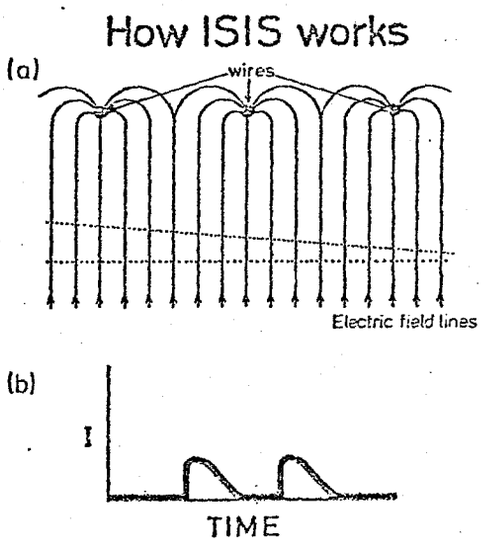

Fig. 3. (a) A schematic diagram showing two "tracks" of ionisation electrons drifting towards a signal-wire plane perpendicular to the diagram. (b) A pair of signals seen on a wire corresponding to two "tracks" arriving displaced in time.

In section 2 we discuss the physical principles of t device. In section 3 we show results gained fro experiments on a 1 m model in a test beam. In sectio we discuss the form that the device would take behi a rapid cycling target.

2. The ISIS method

The ISIS chamber consists of a large volume of gas in a uniform electric field. At one end is a high-voltage negative-polarity planar electrode and at the other is a proportional-wire plane. The latter is sandwiche between a pair of closely spaced high-voltage wire planes and resembles a conventional multi-wire proportional-chamber (MWPC) assembly. Fig. 3a shows a schematic diagram in which the proportional wires are perpendicular to the plane of the figure and the high-voltage wire planes are not shown*. The particle trajectories are roughly parallel to the plane but displaced some way from it. The primary ionisation electrons along each particle trajectory drift parallel to the electric field* without amplification until they reach

* The arrows on the electric field lines indicate the direct electron drift, not the sense of the electric field.

e neighbourhood of the signal wires where amplifi-ion takes place. If the signal-wire spacing is d, then ch wire collects a charge proportional to the energy s in a thickness of gas d†. Considering now the rrent seen by each wire as a function of time, different rticle tracks in general arrive at different times and erefore may be handled sequentially. Clearly sophis-ated techniques are required but the problems can be lved with available signal-processing methods.

The electronics associated with each wire of the vice does two things. The first is to record the time arrival of each pulse so that the position of the track space may be known; the second is to integrate each rrent pulse such that a shape-independent estimate the primary ionisation is made. Each channel erates independently in a self-triggered mode hand-g up to 20 or 30 tracks between read-out to a mputer.

Drifting electrons over a few cm in non-uniform lds is standard practice in conventional "drift ambers"[5]). Some successful work has been reported olving drifting up to 50 cm in high uniform fields a single wire[6]). In this work we consider drift stances of the order of a meter. This allows a device th the largest solid-angle acceptance to be built.

Given an adequate electrostatic structure to main-in a uniform electric field, there are two principal oblems:

1) *Diffusion.* The primary electrons must not diffuse ring the drift time such that either they reach the rong signal wire giving rise to statistically correlated mples (cross-talk) or spread along the drift di-ction thereby making it impossible to identify close cks.

2) *Attenuation.* The primary electrons must have a ng lifetime in the gas, otherwise losses will dominate e observed pulse height.

These properties depend critically on the choice of s and its purity.

The diffusion of electrons in a gas depends on their ean energy, kT_e, where T_e is the electron tem-erature[7,8]). One can show quite simply from kinetic eory that

$$\sigma = l\left(\frac{2kT_e}{eV}\right)^{\frac{1}{2}} = \left(\frac{2lkT_e}{eE}\right)^{\frac{1}{2}}, \qquad (1)$$

ere σ is the rms projected spread of an electron cloud due to diffusion after drifting a distance, l, over a potential drop, V. This expression does not depend explicitly on the electron mean free path. The electron temperature is known as a function of reduced electric field, x/p, for a number of gases[8]) as shown in fig. 4. This shows that CO_2 is much more efficient at cooling the electrons than the other gases shown. It is well known that due to the Ramsauer–Townsend effect[7]) argon is almost transparent to electrons at thermal energies. As a result, in argon–CO_2 mixtures the behaviour of the electrons should be determined solely by the partial pressure of CO_2. Thus considering an argon +20% CO_2 mixture these data allow us to predict the value of σ after a 1 m drift for various electric field strengths.

We have measured the diffusion by studying the dispersion in arrival time of electrons in a blob originating from a ^{55}Fe X-ray* and collected on a proportional-wire plane after drifting 8.5 cm in a

† In the statistical analysis of the measurements the larger energy losses must be excluded to remove the direct effects of the Landau tail and also to eliminate the correlations intro-duced by long-range δ-rays.

* The range of a primary electron from the conversion of a 5.9 keV X-ray is less than a few tenths of a mm in argon. We therefore consider the blob of electrons to start localised at a point.

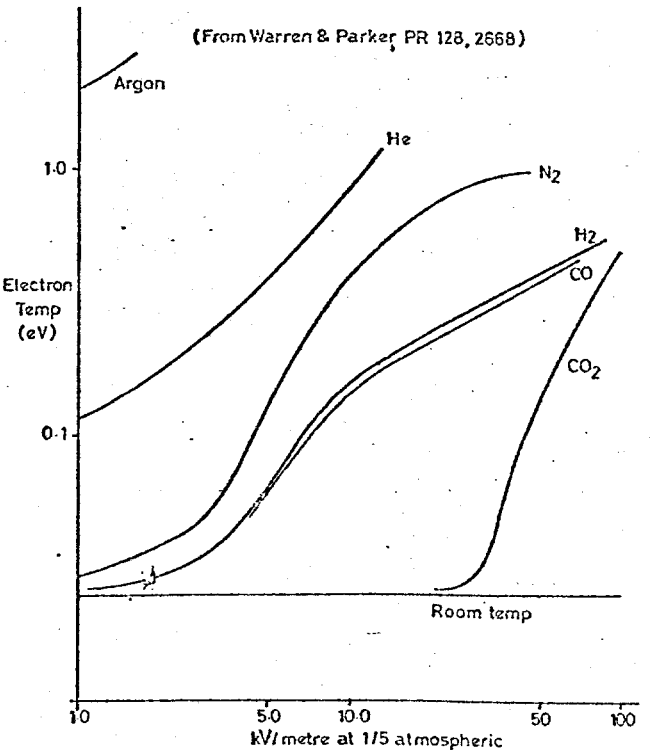

Fig. 4. The electron temperature as a function of electric field for various gases at $\frac{1}{5}$th atmospheric pressure. The curves represent eyeball fits to the data quoted in ref. 8.

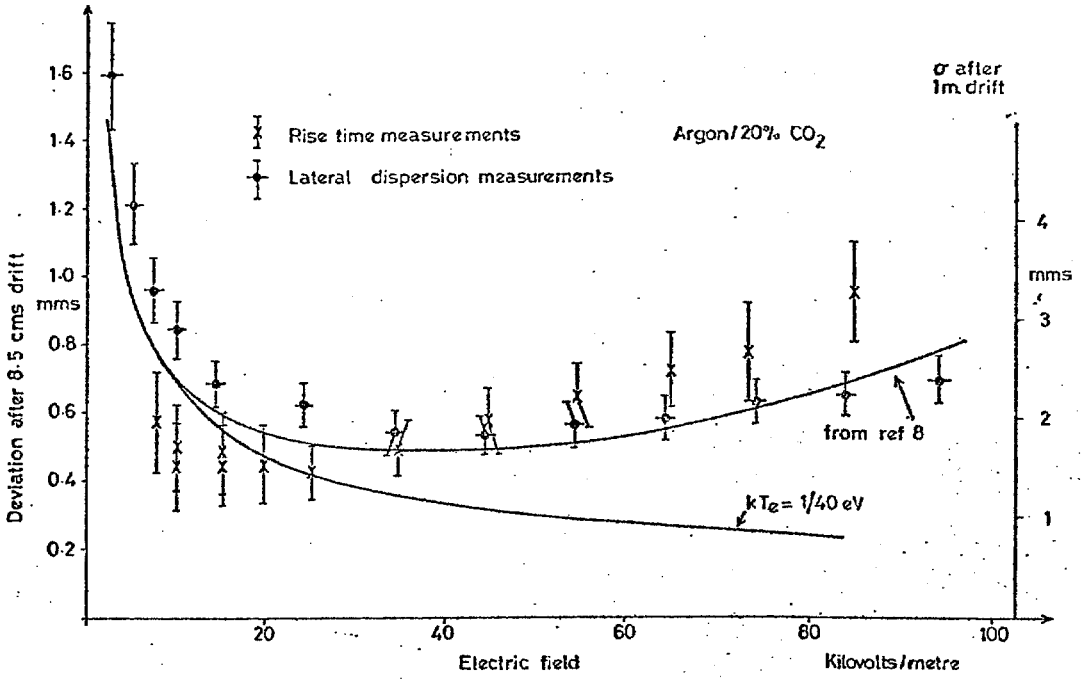

Fig. 5. The expected and observed effects of diffusion after drifting 1 m and 8.5 cm in argon+20% CO_2.

uniform electric field[9]). Using the measured drift velocity (see fig. 7) we obtain σ and eq. (1) allows us to extrapolate to 1 m. The results are shown in fig. 5. We have also measured the lateral dispersion of the bunches by comparing pulse heights on adjacent wires separated by 2 mm (see fig. 5) but note that this is susceptible to cross-talk effects. We find excellent agreement between the two methods and with published data on electron temperatures[8]). Values of σ between 1.5 and 2.5 mm apply over a wide range of electric fields. This means that the position of the blob may be measured to approximately 2 mm but that for two blobs to be integrated to the 1% level they must be at least 1 cm apart.

Unfortunately CO_2 catalyses the attachment of electrons to residual oxygen and the rate is given by[10])

$$\nu = (3.1 \pm 0.3) \times 10^{-30} \times [O_2] \times [CO_2] s^{-1},$$

where concentrations are expressed in molecules per cm^3.

With 20% CO_2 this is expected to be the dominant cause of electron loss. With 2 ppm of oxygen it predicts an electron lifetime of 1.4 ms. With the observed drift velocity gas of such a purity should therefore give an attenuation length of 20–30 m.

We conclude that argon/20% CO_2 is a suitable gas mixture to use.

3. Tests

To confirm these expectations we h[illegible] buil[illegible] device with a 1 m drift path (fig. 6). T[illegible] was vertical and surrounded by guard planes co[illegible] to a resistor chain to ensure uniformity. At the [illegible] a 30 cm × 30 cm proportional chamber wit[illegible] 30 μm diameter stainless-steel signal wire[illegible] 1.5 cm apart. The high-voltage planes we[illegible] above and below the signal plane* and were at 2130 V. Each channel contained a pre-amp[illegible] an 8-bit CAMAC ADC unit. The ADCs were discriminator logic looking at one or mor[illegible] signals. The tests were carried out in the P71 [illegible] at the Rutherford Laboratory with particle [illegible] cation by time of flight, a Cherenkov counte[illegible] shower counter (see fig. 6). A geometrical [illegible] defined by the passage of a particle through finger counters placed in front of and beh[illegible] chamber in coincidence with other beam cou[illegible] in the absence of other beam or backgrou[illegible] within ± 10 μs. The data were collected by with an on-line display and written out on tape. Further processing was done off-line. [illegible] chamber which was positioned at a vertical the beam was raised and lowered on a hydrau[illegible]

* With this geometry the induced-pulse cros[illegible]lk is to be small.

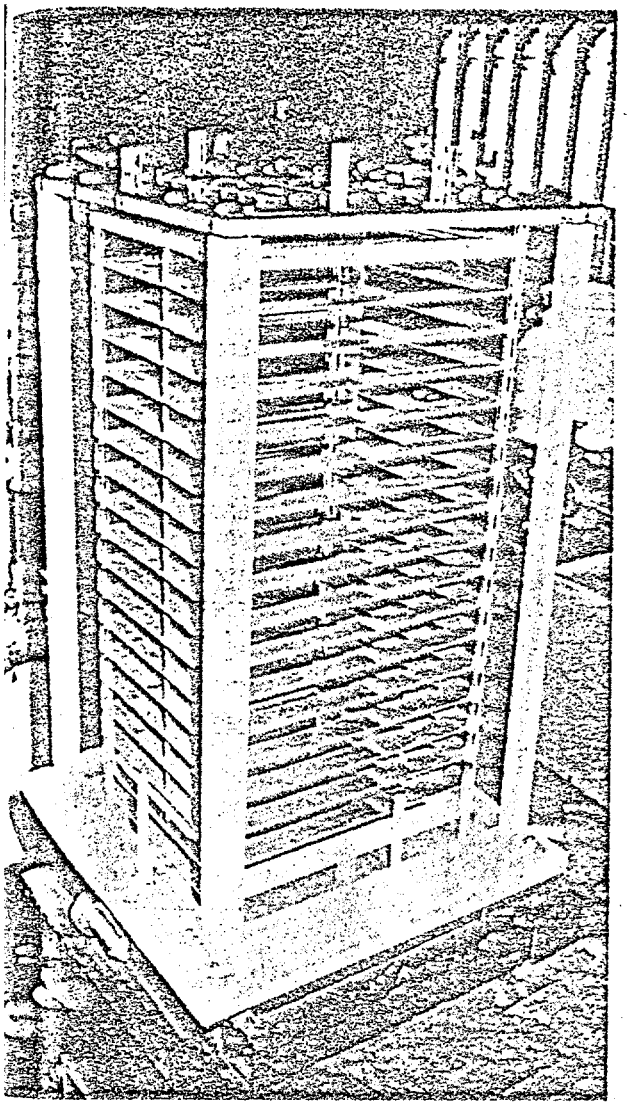

so that the beam could be passed through the drift volume at any desired height. The premixed argon/20% CO_2 was flushed continuously through the chamber, one of the double walls acting as a gas-inlet manifold to ensure efficient flushing of the whole volume.

Fig. 7 shows the results of measurements of the drift velocity at various drift field strengths. These were made using a time-to-pulse-height converter and a 1000-channel pulse-height analyser. The data show a linear dependence of the velocity on field strength characteristic of thermalised electrons. During this study we observed a change in the drift velocity with high beam intensities and gas amplification. This has been related to the presence of positive-ion space charge in the drift region[11]). A 3% effect was observed with $G\Phi \approx 5 \times 10^7$, were G is the gas gain and Φ is the flux in particles per second.

We have studied electron attenuation using a gas mixture assayed to contain 80–100 ppm of oxygen. The experiments of Pack and Phelps[10]) predict an electron lifetime for attachment of 28–35 μs. Fig. 8 shows how the peak of the pulse-height spectrum varies as a function of drift time. Data taken with different drift voltages lie on the same line and correspond to a lifetime of 35.3 μs. We conclude that the electron loss mechanism is that studied by Pack and Phelps and that oxygen contamination of 2 ppm corresponding to an attenuation length of 20–30 m is tolerable. In fig. 9 we show the single-wire pulse-height spectrum obtained using a gas mixture with less than 2 ppm oxygen. The beam was 1 GeV/c π^- and the drift voltage was 50 kV. The three spectra correspond to three different drift-path

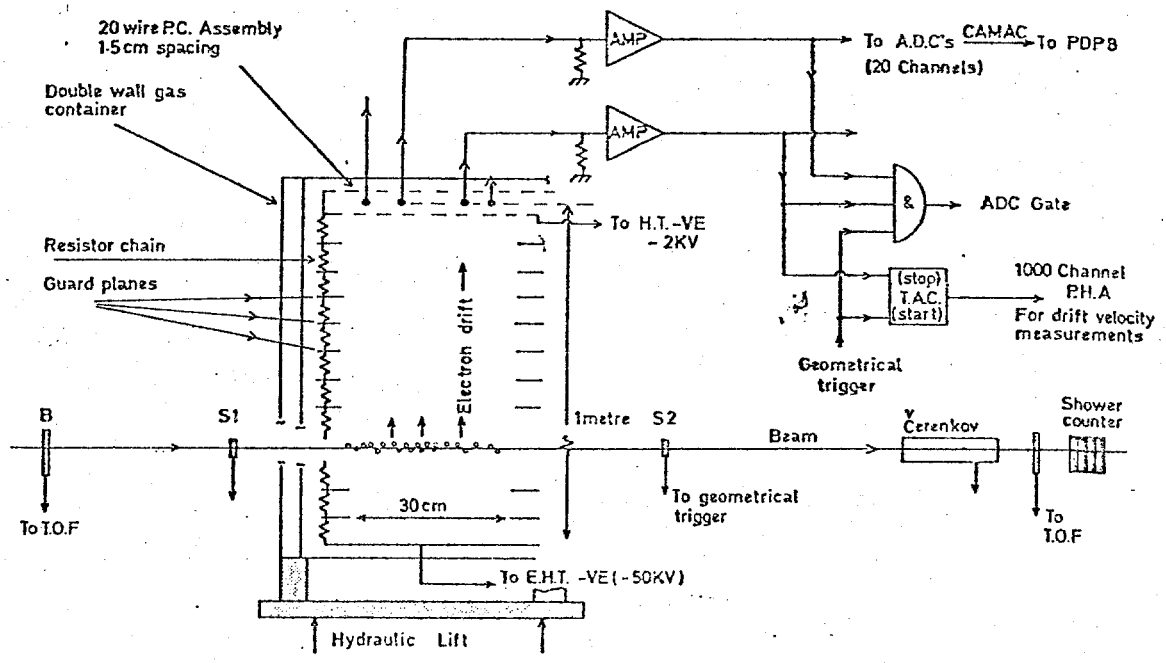

6. (top) The prototype during construction. The proportional-plane assembly is near the top. (bottom) Schematic diagram of prototype in test beam at Rutherford Laboratory.

lengths, and are compared with identical reference curves. No effect of drifting on either the peak value or the width of this Landau distribution is apparent.

In fig. 10 we compare the width of the distribution with that measured in conventional MPWC filled with argon/7% methane for pions of the same momentum[1]). The ISIS data was a fwhm of 83% compared with 96%. This may be understood in terms of the com effects of double-particle data in the MWPC[1]) emerging from the walls of the MWPC[1] talk in the ISIS data.

In fig. 11 we show the single-wire sample distributio for π^+ and protons in a 1 GeV/c beam as measure the chamber after a drift of 86 cm in a field of 50 k The distributions should peak at energies in the 1.05/1.6 (see fig. 1) as indicated by the dotted The agreement is excellent.

Next we looked for the effects of diffusion. proved difficult in our apparatus due to the length of track seen by each wire (1.5 cm). By stu the rise time of track pulses after drifting 85 were able to establish a conservative upper limi of 5 mm at a field of 40 kV/m. In addition if we at all the observed cross talk (20%) between bouring samples we get a limit of 4 mm. Both results include systematic effects inherent in the

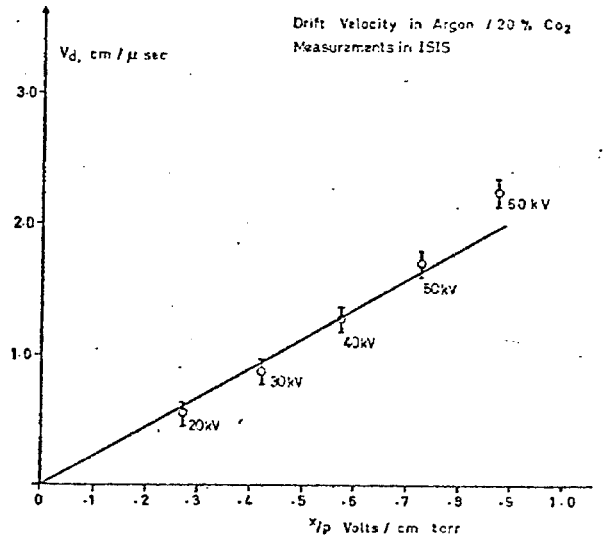

Fig. 7. Drift-velocity measurements.

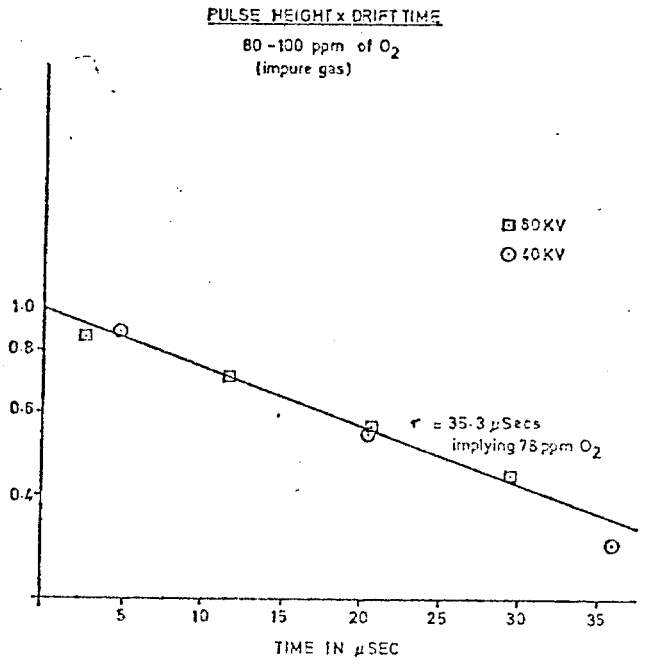

Fig. 8. Measurement of electron lifetime in argon/20% CO_2 in the presence of residual oxygen.

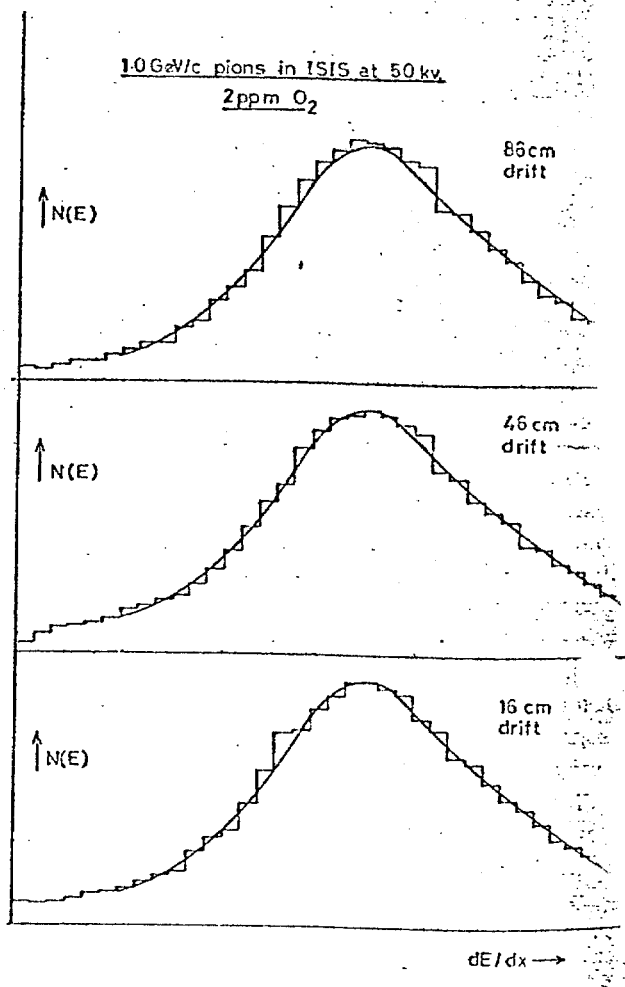

Fig. 9. The pulse-height spectra observed at different dr distances with identical superimposed curves to guide the ey

the prototype and we believe that the diffusion is correctly described by our earlier results shown in fig. 5.

Design of an ISIS chamber for use with a rapid cycling target

We have used the actual data for the energy loss in 3 cm of gas as seen by a single wire in ISIS for 1 GeV c pions to make a Monte Carlo study of the resolution attainable by a large device with many channels. We plot the ionisation resolution against the total device length in fig. 12. To reduce the effect of the Landau tail we used as estimater the mean of the lowest 70% of the samples generated for each track. Studies showed that for a wide variety of detector parameters the percentage used mattered little provided it lay in the range 50–80%, and we calculate that a cut of this size should be sufficient to remove the effects of long-range δ-rays. In the calculation of the crosses in fig. 12 we have included a 15% cross talk from sample to sample. In fact it makes rather little difference. To maximise the angular acceptance the device must be as short as possible consistent with the required resolution. Similarly the sample size should be short enough that wide-angle tracks do not generate broad pulses which will not be integrated correctly. For these reasons we choose a 1.5 cm sample size and a total active device length of 5 m (330 samples). The expected ionisation resolution of 6.2% does not differ significantly from that derived from the analysis of Lehraus and co-workers[3]) for such a device. The corresponding separations of K/π/p are shown in fig. 13.

We now turn to the design and position of an ISIS chamber with respect to a rapid cycling target (RCT). Such a chamber is shown in fig. 14. The device is

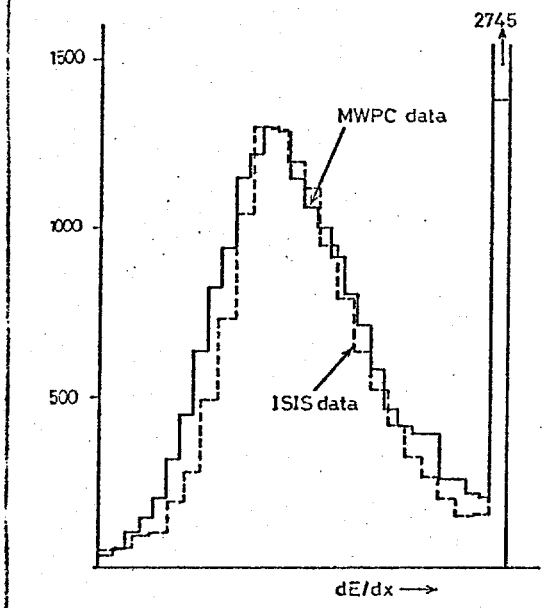

Fig. 10. A comparison of the shape of the spectrum of ISIS data with comparable data from the experiment of ref. 1. The scales of the two histograms have been adjusted.

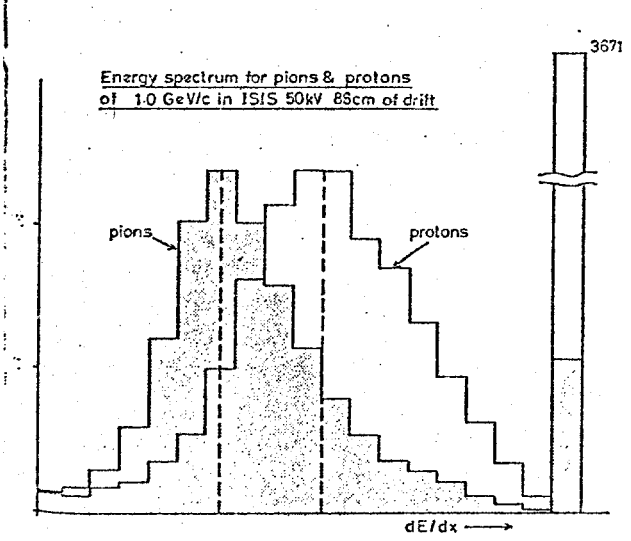

Fig. 11. The observed ionisation-energy spectra for pions and protons at 1 GeV/c. The relative separation expected from fig. 1 is shown by the dotted lines.

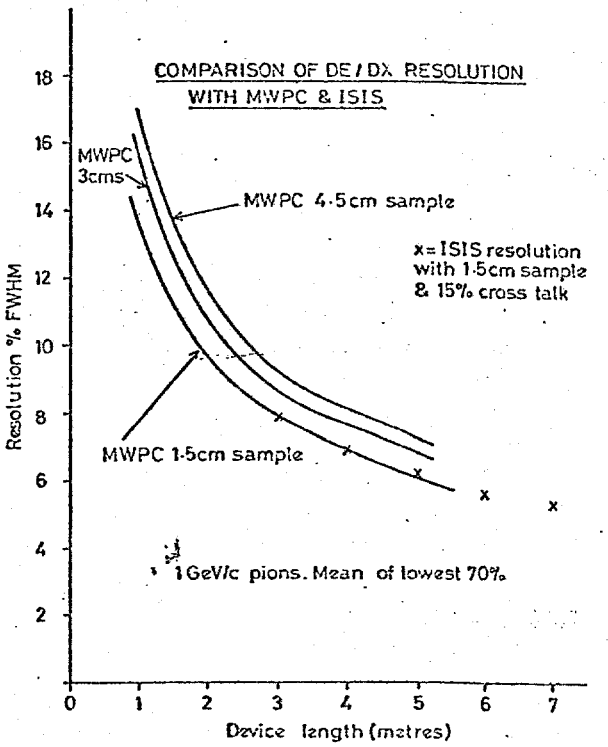

Fig. 12. The ionisation resolution predicted for devices of various lengths based on the data of ref. 1 and of this experiment.

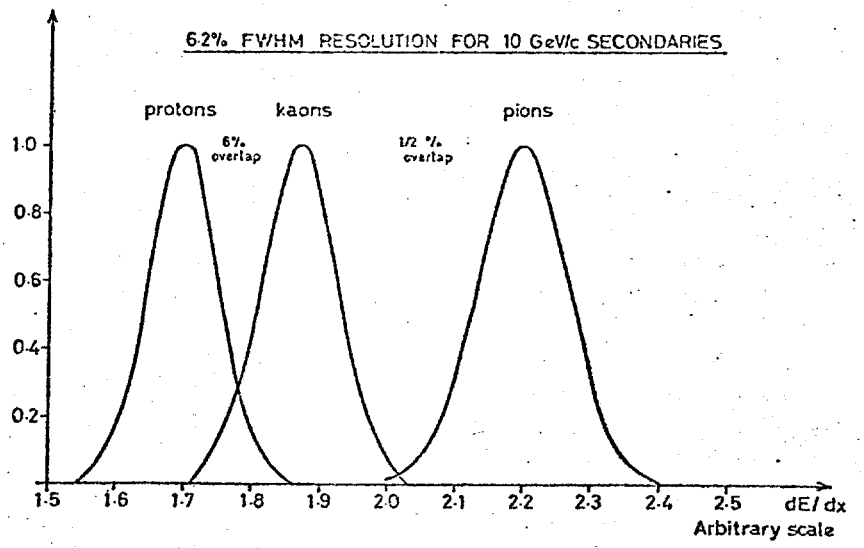

Fig. 13. The separation expected with a 5 m deep ISIS device at 10 GeV/c.

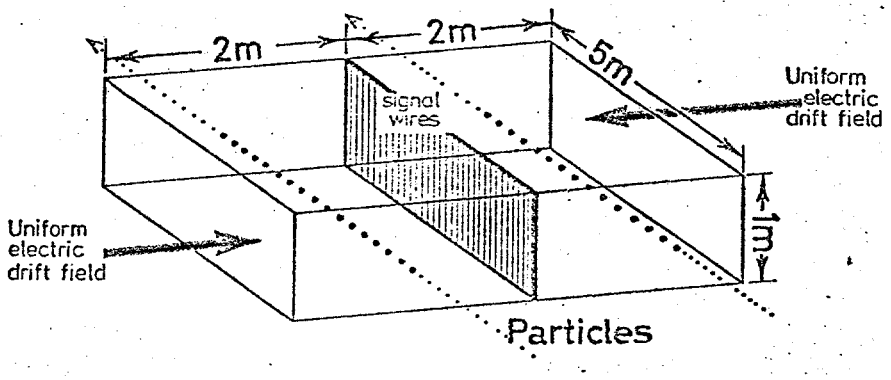

Fig. 14. The geometry of an ISIS behind an RCT.

4 m wide, 1 m high and the 5 m depth would be divided into 5 × 1 m modules or tanks. The upstream end of it is 5 m from the centre of the RCT, which might be an 80 cm diameter chamber with a 3 T magnetic field. Even without allowance for any iron the magnetic field gradient due to such an RCT is less than 25 G/m at 5 m – at least a factor 2 below having any effect on ISIS. The left and right halves of the detector are formed by two 2 m drift spaces with a common central wire plane. All secondaries above about 2 GeV/c will enter the detector to give up to 330 transverse-position measurements on each track to an accuracy of 2–3 mm*. Those above 5 GeV/c will remain within ISIS for its whole depth and will be identified. Tracks within 1 cm of one another in the folded horizontal plane for an appreciable fraction of the 5 m depth will not be identified – in fact this is expected to be an unusual occurrence. Of course no vertical-position information on each track is obtained.

In this device at the cost of the ambiguity between the left and right sides of the apparatus each and every track is sampled by each and every signal wire and its associated electronics. This has the advantage that systematic effects of imperfect calibration are minimised. Further, since each channel sees the non-interacting beam tracks, each may be monitored during an experiment.

5. Conclusion

The physical principles of a device to identify particles from 5–100 GeV/c with high efficiency have been established. The effect of space charge limits the average particle flux to a few × 10^4 per second (without pulsing the amplification voltage). We are undertaki

* To extract position information from the time of arrival of the drift electrons the precise time of the event must be known. This pattern recognition problem is made easier if the events do not overlap within the memory time of the device (~100 μs).

ailed studies in relation to a rapid cycling target use with beams up to 400 GeV/c, where such flux itations are not a problem. Work is in progress on construction and testing of prototype electronics h the required multitrack capability.

We would like to thank the Rutherford Laboratory their support and acknowledge the assistance and vice of Dr G. Parham and Dr J. H. Mulvey. Finally, thank the Nuclear Physics Laboratory main rkshop for their enthusiastic efforts and Mr P. ield for his work on the electronics.

eferences

F. Harris et al., Nucl. Instr. and Meth. 107 (1973) 413.
P. V. Ramana-Murthy et al., Nucl. Instr. and Meth. 56 (1967) 93; P. V. Ramana-Murthy, Nucl. Instr. and Meth. 63 (1968) 77.
3) D. Jeanne et al., Nucl. Instr. and Meth. 111 (1973) 287; M. Aderholz et al., CERN/D. Ph 11/BEAM 74-1.
4) J. D. Jackson, *Classical electrodynamics* (J. Wiley, New York, 1960) Ch. 13.
5) G. Charpak et al., Nucl. Instr. and Meth. 62 (1968) 235; G. Charpak et al., Nucl. Instr. and Meth. 108 (1973) 413.
6) J. Saudinos et al., Nucl. Instr. and Meth. 111 (1973) 77.
7) A. von Engel, *Ionised gases* (Oxford Univ. Press, Oxford, 1960).
8) R. W. Warren and J. H. Parker, Phys. Rev. 128 (1962) 2668.
9) J. H. Cobb, ISIS internal note 15, Nuclear Phys. Lab. Oxford (1974) unpublished.
10) J. L. Pack and A. V. Phelps, J. Chem. Phys. 45 (1966) 4316.
11) J. H. Cobb, ISIS internal note 12, Nuclear Phys. Lab. Oxford (1974) unpublished.
12) J. H. Cobb et al., to be published.
13) Sternheimer and Peierls, Phys. Rev. B3 (1971) 3681; and earlier work.

CERN/D.Ph.II/RCBC 75-6
20 May 1975

This proposal, which was submitted by the Oxford Group to the Rutherford Laboratory Selection Panel, contains new information on ISIS and it is therefore distributed as an RCBC note.

W.W.M. Allison

To the Members of the

Rutherford Laboratory Selection Panel

PROPOSAL TO STUDY MULTIHADRON EVENTS INVOLVING IDENTIFIED PARTICLES IN HIGH ENERGY INTERACTIONS AT THE SPS

CERN-ORSAY-Oxford**-Rutgers-Stockholm

(**W.W.M. Allison, J.L. Lloyd, L. Lyons)

1. Introduction
2. Physics Philosophy
3. The apparatus
4. Status of Particle Identifier, ISIS
5. Timescale and support required

Spokesman: W.W.M. Allison

1. Introduction

This experiment has been proposed to the SPSC at CERN (CERN/SPSC/75-15 P42 attached) to be run in the North Area in 1978/79. After an open session presentation the committee appointed referees (I. Butterworth, E. Gabathuler, A. Miller). It is expected that their reports will be discussed at the meeting at the end of May.

The full proposal is rather bulky and so in the next sections of this document we give a brief description of the physics and the apparatus - further details may be found in the full proposal. Following this we describe the present status of the Oxford Particle Identifier (ISIS) which forms an important part of the facility. Finally we outline the support needed to complete ISIS, the technical assistance required and the testing facilities needed.

2. Physics Philosophy

Strong interaction physics at SPS energies is dominated by high multiplicity processes with large cross-sections. In studying physics in this range the experimentalist has a choice, either,

(a) to study exceptional processes which are in principle easier to detect and easier to interpret (e.g. high transverse momentum, low multiplicity, lepton production etc.), or

(b) to study the unexceptional high cross-section interactions which represent a major challenge for interpretation, but which, at the same time, are the meat of what actually occurs in strong interactions.

Intensive studies (a) call for high fluxes of incident beam to achieve the required counting rate on channels of interest. Equally important is the use of an efficient trigger to reduce dead time losses. It is

often necessary to trade some systematic losses to optimise these flux and trigger requirements. Most SPS experiments currently proposed are intensive in character.

Extensive experiments (b) concentrate on collecting bias-free data for many channels simultaneously. Tight triggers are avoided as a source of possible bias and a high data rate is achieved with a very modest incident flux. In the case of high multiplicity events the effects of relatively small systematic losses due to acceptance or close track problems can be severe. To avoid bias in the detection of 10 or 20 prong events a very high degree of spatial redundancy is needed in the track measurements. As a result the amount of data needed for each event is extremely large and to handle this rapidly is very expensive.

This proposal is for such an extensive study of 200 GeV/c π^- with hydrogen. The apparatus consists of an 80 cm 30 Hz rapid cycling bubble chamber at the head of a spectrometer and is well suited for use with other extensive experiments. Indeed 3 other proposals are currently before the SPSC and other letters of intent have been received.

The efficiency with which high multiplicity events can be handled is complicated by the requirement that, in addition to measuring the vector momentum of each outgoing particle by magnetic analysis, the mass or velocity must also be measured. Below about 1 GeV/c the track density of each charged secondary in the bubble chamber provides the necessary information. Above this momentum a major contribution can be made by the Oxford "ISIS" (Identification of Secondaries by Ionisation Sampling).

In extensive studies to date in the FNAL 30" bubble chamber there has been an almost complete lack of particle identification. As a result it is not even possible to make a Lorentz transformation to the centre of mass system except in the approximation that all fast charged particles are pions. While this approximation is almost true, it is the belief of this collaboration that it is just in the departures from this approximation that most of the useful physics information resides in brief, that multiparticle hadron physics should be studied by concentrating on the role of strangeness and baryon number as a probe of strong interactions. Neutral kaons, while a useful adjunct, have disadvantages compared with charged kaons. Thay are observed with less than 30% efficiency, their strangeness is ambiguous and in certain cases not more than one kaon of a pair may be observed (as in $\emptyset^\circ$ decay).

The experimental proposal should be compared with the ideal of accurate momentum determination and efficient particle identification over the whole of phase space for charged particle multiplicities up to 12 at least. Of course it falls short of this ideal but we believe it will be substantially better than any other existing or proposed at CERN or FNAL and as such is essential if extensive studies are to be undertaken.

3. The apparatus

The apparatus consists of:-

(1) A rapid cycling hydrogen bubble chamber, RCBC

(2) the Oxford particle identifier, ISIS

(3) a multicell Cerenkov system for slow secondaries at wide angles

(4) sets of drift and proportional chambers and a downstream bending magnet for improved resolution

(5) 3 sets of beam defining chambers and a Cerenkov counter for identification of the incident particle.

The layout is shown in fig. 3.0 (page 33) of the full proposal and is described there. The bubble chamber provides the features of high spatial redundancy and high geometrical efficiency for all tracks, good momentum resolution and particle identification for low momentum tracks. The downstream spectrometer and ISIS provide good momentum resolution and particle identification respectively for high momentum tracks. For tracks of intermediate momentum important additional resolution is provided by the bubble chamber magnet which is significantly bigger than the chamber itself on the downstream side. Particle identification coverage is improved by the use of the multicell Cerenkov counter. The latter is in fact being redesigned as two separate tanks with a gap for the higher momentum tracks to pass between. This and other developments in the design of the experiment are to be described in an addendum to the full proposal. This should be completed by mid-May.

How does this spectrometer measure up to the ideals of high efficiency, good resolution and complete particle identification?

The situation with respect to momentum is shown in Fig. 3.6.1 (page 37) and 3.7.2 which, when combined with the proven ability of bubble chamber photographs to resolve close tracks, leaves the main difficulties in the region of particle identification. There are two aspects of this, the geometrical efficiency of each stage of particle identification and the confidence with which the identification can be made when the particle enters the detector. A full study of the combined system is in progress and will be reported in the addendum.

Fig. 1 of this proposal shows the momentum ranges over which separation of kaons, pions and protons is possible. In the range 3-5 GeV/c there is significant overlap between the capability of ISIS and the Cerenkov counter. This is necessary because of the difficulty of achieving a high geometrical efficiency for these dispersed tracks

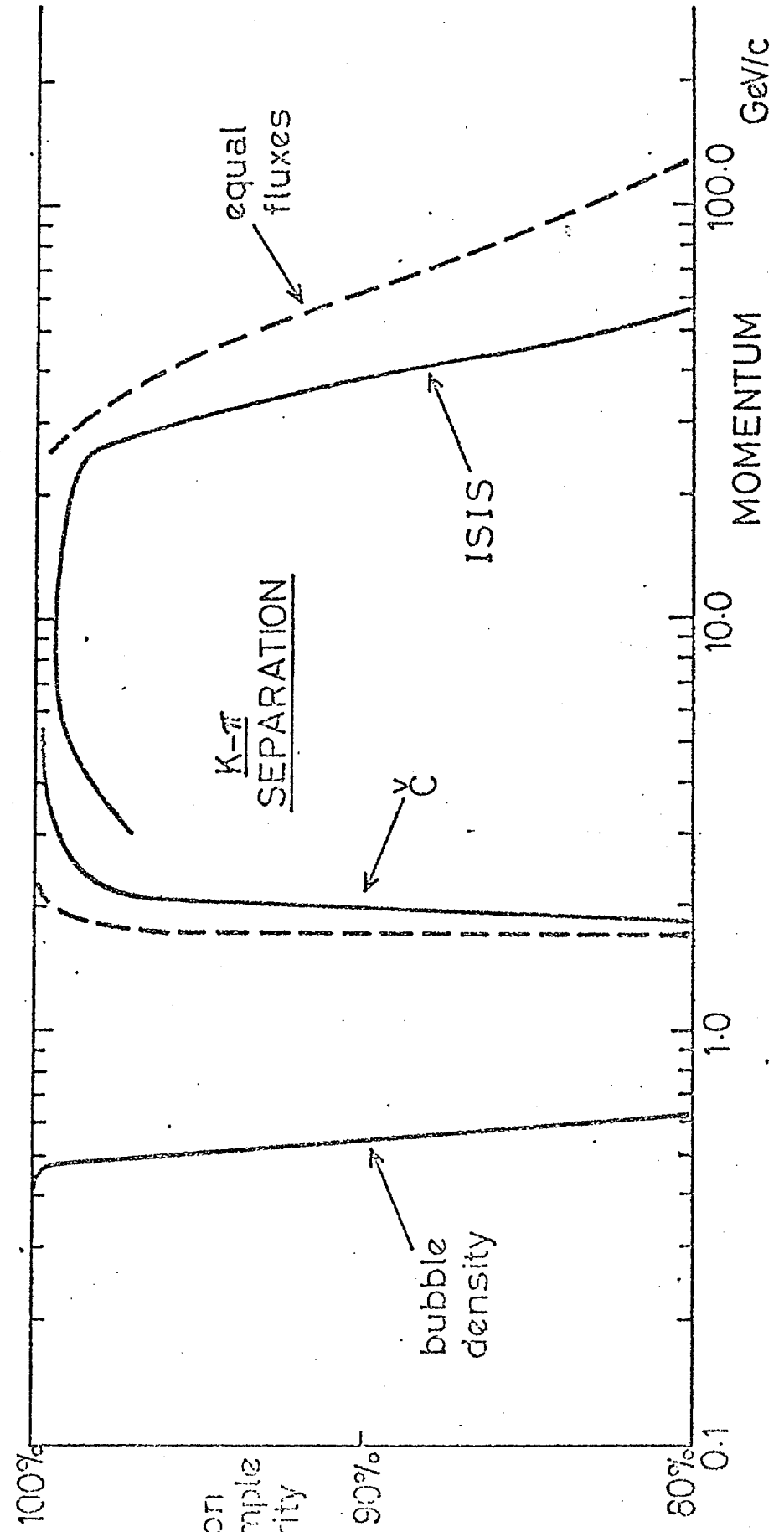

Fig. 1a

Assumed π/K/P ratio: 10/1/1

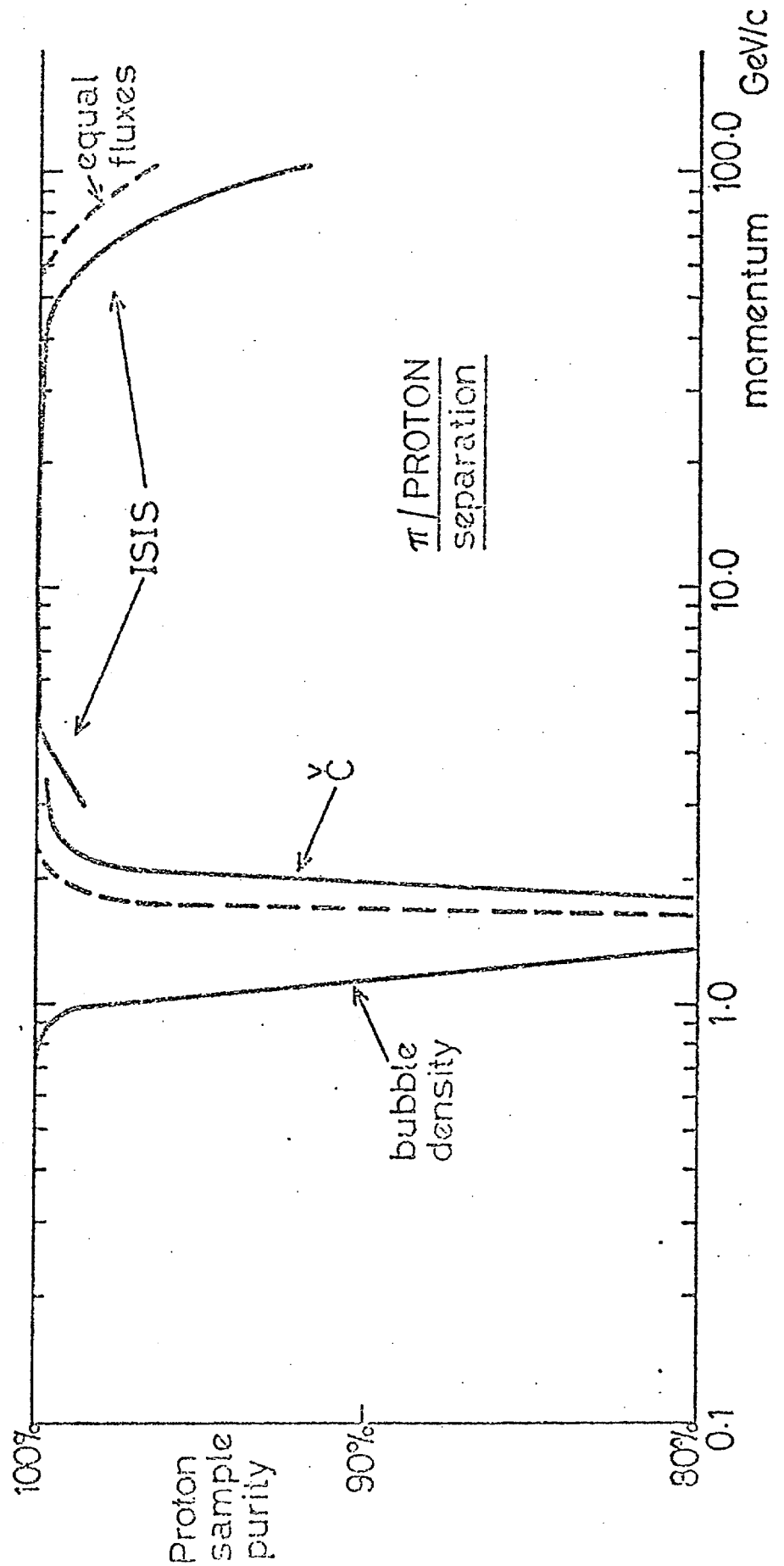

Fig. 1b

Assumed π/K/P ratio: 10/1/1

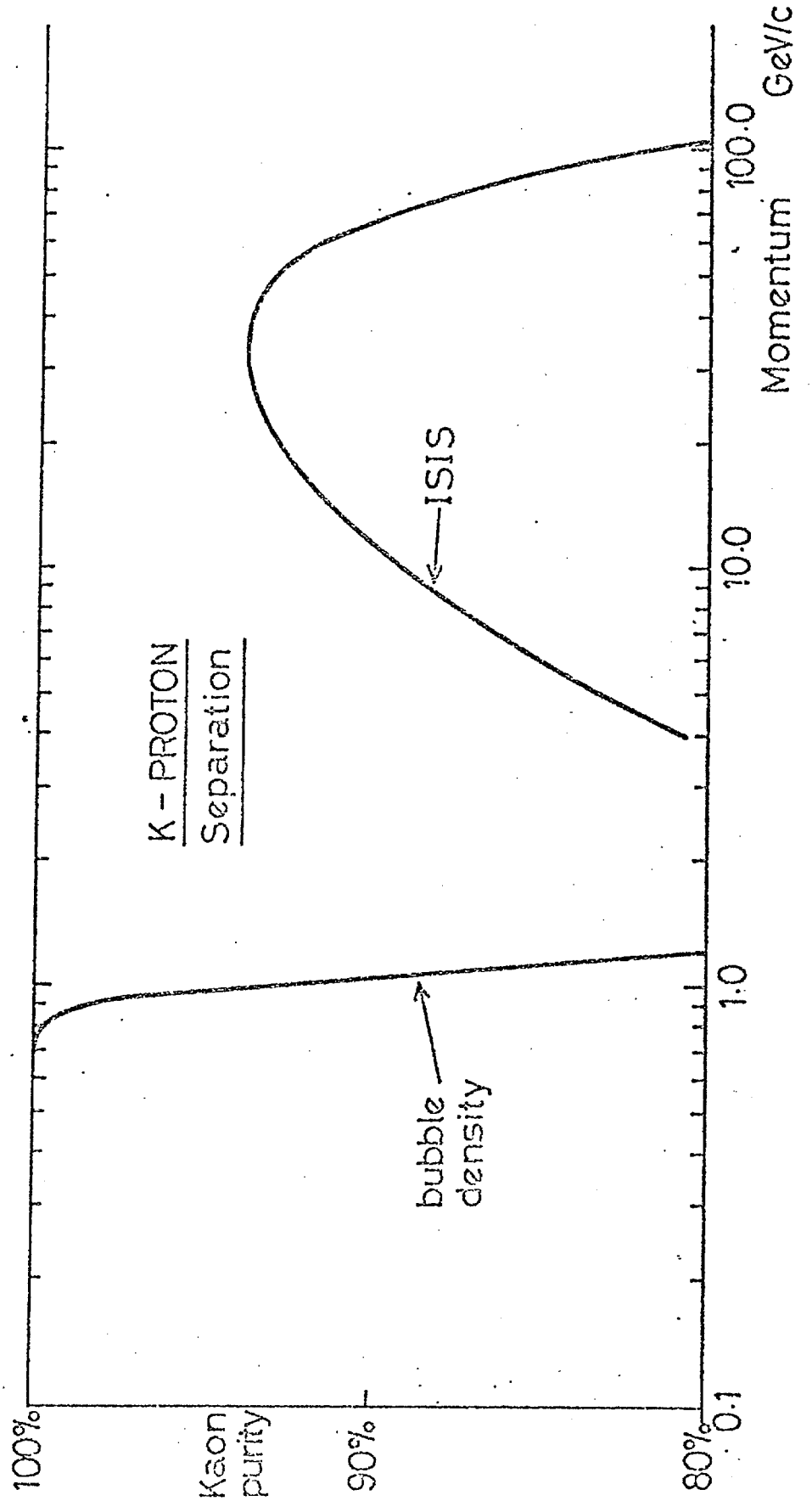

Fig. 1c

Assumed π/K/P ratio: 10/1/1

in ISIS. The logarithmic momentum scale is chosen to give a realistic picture of the relative importance of different momentum ranges in terms of secondary particle flux (see Fig. 3.7.2 following page 39). The ordinate of Fig. 1 represents the purity of an identified sample of kaons or protons associated with a flux of an order of magnitude more pions. In some cases useful physics may be done with equal fluxes (dashed lines in Fig. 1). For instance, most tracks above 50 GeV/c involve leading particle or diffraction dissociation effects where ambiguities are characterised by simple choices e.g. a K^+/π^+ pair. In any case above 100 GeV/c the efficiency of ISIS suffers some losses due to overlapping tracks. In our view the most serious losses are those in the K/π separation from 0.7 to 1.8 GeV/c. These would not be separated by ISIS or the Cerenkov counter even if they could be extracted from the magnet. We have to admit failure in this region. The poor quality of the K/p separation is less important since the proton flux above 1 GeV/c will be small and the resulting contamination of kaons likewise.

Finally we note that there is plenty of room in the spectrometer for the addition of further apparatus to detect forward γs (this is the subject of active work by the Padua group), a Cerenkov counter for leading particle triggering (as proposed by the Cambridge group) etc. However, we do not regard these as being essential to the P42 proposal.

4. Current status of ISIS

The performance of ISIS claimed in the preceding section depends on two separate properties:

a) its ability to handle a large number of simultaneous tracks over a large area, and

b) its ability to resolve different velocities in the region of the relativistic rise of ionisation loss in argon.

The principles of ISIS are described on page 60 of the full proposal. Over the last 2 years extensive tests have been made and the present situation is as follows:

Property a). Problems of diffusion, attenuation, drift velocity etc. have been studied extensively with sources and charged particles (W.W.M. Allison et al., Nucl. Inst. and Meth., 119 (1974) 499 and further tests in J.H. Cobb D. Phil thesis (1975) Oxford). The status of the electronics and its ability to handle multiple tracks is discussed below.

Property b). This depends on three things: (i) the magnitude of the relativistic rise, ii) the shape of the Landau distribution or energy loss spectrum of single measurements and (iii) the ability to make a large number of independent measurements ($\sim$300) on every track without being limited in resolution by systematic effects. These three aspects were the subject of a test experiment performed by the Oxford group at FNAL in January and February 1975. (FNAL experiment 327).

In fact it has been known for many years that measurements of (i) and (ii) are in poor agreement with accepted theoretical calculations for thin gas samples. A programme of improved theoretical calculations is in fact in hand at Oxford. In any event the results of the FNAL measurements permit us to make reliable statements about the particle identification that can be achieved. Fig. 2 shows the separation observed with raw data

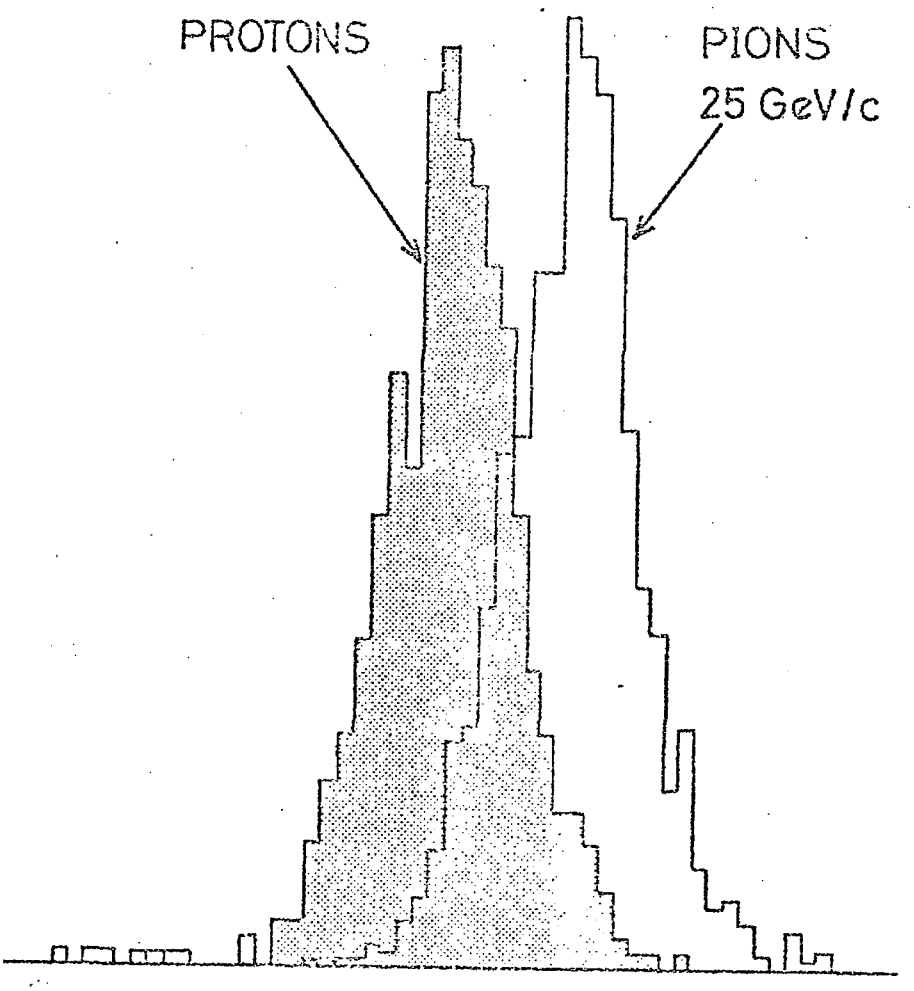

Fig. 2

between pions and protons of 25 GeV/c. The spectra are the distributions of mean* ionisation for protons and pions as identified by a Cerenkov counter. The ionisation is sampled 58 times on each track over 90 cms - this is to be compared with 330 times over 500 cms in the final ISIS. In table I we give some preliminary results on the difference between π and proton as observed and as expected according to our theoretical calculations. The agreement is encouraging. We are not in a position to quote errors on these numbers until the data has been fully calibrated and checked out. A typical Landau distribution is shown in fig. 3.

TABLE I

π/p ionisation ratio	Experiment	Theory
9 GeV/c	1.21 (EPI group)	-
25 GeV/c	1.18	1.17
50 GeV/c	-	1.16
100 GeV/c	1.10	1.09
150 GeV/c	1.07	1.06

To estimate the theoretical resolution, ΔI, of a full scale ISIS we may sample by Monte Carlo from this distribution 330 times. The confidence levels of fig. 1 were computed by comparing ΔI with the theoretical difference of ionisation for π/K and proton of known momentum. Is this realistic? This cannot be answered for certain since we have still to build such a device. What we can do however is compare such a ΔI computed by Monte Carlo method for a 58 sample device with the resolution actually observed at FNAL. The experimental value of ΔI was 18% larger than the result of the Monte Carlo calculation. We expect this discrepancy to be

---

* In order to remove the effect of the Landau tail the abscissa is in fact the mean of the lowest 35 measurements out of the 58. This gives close to optimal resolution.

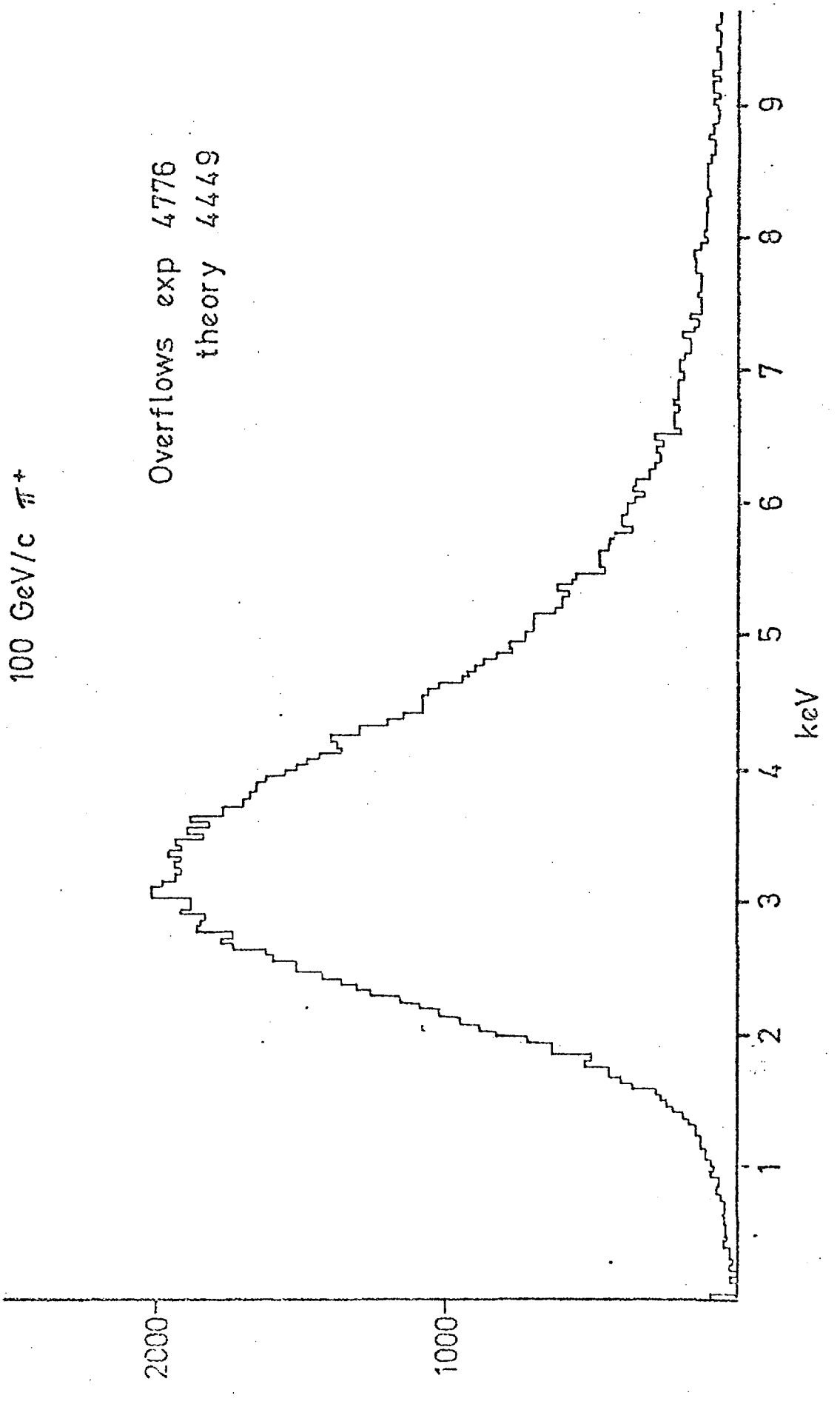
100 GeV/c π+
Overflows exp 4776
theory 4449
2000
1000
1
2
3
4
5
6
7
8
9
keV

Fig. 3

further reduced when better correction for gain drift during the runs due to temperature and pressure variation becomes available. The results of this experiment and therrelated theoretical calculations will be published in due course.

A full discussion of the electronics as currently designed will be included in the proposal addendum. We present here a brief summary of the present status. Each sampling channel, of which there are 330, operates essentially independently of the others. It has to be able to integrate the track signal for up to 32 tracks (including background) with systematic effects not exceeding 1% and record the arrival time of tracks in a 400 position bit map. The collection (drift) time is 50 μ secs and thus the bit map is scanned at 8 MHz and each slot represents 5 mms in space. Each track profile is integrated for 250 n secs which is calculated to provide a shape-independent pulse height at the 1% level for the shape variations expected from diffusion and track inclination to ± 25°. A block diagram of the electronics is shown in fig. 4. The modest bandwidths involved mean that most of the problems can be handled by standard techniques. There are a number of areas where work is or remains to be done.

(1) The multi ADC (MADC) which integrates up to 32 separate pulse heights each on its own capacitor and then digitises them sequentially (one digitiser per channel) during the read out phase. Such a unit has been built and tested in Oxford with test pulses and signals from a proportional chamber illuminated by an Fe source. Pulse height memory times at least one order of magnitude longer than is needed can be achieved and cross-talk problems can be made negligible. None the less much further work remains to be done.

(2) The signal-to-noise ration as far as it affects the trigger circuit depends on the gas amplification factor, the design of the preamplifier and the bandwidths. This is under intensive study by computer simulation.

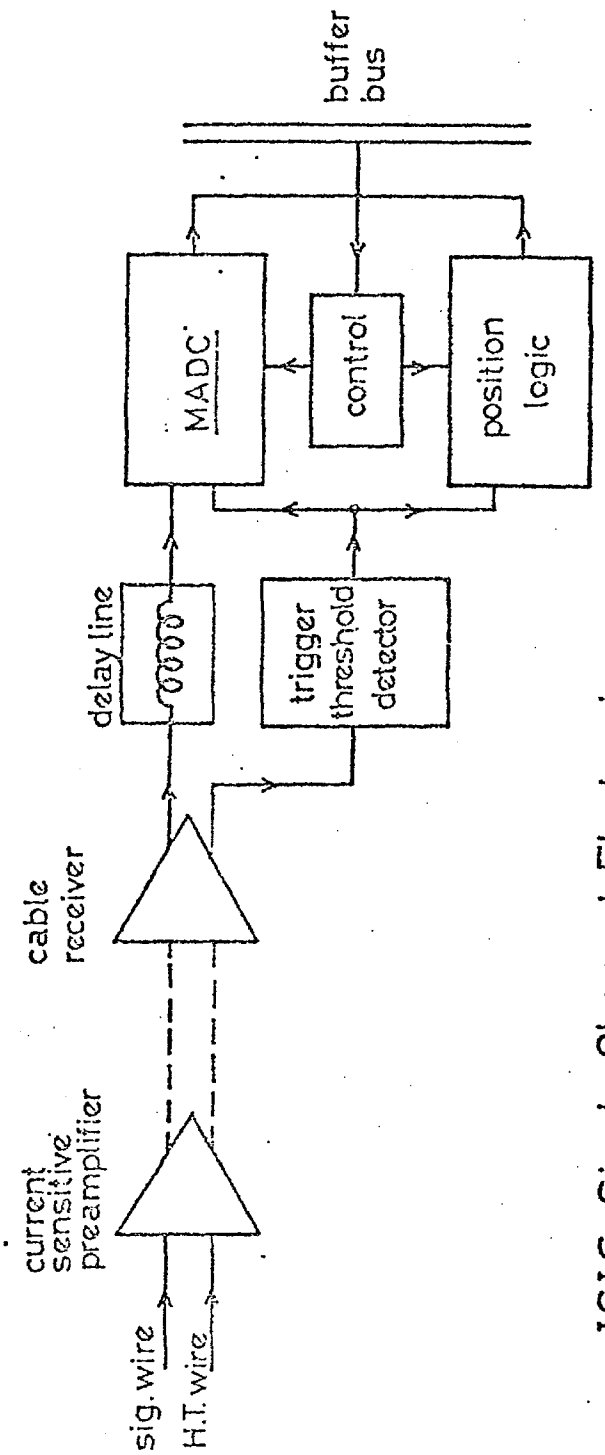

ISIS Single Channel Electronics

Fig. 4

(3) The use of differential input to the preamplifier using high voltage and signal wires. This is being studied as a method of reducing both external pick up and also capacitative coupling between channels. Failure to understand the latter problem caused serious (but recoverable) deterioration in the quality of the data from the FNAL experiment.

(4) Gain switching. To avoid the build up of space charge in ISIS (see proposal page 62), it is necessary to "turn off" the gas amplification of the electrons at the signal wires by lowering the amplification voltage by a few hundred volts, except during the bubble chamber sensitive time when the voltage stability must be ± IV to ensure ± 1% gain stability. Design work remains to be done in this region.

The structure of the chamber itself will incorporate the results of useful experience gained with the FNAL chamber. The most important of these is the use of a single wire plane incorporating both HT and signal wires. The former provide control of the gas amplification independent of the drift field, improve the electromechanical stability of the plane allowing the use of 2 metre long wires, act as a screen between neighbouring channels and remove the difficulties associated with multiplane geometries. Wire gain uniformity of 2% was achieved in the FNAL chamber.

Work remains to be done on other aspects of the chamber design, safety, environmental monitoring, gas handling, calibration, testing and debugging, surveying, computer interface and software, although important steps have been made towards understanding the problems in most cases.

Appendix G 88-43

THE IONISATION LOSS OF RELATIVISTIC CHARGED PARTICLES IN THIN GAS SAMPLES AND ITS USE FOR PARTICLE IDENTIFICATION: I THEORETICAL PREDICTIONS

J.H. Cobb*,, W.W.M. Allison, J.N. Bunch

Nuclear Physics Laboratory, Oxford.

(Submitted to Nuclear Instruments and Methods)

Abstract

A brief review shows a significant discrepancy between available data and theoretical predictions on the ionisation loss of charged particles in thin gas-filled proportional counters. The discrepancy relates both to the increase of the most probable loss at relativistic velocities ("relativistic rise") and to the spectrum of such losses at a given velocity (the "Landau distribution"). The origin of this relativistic rise is discussed in simple terms and related to the phenomena of transition radiation and Cerenkov radiation. We show that the failure of the predictions is due to the small number of ionising collisions in a gas. This problem is overcome by using a Monte Carlo method rather than a continuous integral over the spectrum of single collision processes. A specific model of the atomic form factors is used with a modified Born approximation to yield the differential cross-sections needed for the calculation. The new predictions give improved agreement with experiment and are used to investigate the problem of identifying particles of known momenta in the relativistic region. We show that by measuring the ionisation loss of each particle several hundred times over 5 metres or more, kaon, pion and proton separation with good confidence level may be achieved. Many gases are considered and a comparison is made. The results are also compared with the velocity resolution achievable by measuring primary ionisation.

* Now at CERN.

Introduction

The mean energy loss of high velocity charged particles in thin absorbers is a function only of the velocity, β, of the particle and not of its mass[1]. In fact it is more convenient to consider its dependence on

$$P/mc = \beta\gamma = \beta(1-\beta^2)^{-\frac{1}{2}} \qquad (1)$$

In terms of this there are three relatively well defined regions:

(a) For $P/mc < 4$, the familiar non relativistic region in which the energy loss goes like $1/\beta^2$ for all media.

(b) For $P/mc > 4$, there is a slow logarithmic increase (the "relativistic rise") which extends up to a value of P/mc depending on the nature of the absorber and its density.

(c) A flat region beyond the region of the rise where no further increase takes place (the "Fermi Plateau").

In this paper we explore what is known about the logarithmic increase and the plateau region as observed in thin gas counters and how it may be applied to the problem of particle identification at high energy.

In section 2 we review existing data and current models. In section 3 we discuss the origin of the "relativistic rise" and other relativistic phenomena in terms of simple models. In section 4 we set up a specific model for the calculation of energy loss spectra and in section 5 we apply it to a variety of gases. These results are used to estimate the particle identification efficiency of ionisation sampling chambers[2] with different gas fillings.

2. Status of Theory and Experiment

The experimental and theoretical status of the relativistic rise region has been reviewed by Crispin and Fowler[1]. In the case of measurements which can be simply related to calculations there is good agreement for dense materials for which the relativistic increase rarely exceeds 20%. Some

difficulty surrounds the interpretation of emulsion and bubble chamber data since they are not related in a simple way to the energy loss. This is not serious. In the case of ionisation loss in gases on the other hand the interpretation of the measurements is simpler but the discrepancy with calculation appears large.

Fig. 1 shows the results of a variety of measurements of the relative ionisation loss of relativistic particles in thin proportional chambers filled with argon at 1 atmosphere[3-5]. The dashed curve I has been calculated according to the model of Sternheimer[6] for the most probable ionisation loss in a chamber 1.5 cms thick. The measurements favour a relativistic rise of about 50% whereas the model predicts about 70%[5,7]. Fig. 2 shows that the discrepancy goes further. The histogram is the observed ionisation loss spectrum of 3 GeV/c π^- in 1.5 cms (2.7 mg/cm^2) of argon[3,9]. The distribution is remarkable for its width and long tail. Curve I is the prediction of the original Landau theory[10] which is used explicitly in the derivation of the most probable energy loss (curve I in Fig. 1[6]). It is an extremely bad fit to the experimental distribution. The model of Blunck and Leisegang[12] does not fit the data either (curve II). The reason is clear. The number of ionising collisions is small ($\sim$30/cm) and the most probable energy loss cannot involve any contribution from inner electrons with large binding energies[11]. For instance, in argon the most probable loss is about 2 keV per cm, whereas the K shell binding energy is already 3 keV. This shows that we should try first to abandon the use of a "mean ionisation potential" and work with a specific spectrum of atomic oscillator strengths and second to replace the continuous integral over possible collisions by a corresponding random summation of discrete energy losses by a Monte Carlo method. Ispiryan[13] et al have already shown that the technique gives improved agreement with the Landau distribution.

3. The Origin of the Relativistic Rise

Before pursuing quantitative questions further we pause to discuss the origin of the relativistic rise and the Fermi plateau. This will suggest qualitatively what rise we can expect in particular gases. In section 5 we confirm these expectations with detailed calculations.

The electromagnetic field of a relativistic charged particle can be represented as a Fourier integral over plane wave components with wave number $\underline{q}$, frequency ω. The energy loss process involves the scattering of one of these virtual photons by the medium resulting in an energy loss $\hbar\omega$ and momentum transfer $\hbar\underline{q}$. The interaction through virtual longitudinal photons ($\underline{E}$ parallel to $\underline{q}$) represents the instantaneous coulomb interaction and is effectively constant at high velocities[15]. The increased range of the transverse photons on the other hand is responsible for the "relativistic rise" of the energy loss.

These virtual photons have a very broad spectrum simply because they relate to the transform of the field of a point charge. This broad spectrum leads in turn to significant ionisation cross-sections over a wide range of energy transfer even for atomic electrons with a unique binding energy. In considering a finite, thickness of absorber we sum over all energy loss processes including the large energy loss collisions which have a low probability. The latter are responsible for the long tail observed in the energy loss spectrum shown in Fig. 2.

Why does the interaction through transverse photons increase and then saturate? It is well known that in vacuum the electric field of a relativistic particle expands in the transverse dimension as γ increases as a kinematic consequence of special relativity. In a medium on the other hand this increase does not continue indefinitely. The effect of the medium may be described by a screening length, χ, which is the Compton wave length of the renormalised photon in a medium of dielectric constant $\varepsilon(\omega)$. In simple terms, since electromagnetic

photons have mass, μ, given by

$$\mu = \frac{\hbar\omega}{c^2}\ (1 - v^2/c^2)^{\frac{1}{2}} = \frac{\hbar\omega}{c^2}\ (1 - (\frac{d}{d\omega}(\omega\sqrt{\epsilon}))^{-2})^{\frac{1}{2}} \qquad (2)$$

where v is the group velocity at frequency ω. Exchange of such quanta will be characterised by a range equal to the Compton wavelength:

$$\lambda\!\!\!^{-} = \frac{\hbar}{\mu c} = \frac{c}{\omega}\ (1 - (\frac{d}{d\omega}\ (\omega\ \sqrt{\epsilon}))^{-2})^{-\frac{1}{2}} \qquad (3)$$

At high frequencies when the binding energy of the electrons may be neglected this reduces to

$$\lambda\!\!\!^{-} = \frac{c}{\omega_p} \qquad (4)$$

where ω_p is the plasma frequency. We may compare this screening length with the maximum impact parameter for which the collision is sufficiently "sudden" to transfer energy $\hbar\omega$ to an atom. Jackson shows that

$$b_{max} = \frac{\gamma v}{\omega}$$

It follows that we may expect the relativistic rise due to the increase of b_{max} to saturate when $b_{max} = \lambda\!\!\!^{-}$ or when

$$\beta\gamma \sim \frac{\omega}{\omega_p} = \frac{\text{ionisation energy}}{\text{plasma energy}} \qquad (5)$$

in the high frequency case.

Before discussing this result we derive it in a different way[9] which brings out relationships with the phenomena of Cerenkov and Transition Radiation and is based on the Uncertainty Principle. A virtual photon associated with a particle of velocity βc along the x-axis must itself have a phase velocity βc along x. Otherwise it would not be seen to an observer travelling in the particle frame as a component of a static coulomb field. It therefore has a momentum projection along x given by

$$p_x = \frac{\hbar\omega}{\beta c} \qquad (6)$$

The range of such a virtual photon is given by Heisenberg's Uncertainty Principle:

$$R_x = \hbar/\Delta p_x \tag{7}$$

where Δp_x is the difference between its momentum and that of a free photon in the medium travelling in the same direction, ψ, with the same energy, $\hbar\omega$.

$$\Delta p_x = \frac{\hbar\omega}{\beta c} - \frac{\hbar\omega}{c}\sqrt{\varepsilon}\cos\psi \tag{8}$$

where $\sqrt{\varepsilon}$ is the refractive index of the medium. This gives a range

$$R_x = \frac{c}{\omega}\left(\frac{1}{\beta} - \sqrt{\varepsilon}\cos\psi\right)^{-1} \tag{9}$$

Of course, when $1/\beta = \sqrt{\varepsilon}\cos\psi$, the range is infinite (for real ε). This describes Cerenkov radiation.

Making further approximations to emphasise the dependence on velocity, we have

$$R_x \simeq \frac{2c}{\omega}\left(\frac{1}{\gamma^2} + \psi^2 + \xi^2\right)^{-1} \tag{10}$$

where we have taken ψ small, $\gamma = (1 - \beta^2)^{-1/2}$ large and $\varepsilon = 1 - \xi^2$. This formula is the same as the expression for the 'formation zone' discussed by Garibyan[14] for transition radiation. It shows that the range of virtual photons increases with γ until γ is of order ξ^{-1}, where for high frequencies $\xi^{-1} \simeq \hbar\omega$/plasma energy. So again we expect the relativistic rise to give way to the Fermi plateau region when

$$\gamma \sim \frac{\text{ionisation energy}}{\text{plasma energy}} \tag{11}$$

This suggests that the largest relativistic rise will be seen in gases because of their low plasma energies, especially those with high Z, for which the ionisation potentials increase faster than the plasma energy. Further, of those with similar numbers of electrons, the rare gases with the

tightest binding will show the largest rise. In addition different electron shells will saturate at different values of γ and calculations should take account of this. In particular if measurements are made which effectively exclude the contribution from inner electrons - such as the most probable ionisation loss in thin gas counters - the relativistic rise will be less than conventional calculations might suggest.

4. The Model

Following Fano[15] we start by considering the differential cross section per atomic electron for the inelastic collision of an isolated atom with the incident particle according to the Born approximation:

$$\frac{d^2\sigma}{dQdE} = \frac{2\pi e^4}{mv^2} \left\{ \frac{|F(E,q)|^2}{Q^2} + \frac{|\beta_t . G(E,q)|^2}{(Q^2 - E^2/_{2mc^2})^2} \right\} \qquad (12)$$

where $v = \beta c$ is the incident particle velocity,

$Q = h^2q^2/_{2m}$ and m is the electron mass

F and G are inelastic form factors discussed by Fano[15]. We have dropped some terms in Q/mc^2 which are only important for large energy losses and are consequently of no interest when considering thin absorbers.

The first term represents the interaction of charges and as such is essentially constant in the relativistic region. It describes ionisation due to the absorption of longitudinal virtual photons. These photons have a range $\sim 1/q$ as in the static coulomb field hence the denominator Q^2. The second term is the current-current term involving the exchange of transverse virtual photons. These two terms add incoherently because they involve transitions to final states of opposite parity.

When q is small, dipole transitions will predominate and we can follow Fano[15] by approximating:

$$|F(E,q)|^2\, dE = \left(Q/E\right) f(E)\, dE \tag{13}$$

and $$|\underline{\beta}_t . \underline{G}(E,q)|^2\, dE = \beta_t{}^2 f(E)\, dE\; E/2mc^2 \tag{14}$$

where $f(E)dE$ is the optical dipole oscillator strength. The definition of small q in this respect is

$$q < (\text{electron orbital size})^{-1},$$

which is essentially: $Q < E_i$, where E_i is the electron binding energy.

The longitudinal term is evaluated in two different regions:

(1) Low Q, i.e. $Q < E_i$ with dipole approximation and the choice $f(E) = \delta(E-E_i)$ so

$$|F(E,q)|^2\, dE = (Q/E_i)\delta(E-E_i)\, dE \tag{15}$$

This choice satisfies the sum rule $\int E|F|^2 dE = Q$

(2) High Q, i.e. $Q > E_i$ with impulse or free electron approximation

$$|F(E,q)|^2 dE = \delta(E-Q)\, dE \tag{16}$$

which also satisfies the sum rule.

Taking these two together and integrating over Q we get

$$\frac{d\sigma_L}{dE} = \frac{2\pi e^4}{mv^2}\; \delta\left(\frac{E-E_i}{E_i}\right)\; \log \frac{2mv^2}{E_i} \quad \text{for } E \lesssim E_i \text{ and } \log \frac{2mv^2}{E_i} \tag{17}$$

$$\frac{d\sigma_L}{dE} = \frac{2\pi e^4}{mv^2}\; \frac{1}{E^2} \quad \text{for } E > E_i. \tag{18}$$

The latter being of course the Rutherford cross-section.

There are two important points here. The first is that our crude approximations satisfy the sum rule, are consistent with the longitudinal part of the Bethe Bloch formula for the mean energy loss[9] and incorporate some not too implausible low energy behaviour. The second is that, by using the sum rule to integrate over energy, traditional calculations avoid having to make some of our crude assumptions. We are unable to do this since an energy integration is inappropriate when the discrete energy loss collisions

are few. This integration must be deferred to the end of our calculation and be carried out as a Monte Carlo process using the spectrum of energy loss probabilities.

The transverse term only contributes significantly in the low Q region[15] and may therefore be evaluated in the dipole approximation. If ψ is the angle between the virtual photon direction and the particle momentum, we have

$$\beta_t^2 = \beta^2 \sin^2 \psi \text{ and } Q = E^2/2mv^2 \cos^2\psi$$

Substituting we get [15]

$$\frac{d^2\sigma}{dE} = \frac{2\pi e^4}{Emv^2} \frac{\sin^2\psi f(E) d(\cos^2\psi)}{(1/\beta^2 - \cos^2\psi)^2} \tag{19}$$

This formula applies to an electron of an isolated atom rather than one in a medium - i.e. in the approximation $\varepsilon = 1$. To see how it is to be modified we refer back to equation 9. The denominator there contains a $\sqrt{\varepsilon}$ factor and a similar denominator appears in equation 19 representing the effect of the finite range or propagator of the virtual photon. Instead of equation 19 we write:

$$\frac{d^2\sigma}{dE} = \frac{2\pi e^4}{Emv^2} \frac{\sin^2\psi \; f(E) \; d(\cos^2\psi)}{(1/\beta^2 - \varepsilon\cos^2\psi)^2} \tag{20}$$

which is related to the formula given by Fano[15]. Further evaluation is simplified by the observation[16] that

$$f(E) = \frac{m\omega}{2\pi^2 e^2 N} \int m(\varepsilon(\omega)) \tag{21}$$

where N is the electron density.

$$\frac{d^2\sigma}{dE} = \frac{e^2\omega}{E\pi mv^2 N} \left[\int m\varepsilon(\omega)\right] \frac{\sin^2\psi \; d(\cos^2\psi)}{|1/\beta^2 - \varepsilon(\omega) \cos^2\psi|^2} \tag{22}$$

$$\frac{d\sigma}{dE} = \frac{e^2}{\pi\hbar^2 v^2 N} \left\{ \frac{\varepsilon_2}{|\varepsilon|^2} \log \left[(1-\beta^2\varepsilon_1)^2 + \beta^4\varepsilon_2^2\right]^{-1/2} + \left[\beta^2 - \frac{\varepsilon_1}{|\varepsilon|^2}\right] \arctan \frac{\beta^2\varepsilon_2}{1-\beta^2\varepsilon_1} \right\} \tag{23}$$

by integrating $\cos^2\psi$ from 0 to 1 and taking $\mathcal{E} = \mathcal{E}_1 + j\mathcal{E}_2$.

For ε we use

$$\varepsilon = 1 + \omega_p^2 \sum_i \frac{f_i}{E_{i/\hbar}^2 - \omega^2 - j\gamma_i\omega} \tag{24}$$

where we take $\gamma_i = E_i$†. γ_i is the "width" of the effective ionisation level which takes account of the finite kinetic energy of the electron in the continuum on the one hand and energy loss through excitation levels on the other. This is crude but it is a significant improvement over the use of a mean ionisation potential.

5. Results of Calculations

We have calculated[17] the energy loss spectra in 1.5 cms of gas at NTP at values of p/mc from 2 to 2000 in powers of 2 and also 5×10^4. For each gas or gas mixture a knowledge of the atomic levels E_i and the plasma frequency were sufficient to determine the different parts of the cross-section according to the model described in the previous section. The results are only weakly dependent on the values of E_i used. These are shown in Table I and are taken from Sternheimer (1952)[6]. A simple Monte Carlo calculation then gave the differential energy loss distribution in 1.5 cms of gas. The full curve in Fig. 2 shows the result for 3 GeV/c pions in argon[9]. The agreement with the data is significantly better than for the Landau and Bunck and Leisegang models. By plotting the peak of the Monte Carlo energy loss distribution as a function of p/mc, a prediction for the relativistic rise is obtained

† The results of calculations are essentially unaffected by other choices e.g. $\gamma_i = 0.2\ E_i$.

which is also in better agreement with available data. This is shown as curve II on Fig. 1. Of course different experiments use different gas mixtures, sample thicknesses and methods of estimating the peak or most probable ionisation loss. We defer to paper II[18] a comparison of the model with new data where these effects are treated in detail. However, neither in the case of the old data nor in the case of the new is there any indication of a real discrepancy with the model.

Next we use the model to discuss the use of the relativistic rise in different gases for identifying particles of known momentum. As discussed elsewhere[2], the combined effect of the slow rise giving little difference between masses and the broad energy loss spectrum giving poor resolution is to require more than 100 energy-loss measurements on each track if individual pions, kaons and protons are to be distinguished. In a second Monte Carlo program we have simulated such a multiple sampling device and studied the mass resolution that may be derived from the measurements on a single track. The larger and less probable measurements (the Landau tail) contain little information and only serve to degrade the variance of the smaller more probable measurements. Traditionally the peak of the distribution, the most probable energy-loss, is used but this is notoriously hard to estimate with small statistics. It has been shown[5] that the resolution is close to optimum if a fixed fraction of the measurements (20-50% of the largest) is discarded and the mean of the remainder is used as the estimator. This is the method we have used. Fig. 3a shows how the resolution of 330 x 1.5 cms samples of argon varies as a function of this cut. Both this resolution and the corresponding relativistic rise are rather insensitive to the size of this cut - in fact according to the calculations the rise is only 3-5% larger with a 50% cut than a 10% cut. In all of the following results we have used a 40% cut.

In Fig. 3b we show how the resolution behaves as a function of number of samples and device length. Typically a 5m device with 1.5 cms samples is

TABLE I

ATOMIC DATA USED IN CALCULATIONS

	Helium	Neon	Argon	Krypton	Xenon	Methane	Ammonia	Nitrogen	Carbon Dioxide
Plasma energy	0.272	0.609	0.816	1.156	1.414	0.609	0.609	0.721	0.902
Binding energies (eV) and electrons per molecule	24.5(2)	870 (2) 54.4(8)	3196 (2) 294 (8) 39.5(8)	14280 (2) 1754 (8) 152 (18) 39.4(8)	34612 (2) 5073 (8) 831 (18) 169 (18) 25.8(8)	313 (2) 55.8(2) 17.7(2) 13.6(4)	412 (2) 47.6(2) 31.3(3) 13.6(3)	412 (4) 47.6(4) 31.3(6)	313 (2) 55.8(2) 17.7(2) 575 (4) 54.4(4) 39.4(8)

Argon/20% Co_2 Plasma energy = 0.834eV

He/50% Ne Plasma energy = 0.472eV

Atomic data from Sternheimer (1952) Ref. 6. Chemical effects neglected.

comparable to a 7m device with 3 cms samples. There is no easy cheap way to get the required resolution (5-6%). A device of several metres depth and several hundred samples is needed. In the real world there are systematic effects also. Fig. 3c shows the effect of a small amount of nearest neighbour inter-sample crosstalk as simulated by the Monte Carlo program. The effect on the resolution is small. These problems are discussed at greater length in paper II[18]. In the following analysis we are concerned primarily with the efficacy of different gases and therefore restrict our calculations to a 5m device yielding 330 x 1.5 cms samples and ignore possible systematic effects.

Fig. 4a shows the response* expected from such a device filled with argon and exposed to a mixture of pions, kaons and protons at 25 GeV/c in the ratio 10:1:1. In this case we can identify particles with good confidence. At 60 GeV/c on the other hand the separation is marginal as shown in Fig. 4b. An optimum cut between kaons and pions would result in a loss of about 10% of kaons into the pion peak and the same number of pions misidentified as kaons. In order to make a definitive comparison between different gases we have calculated at what momentum the kaon/pion separation is 90% pure in the above sense.

For each gas and value of $^{P}/_{mc}$ in turn we generated an energy loss distribution appropriate to 1.5 cms of gas at NTP (20000 points). In the second Monte Carlo program we simulated 2000 traversals of the detector described above. Some of the results are given in Table II. We estimate that the statistical inaccuracies on these results are less than 1%. For reference we have also calculated the value of the most probable ionisation loss.

* The "response" is the mean of the 60% smallest signals discussed above.

The full results will be available elsewhere[17].

The rare gases are treated in the first section of Table II. In spite of a big increase in the energy loss with atomic number the resolution is essentially constant at around 5%. The relativistic rise on the other hand increases from 40% to 70%. This is due to the binding energy which is increasing faster than the plasma frequency (see section 3). The kaon/pion separation limit which is 55-60 GeV/c for argon and krypton is 95 GeV/c for pure xenon. (The lower limit for K/π separation is 1.8 GeV/c for all gases.)

The second group in Table II compares the first chemical period gases methane, ammonia, neon and nitrogen*. The first three of these all have the same plasma frequency. They show that as the binding energy increases, so does the relativistic rise, while the mean energy loss gets smaller. There is also an improved resolution when the binding energy is smaller due to the increased statistics of small energy-loss collisions. However, these have a small contribution to the rise and therefore the K/π separation limit is still worse for methane and ammonia than neon.

The third section of Table II shows how gas mixtures behave. The argon-carbon dioxide system is the example. It shows that the addition of small quantities of a low Z quenching gas has a small effect. The ionisation of gas mixtures is essentially additive in the Born approximation except for the modification due to the dielectric constant.

In the last section of Table II we show figures for the total ionisation cross-section in the form of the number of ionising collisions per metre of gas ("primary ionisation"). Davidenko[19] has proposed that particles could be identified by measuring their primary ionisation in a streamer chamber operating in the avalanche mode. The resolution of such a technique would be limited under ideal conditions by Poisson statistics. In Table II we assume such a limit and calculate the K/π separation limit discussed above for

---

* We ignore all chemical effects.

TABLE II

CALCULATIONS OF dE/dx for 1.5 cms OF GAS AT NTP

	Truncated mean ionisation loss (eV)					Resolution of mean (FWHM)		Relativistic Rise	K/Π limit GeV/c	Most probable ionisation loss (eV)					Relativistic Rise
$P/_{mc}$	4	32	128	512	$5x10^4$	4	5.10^4			4	32	128	512	$5x10^4$	
RARE:															
Helium	254	298	342	358	359	5.2%	4.9%	1.41	45	275	325	372	389	390	1.42
Neon	1115	1359	1583	1696	1714	5.4%	5.1%	1.54	50	1117	1380	1616	1724	1760	1.58
Argon	1961	2408	2783	2995	3095	5.3%	4.8%	1.58	55	2062	2495	2891	3103	3168	1.54
Krypton	3886	4788	5546	5978	6199	5.2%	4.7%	1.60	55	3921	4905	5699	6156	6365	1.62
Xenon	5323	6655	7734	8581	9025	5.5%	5.0%	1.70	95	5339	6704	7878	8726	9242	1.73
FIRST PERIOD:															
Methane	1417	1685	1851	1918	1922	3.9%	3.9%	1.36	30	1459	1744	1916	1988	1992	1.37
Ammonia	1356	1615	1797	1876	1889	4.2%	4.1%	1.39	45	1390	1664	1855	1936	1970	1.42
Neon	1115	1359	1583	1696	1714	5.4%	5.1%	1.54	50	1117	1380	1616	1724	1760	1.58
Nitrogen	1778	2154	2452	2568	2636	4.6%	4.1%	1.48	45	1858	2255	2570	2703	2743	1.48
MIXTURES:															
Argon	1961	2408	2783	2995	3095	5.3%	4.8%	1.58	55	2062	2495	2891	3103	3168	1.54
Argon/20% Co_2	2152	2633	3022	3227	3325	4.9%	4.5%	1.55	55	2244	2713	3096	3363	3404	1.52
Carbondioxide	2915	3523	3969	4167	4226	3.9%	3.7%	1.45	50	3014	3668	4110	4354	4394	1.46
	Number of Collisions/metre														
PRIMARY IONISATION:															
Argon/20% Co_2	2457	2915	3370	3486	3497	2.1%	1.8%	1.42	65						
He/50% Ne	1050	1242	1442	1544	1545	3.3%	2.6%	1.47	85						

For both dE/dx and primary ionisation the quoted resolutions and separations refer to a 5 metre track length.

a helium/neon mixture and an argon/CO_2 mixture. The relativistic rise is smaller due to the equal weighting of large and small energy-loss collisions. In dE/dx measurements on the other hand the large energy loss collisions which show the larger relativistic rise are weighted more than the small energy loss collisions. On the other hand the ideal resolution is much better than in dE/dx measurements although there are major technical difficulties in achieving this.

Finally, we note that there is no discernible difference between the relativistic rise of the most probable and the truncated mean ionisation. This is related to the fact that the shape of the energy loss distribution does not appear to change much as a function of p/mc. Fig. 5 shows a few of the calculated relativistic rise curves.

Conclusion

The discrepancy between theoretical predictions and experimental results for the energy-loss in thin gas samples seems to be resolved. Simple qualitative pictures and detailed quantitative calculations together give insight into the mechanism of the relativistic increase of ionisation loss and its saturation at the highest velocities. These calculations give agreement with existing data and show quantitatively the efficacy of different gases for measuring velocities or identifying charged particles of known momentum. Argon is both effective, practical and cheap. Xenon is the only gas examined which is more effective, achieving this especially over a 5 metre track length.

488-51

REFERENCES

1. J.D. Jackson "Classical Electrodynamics" (Wiley) Ch. 13.
   A. Crispin and G.N. Fowler, Rev. Mod. Phys. 42 290 (1970).

2. W.W.M. Allison et al., NIM 119 499 (1974)

3. F. Harris et al., NIM 107 413 (1973)

4. P.V. Ramana Murthy, NIM 63, 77 (1968).

5. D. Jeanne et al., NIM 111, 287 (1973)
   M. Aderholz et al., NIM 118, 419 (1974).

6. R.M. Sternheimer and R.F. Peierls, Phys. Rev. B3, 3681 (1971).
   R.M. Sternheimer, Phys. Rev. 88, 851 (1952).

7. Z. Dimcouski et al., NIM 94, 151 (1971).

8. A.V. Alakoz et al., NIM 124, 41 (1975).

9. J.H. Cobb, D. Phil. thesis (Univ. of Oxford) 1975. Available from Rutherford as HEP/T/55.

10. L. Landau, J. Phys. (USSR) 8, 201 (1944)

11. G. Knop et al., Zeit. für Phys. 165, 533 (1961).

12. O. Blunck and S. Leisegang, Zeit. für Phys. 128, 500 (1950)

13. K.A. Ispiryan et al., NIM 117, 125 (1974).

14. G.M. Garibyan, Yerevan Report: "Theoretical Foundations of Transition Radiation", (1970).

    See also L. Durand, Phys. Rev. D11, 89 (1975).

15. U. Fano, Ann. Rev. Nucl. Sci. 13, 1 (1963).

16. L. Landau and E. Lifshitz "Electrodynamics of Continuous Media", Ch. 62 equation 13.

17. J.N. Bunch D.Phil. thesis (Univ. of Oxford). In preparation.

18. The Ionisation Loss of Relativistic Charged Particles in Thin Gas Samples and its Use for Particle Identification: II Experimental Results. (following paper). W.W.M. Allison et al.

19. V.A. Davidenko, NIM, 67 325 (1969).

FIGURE CAPTIONS

Fig. 1

Calculations and measurements of the relativistic rise of energy loss in argon filled proportional chambers.
Curve I is based on the method of Sternheimer (1971) ref. 6.
Curve II is based on the method described in this paper.

Fig. 2

A histogram of a typical pulse height distribution from a thin proportional chamber. The smooth curve is based on the model described in this paper and Ref. 9. It does not include any instrumental or resolution effects.

Fig. 3

The dependence of ionisation resolution on various parameters of a multiple sampling technique as found in Monte Carlo studies:

(a) Fraction of samples rejected by cut to remove the Landau tail (see text).

(b) Device length and sample size.

(c) Nearest neighbour intersample cross-talk.

Fig. 4

Ideal response of a 5 metre detector to a mixture of π, K and protons in flux ratio 10:1:1.

(a) shows the separation at 25 GeV/c

(b) shows the separation at 60 GeV/c. This is very close to the case described as "90% separation" (see text).

Fig. 5

Plots of the calculated ionisation loss for some interesting cases

Fig. 1

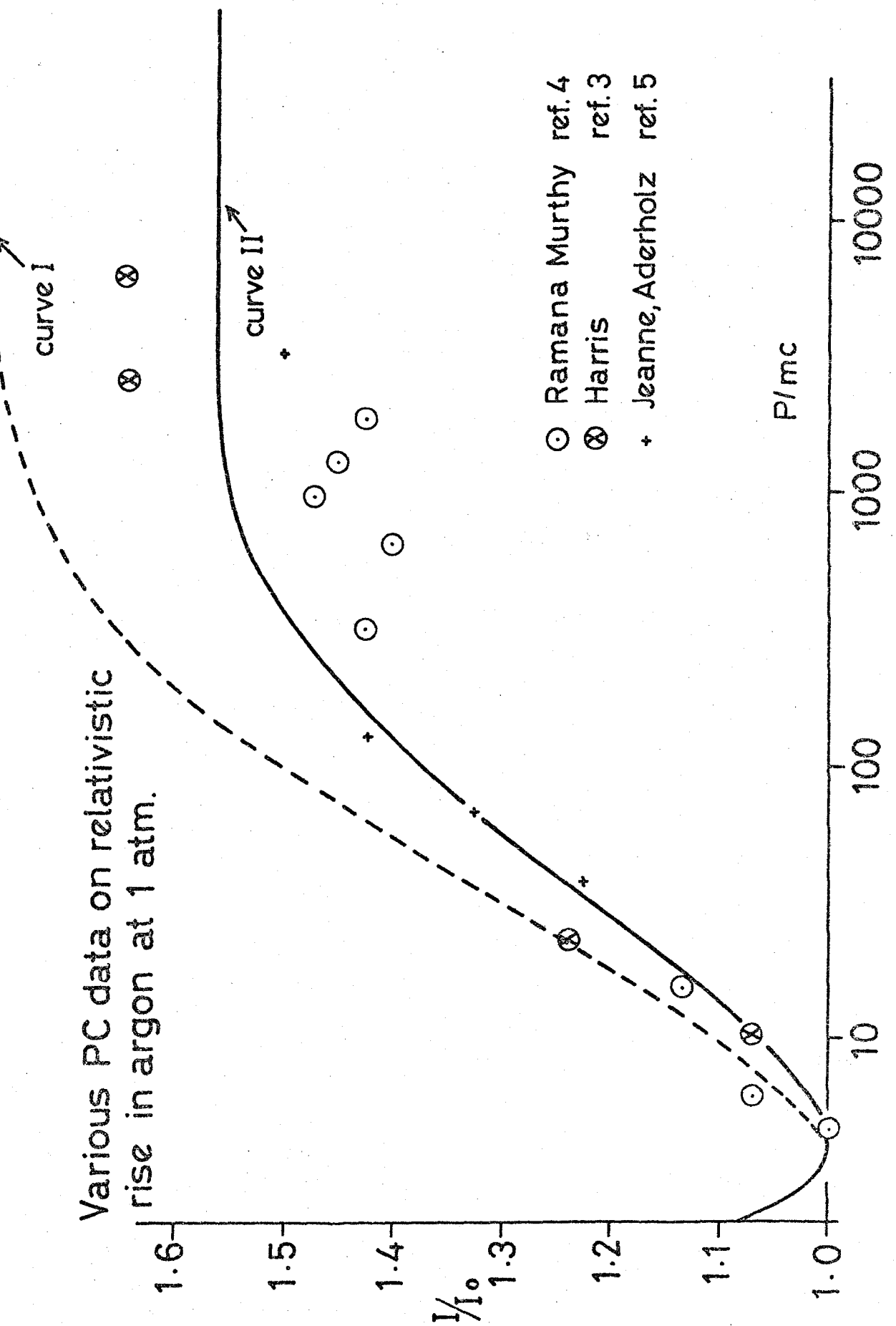
Various PC data on relativistic rise in argon at 1 atm.
curve I
curve II
Ramana Murthy ref. 4
Harris ref. 3
Jeanne, Aderholz ref. 5
I/I₀
P/mc
1.0
1.1
1.2
1.3
1.4
1.5
1.6
10
100
1000
10000

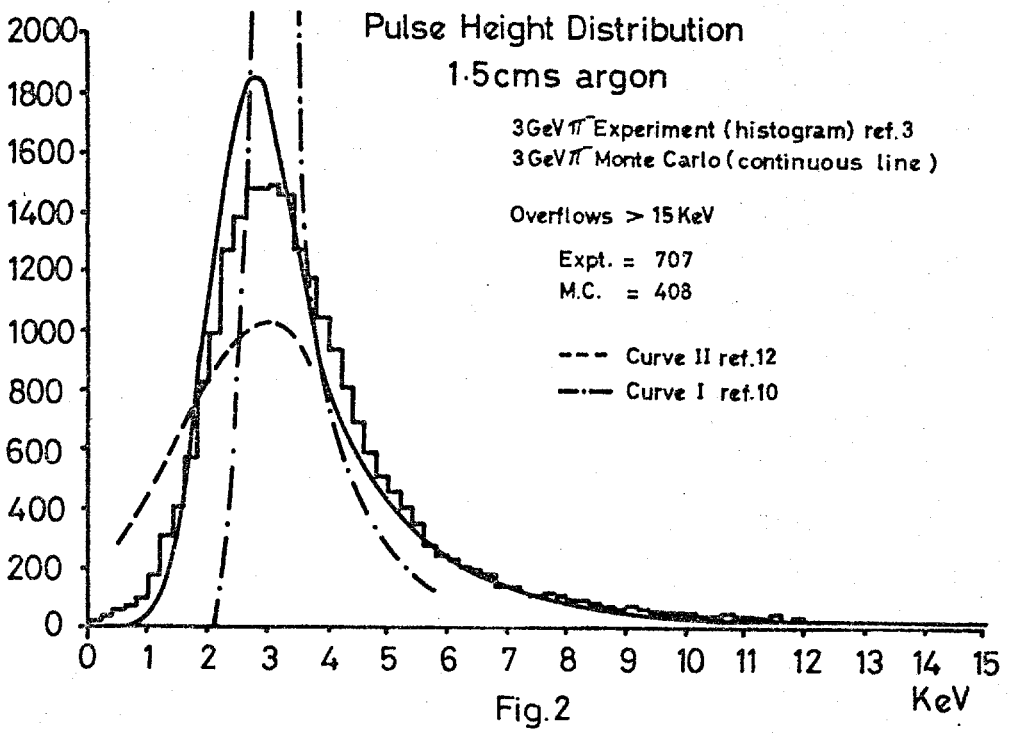
Pulse Height Distribution
1·5cms argon
3GeV π⁻ Experiment (histogram) ref.3
3GeV π⁻ Monte Carlo (continuous line)
Overflows > 15KeV
Expt. = 707
M.C. = 408
Curve II ref.12
Curve I ref.10
2000
1800
1600
1400
1200
1000
800
600
400
200
0
0 1 2 3 4 5 6 7 8 9 10 11 12 13 14 15
KeV

Fig.2

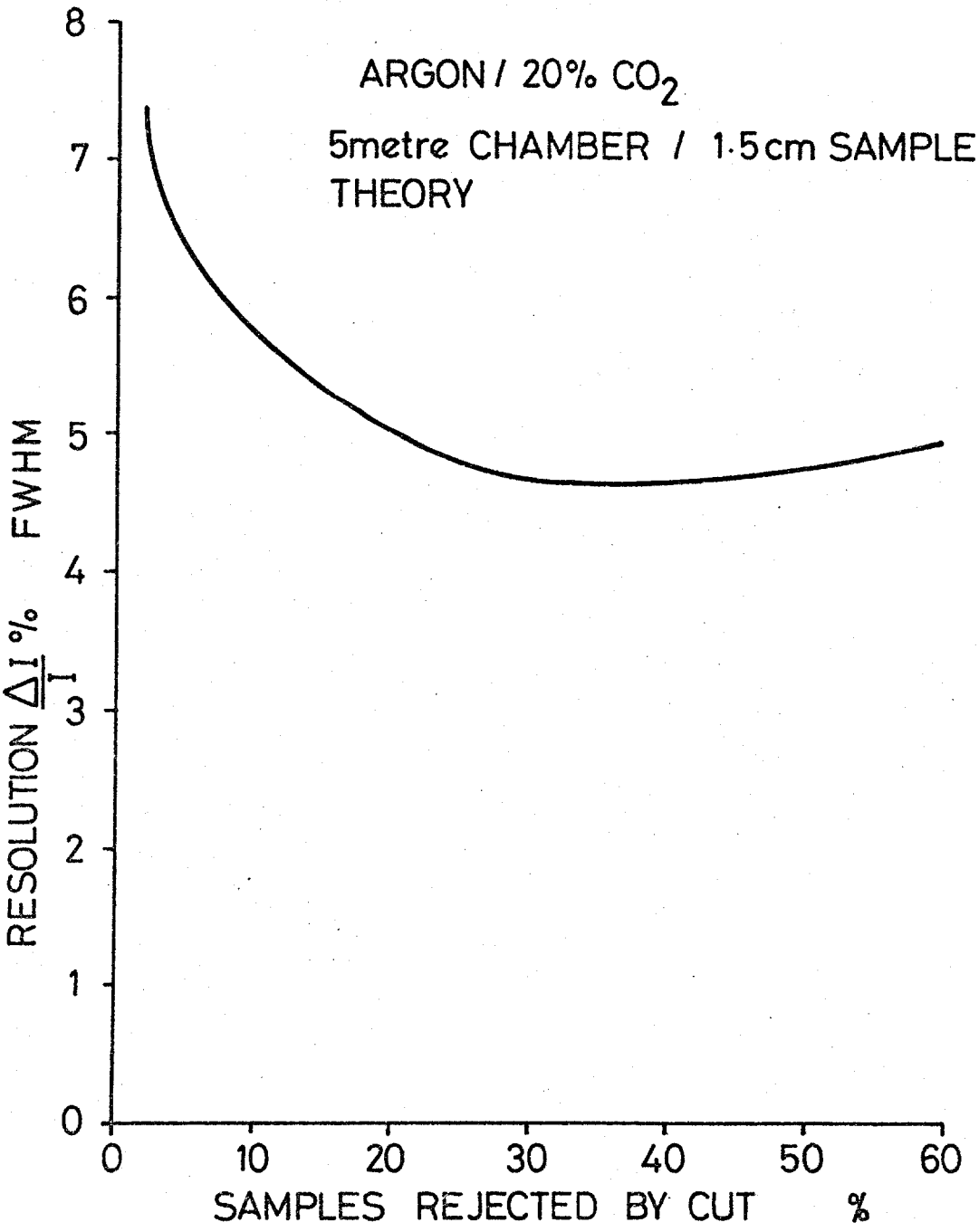
ARGON / 20% CO_2
5metre CHAMBER / 1·5cm SAMPLE
THEORY
RESOLUTION $\frac{\Delta I}{I}$ % FWHM
0
1
2
3
4
5
6
7
8
0
10
20
30
40
50
60
SAMPLES REJECTED BY CUT %

Fig. 3a

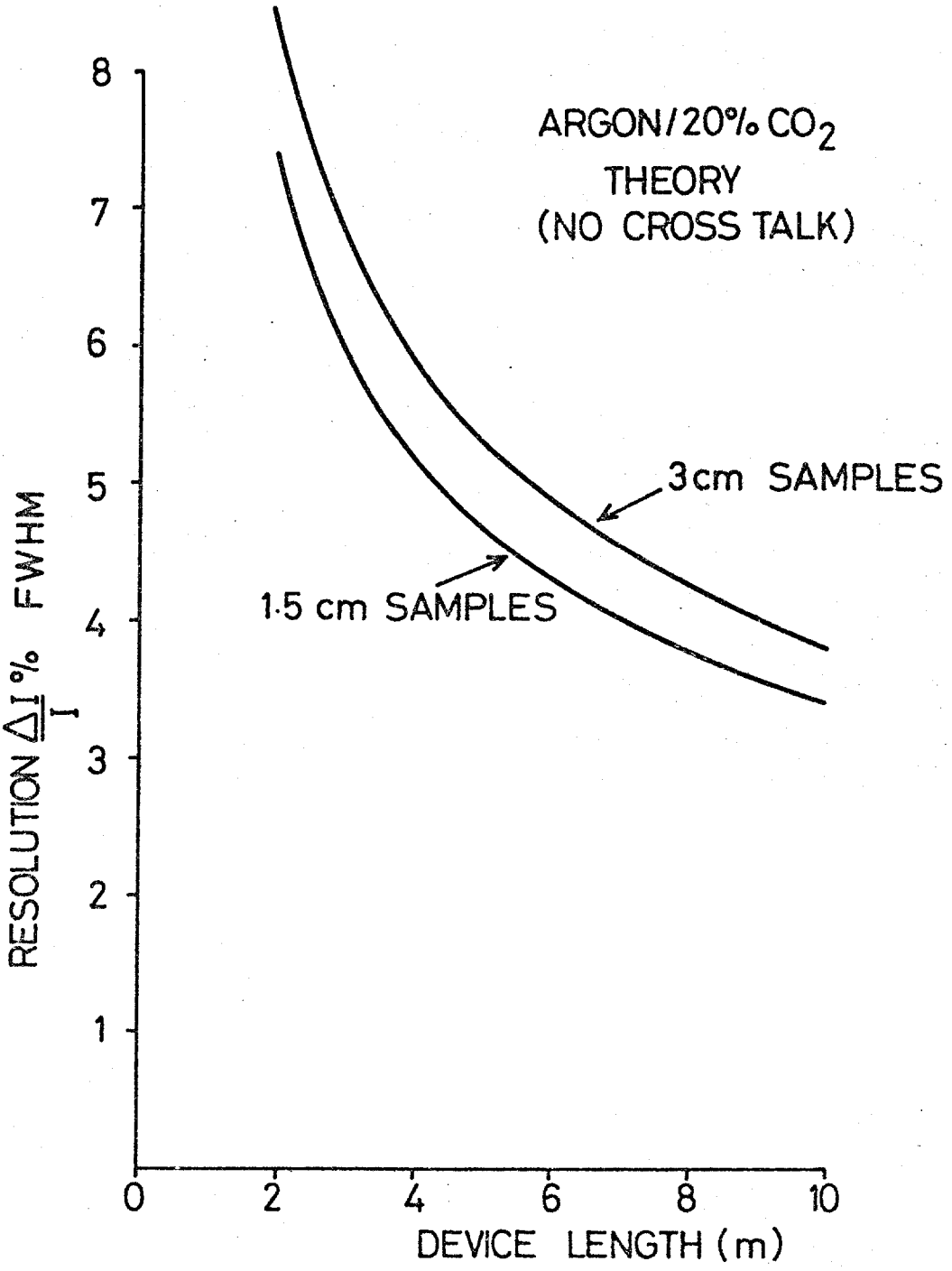
ARGON/20% CO_2
THEORY
(NO CROSS TALK)
3cm SAMPLES
1·5 cm SAMPLES
RESOLUTION $\frac{\Delta I}{I}$ % FWHM
8
7
6
5
4
3
2
1
0
2
4
6
8
10
DEVICE LENGTH (m)

Fig. 3b

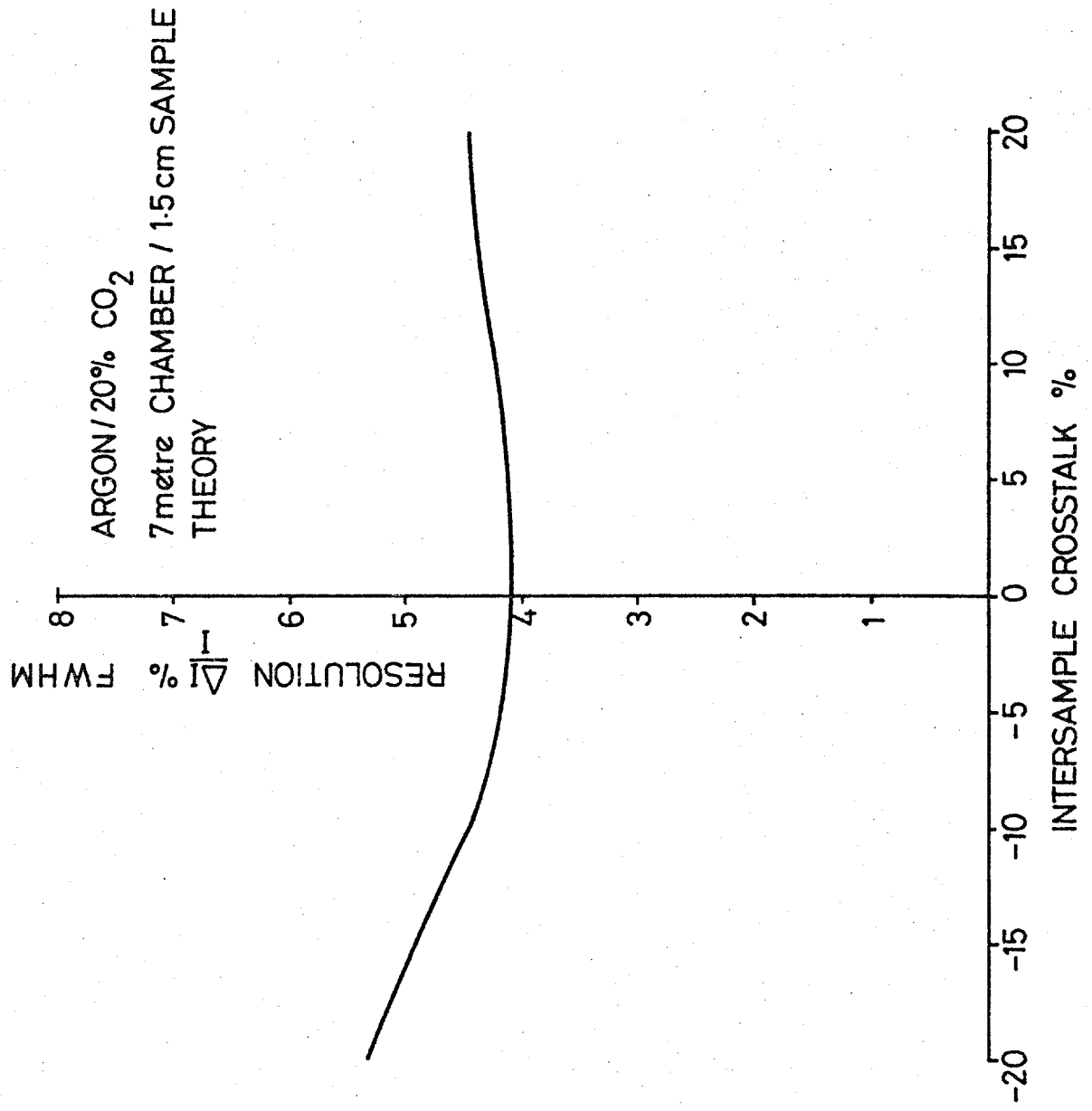
ARGON/20% CO_2
7 metre CHAMBER / 1·5 cm SAMPLE
THEORY
RESOLUTION $\frac{\Delta I}{I}$ % FWHM
8
7
6
5
4
3
2
1
-20
-15
-10
-5
0
5
10
15
20
INTERSAMPLE CROSSTALK %

Fig. 3c

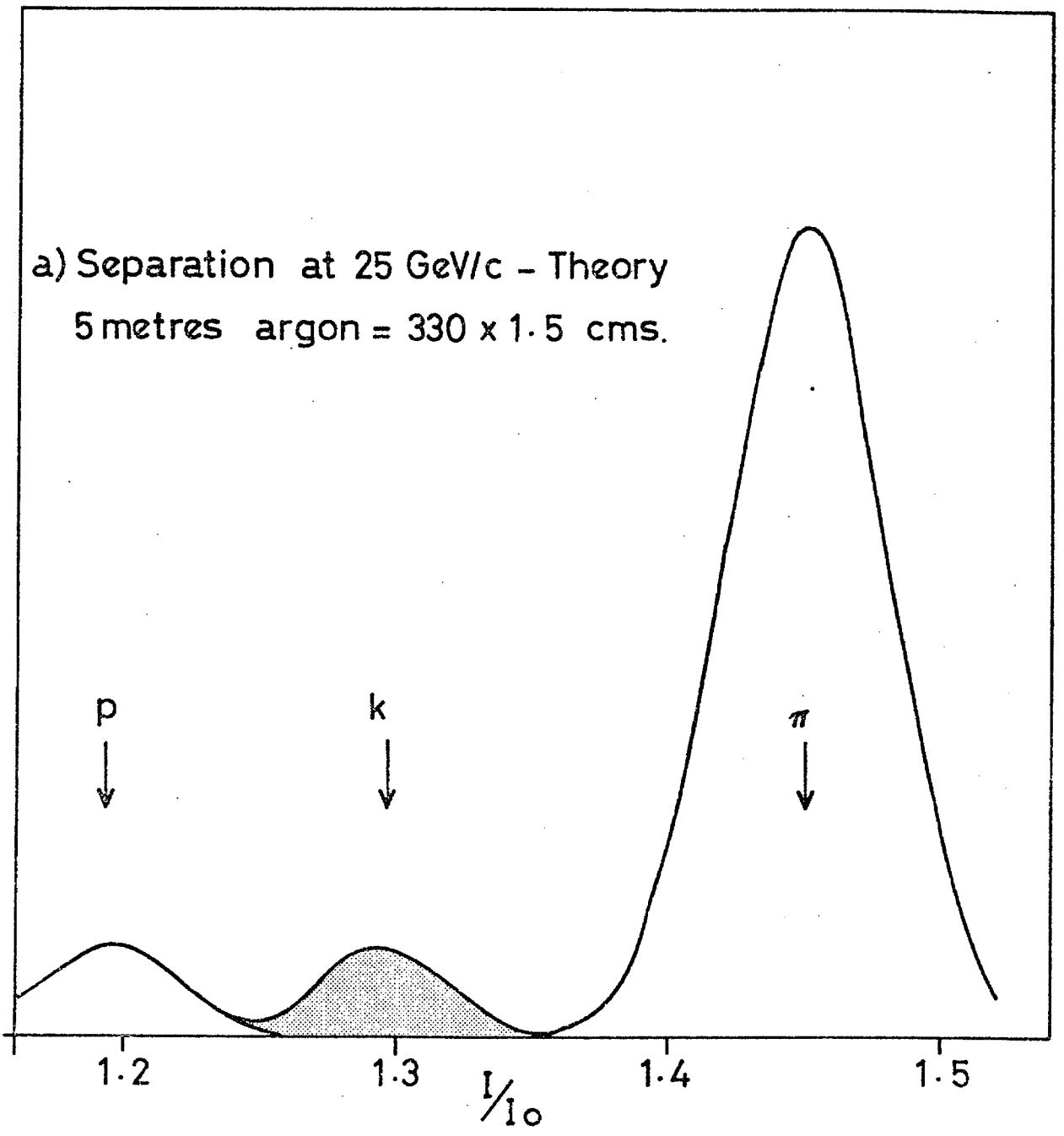
a) Separation at 25 GeV/c - Theory
5 metres argon = 330 x 1·5 cms.
p
k
π
1·2
1·3
1·4
1·5
I/Io

Fig. 4a

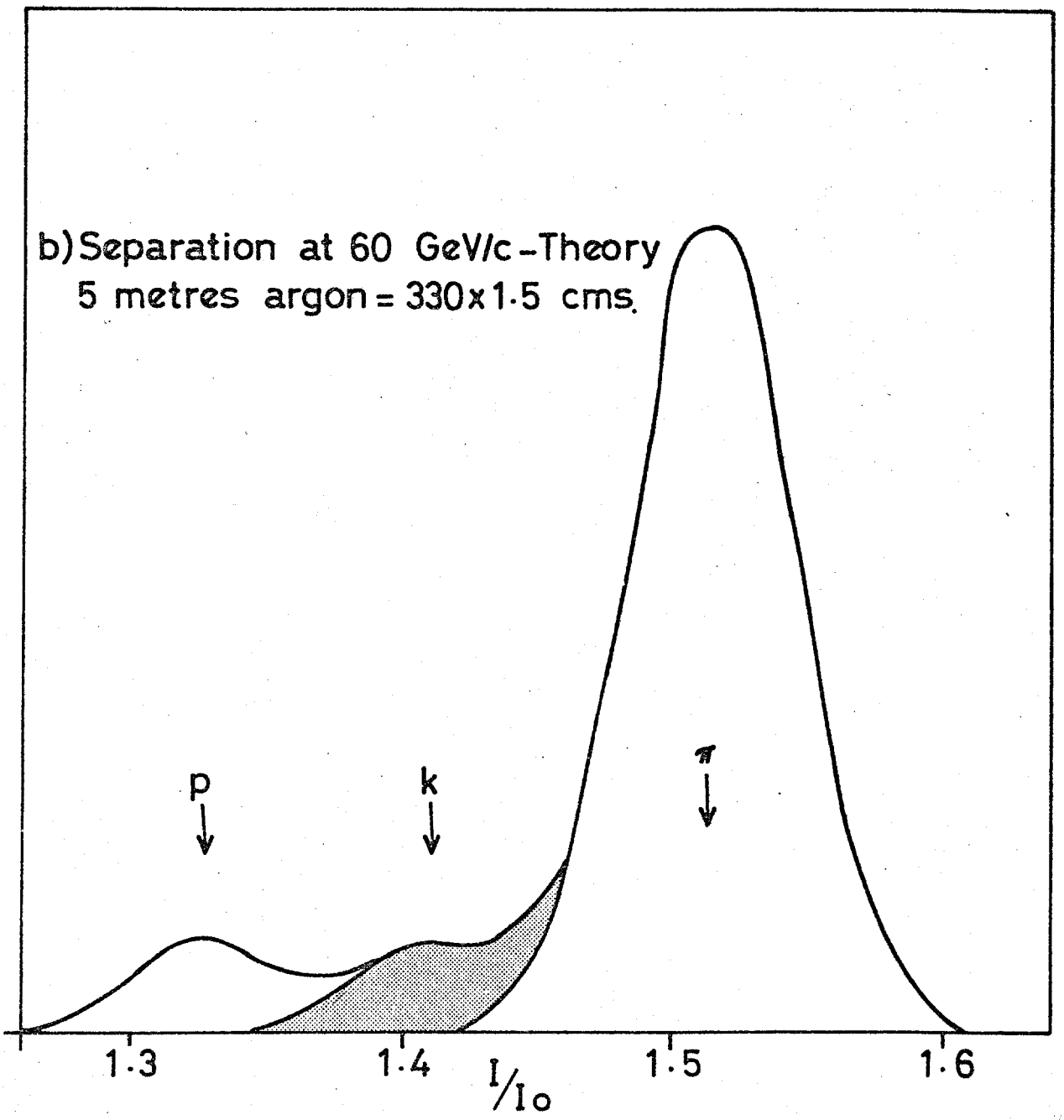
b) Separation at 60 GeV/c - Theory
5 metres argon = 330 x 1·5 cms.
p
k
π
1·3
1·4
1·5
1·6
I/Io

Fig. 4b

Fig.5

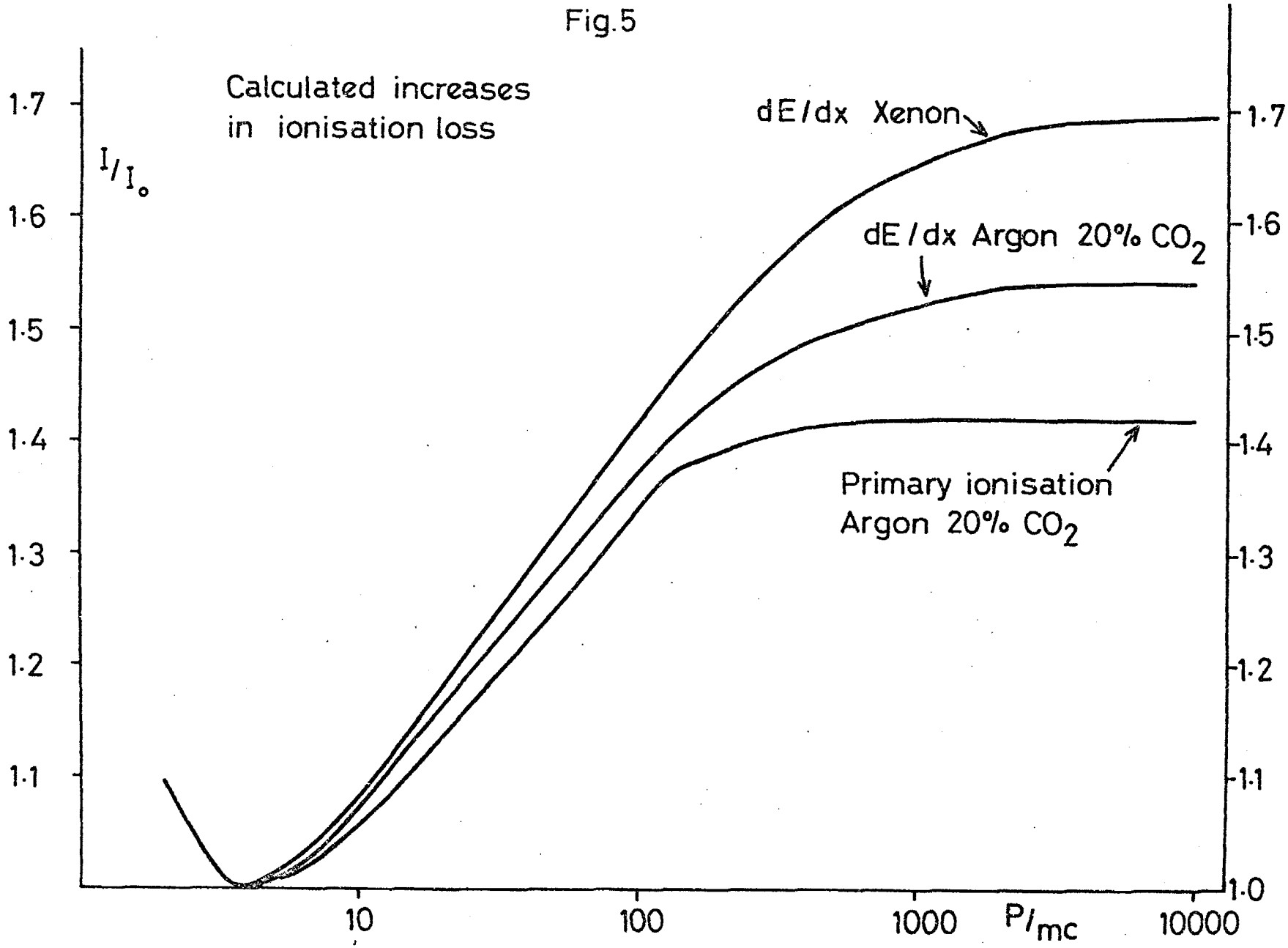
Calculated increases
in ionisation loss
I/I₀
dE/dx Xenon
dE/dx Argon 20% CO₂
Primary ionisation
Argon 20% CO₂
1·7
1·6
1·5
1·4
1·3
1·2
1·1
1·0
10
100
1000
P/mc
10000

THE IONISATION LOSS OF RELATIVISTIC CHARGED PARTICLES IN THIN GAS SAMPLES AND ITS USE FOR PARTICLE IDENTIFICATION: II EXPERIMENTAL RESULTS

W.W.M. Allison, C.B. Brooks, J.N. Bunch, R.W. Pleming

Nuclear Physics Laboratory, Oxford.

R.K. Yamamoto, Massachusetts Institute of Technology, Cambridge, Massachusetts.

(Submitted for Publication in Nuclear Instruments and Methods.)

ABSTRACT

We present the results of an experiment in which a proportional chamber samples the ionisation loss of each incident relativistic particle some 60 times. The chamber, filled with 80% argon/20% CO_2 was exposed to a beam of pions, protons and electrons at momenta between 25 GeV/c and 150 GeV/c at the Fermi National Accelerator Laboratory. The observed pulse height spectra were corrected for systematic effects and compared with new Monte Carlo theoretical calculations discussed in paper I. The agreement is good. The relativistic rise is sufficient to enable individual pions and protons to be distinguished even with the present apparatus. Our results suggest that with a larger device kaons, pions and protons may be separated.

1. INTRODUCTION

In paper I[1] we reviewed the apparent discrepancy between theoretical and experimental results on the ionisation loss of relativistic charged particles in thin gas samples. We showed how using a more appropriate Monte Carlo calculation the discrepancy between theory and experiment could be resolved.

In this paper we present new experimental results which confirm the agreement between theory and earlier experiments and also demonstrate that individual particles of known momentum may be identified by their ionisation loss even using raw data. Particular attention is paid to systematic effects and calibration problems that could affect the predicted performance of a larger device[2].

In section 2 we describe the apparatus and in section 3 the energy calibration and factors affecting it. In section 4 we analyse the inter-channel correlation which is shown to be instrumental and to dominate the other sources of error in this case. Section 5 includes the experimental results and the comparison with theory.

2. THE APPARATUS

The experimental layout and chamber are shown in Fig. 1. The chamber was positioned downstream of a differential Cerenkov counter in the N3 beam line at the Fermi National Accelerator Laboratory. The tagged beam particles passed through the 120 cms long chamber parallel to a wire plane as shown in Fig. 1. This plane was sandwiched between two drift electrodes 7 cms apart and the whole mounted in a gas tight box which was flushed continuously with 80% argon/ 20% CO_2*. The ionisation electrons liberated by the incident particle are shown

---

* The gas mixture was chosen because of its convenience, large relativistic rise (Ref. 1) and properties as a drift chamber gas (Ref. 2,3).

symbolically as a row of dots in Fig. 1b drifting without amplification towards the central wire plane. The latter consists of pairs of 25μ diameter anode wires each separated by 250μ cathode wires to reduce capacitative cross coupling and to control the gas amplification. Each pair of anode wires collects and amplifies the electrons from 1.5 cms of gas and each such pulse is further amplified and integrated as discussed below. There were 60 such channels so that each particle traversing the detector yielded 60 pulse heights.

To achieve accurate spacing the wires were held in slots melted in perspex with a hot blade. The signal wires were connected in pairs to the input of the low impedance (20Ω) current sensitive preamplifiers, where typical signal amplitudes were a few μamps. The gas temperature and pressure were measured and recorded continuously by probes mounted in the box. In addition an Fe^{55} X-ray source was exposed between accelerator cycles to measure variations of the gas gain. It was placed in its shutter box above the chamber and shone through the aluminised mylar window of the gas box and through the upper foil drift electrode into the active region of the chamber. Typical counting rates were 20-30 per second. To calibrate the gain of the electronics, test pulses were sent to all channels in parallel from a current source.

The signals were carried from the preamplifiers to the receiver amplifiers in the control room by woven cables of balanced pairs. In the receiver amplifier units discriminator logic allowed the generation of self-triggers singly on a particular channel (for the X-ray source) or in coincidence between two chosen channels for beam particles. In addition each of the analogue signals was delayed by 200 nsecs and shaped to remove the long tail due to positive ion motion.[4] These signals were integrated in Lecroy 8-bit ADC channels with a 500 nsec gate to provide a pulse integral relatively insensitive to input pulse shape and trigger jitter. The ADC gate was triggered by the 2-channel coincidence occurring within the drift time (1 μsec) of a coincidence between the scintillator telescope (S1S2S3) and the particle identification signature required from the

differential Cerenkov counter. Triggers occurring within 2 μsecs of another S1S2S3 coincidence were rejected. The 500 nsec integration gate was fed in parallel to all ADCs. In addition to 57 standard data channels one only of the two data channels contributing to the coincidence was recorded.

The vector of 8 bit quantities together with a status register was read from CAMAC by a 12K PDP8. If a second beam particle (S1S2S3) occurred within 2 μsecs, a bit was set in the status register and the data ignored by the computer. Otherwise the computer stored the data on DEC tape and carried out a preliminary analysis on line. The latter permitted us to show how well particle masses could be separated even without calibration corrections.

3. CALIBRATION

The calibration was performed in two stages. First, non linear effects in the ADCs were determined by observing test pulses of known relative amplitudes. The amplitude of the test pulses was controlled by a power supply whose value was observed with a digital voltmeter. The non-linearity and pedestal current variation of each channel + ADC were determined individually (Fig. 2a) and used to convert all observed ADC bin numbers to a scale linear in input pulse height. Second, this linear scale was converted into energy units using the known energy of the 5.9 KeV Fe^{55} X-ray. These spectra were recorded on DEC tape after every few hundred charged particle events and contain typically 10-20,000 points. A typical spectrum is shown in Fig. 2(b). The peak was determined by a least squares fit of an inverted parabola to the upper half of the main peak. (The calibration was not sensitive to the choice of fitting method.) In this way the major effects of temperature, pressure and gas mixture variation on the gain are corrected. Fig. 2(c) shows to what extent this procedure compensated for gain variations during a particular run. The scatter of points about the line shows that residual gain variations with

TABLE I SOURCES OF GAIN VARIATION

	Source	Measurement	Variation	Effect on Gain % (σ)
1.	Drift voltage stability	Digital voltmeter	$<10^{-3}$	
	" " ripple	Oscilloscope	$<10^{-3}$	
				<0.7%
2.	HT wire voltage stability	Digital voltmeter	$<10^{-4}$	
	" " ripple	Oscilloscope	$<10^{-4}$	
				<0.1%
3.	LT power supply and other sources of short term electronic gain variation	Observed dispersion of test pulse response averaged over all channels. Fig. 2(g) shaded spectrum.	$<10^{-2}$	
				<1%
4.	Gas gain variation with time (temp., press. and composition) after correction with Fe data	See fig. 2(c) and text	16×10^{-3}	
				<2%
5.	Gas gain variation along wire	Fe^{55} scan Fig.2(f)	$\lesssim 20 \times 10^{-3}$	
				<2%
	Gain variation from wire to wire	Fe^{55} scan	20×10^{-3}	
				2%
		Charged particles Fig. 2(e)	$<40 \times 10^{-3}$	
				<4%
These include:				
	Wire diameter variation	Laser diffraction	<0.2μm*	
	Signal wire position	Microscope	<8μm	
	High voltage wire position		30μm	∿2%
	Drift electrode position	Capacitor bridge	40μm	∿2%
6.	Random electronic noise	See fig. 2(g)	120 eV/ channel	
			20 eV on mean	1%

* This is a typical figure. The sample of wire actually used has not been measured. Wires tend to have non-circular but relatively uniform cross-sections.

ionisation loss. The temperature and pressure readings from the probes were used to correct all ionisation data to NTP. Various sources of error are discussed in Table I.

The non-linearity of the ADC has already been discussed and calibrated out. Fig. 2(d) shows the non-linearity of the amplification beyond the range used (shaded). There is no serious saturation in either the electronic or gas amplification stages in the range used. The observed non-linearity above 10 KeV is consistent with the expected electronic saturation. The effect of self triggering on the observed pulse height was negligible in the case of Fe spectra where only the "escape peak" was affected. In the case of the charged particles two channels in coincidence were used for the trigger but only one was recorded. This one was observed to be biassed against low pulse heights due to the finite discriminator level (peak labelled "trig" in Fig. 2(e)). This effect may neglected when taken with the other 57 channels. Fig. 2(e) also shows the gain variation from channel to channel observed with the charged particles. The data have statistical errors of order 2% and are not inconsistent with the gain variations observed with an Fe^{55} source and those expected from the mechanical tolerances of the chamber construction (Table I). Fig. 2(f) shows the gain variation along typical wires which is also small. These variations are relatively unimportant since they are the same for every particle and therefore do not contribute towards the overall mass resolution based on the 58 samples. Fig. 2(g) shows the spread of observed test pulse response which is primarily due to electronic noise on a single channel. This interpretation is confirmed by the effect of averaging over all channels for each test "event" when the width is significantly reduced (shaded spectrum).

At each momentum the particle selection was changed several times during a run so that data for the different masses were interleaved. Table II shows the different runs that were made. The 150 GeV/c runs were taken with a "ping" spill (four 200 μsec bursts per flat top, 20-25 beam particles per burst). The

TABLE II

Data Runs

Momentum	Particle	Spill	Contamination	Cerenkov
150 GeV/c	Proton	"ping"	-	7.1 psia He. Below threshold
"	Pion	"	μ, e	" θ > 5 mr
100 GeV/c	Proton	slow	-	8.5 psia He. Below threshold
"	Pion	"	μ, e	" θ > 5 mr
50 GeV/c	Proton	"	K	7.0 psia He. Below threshold
25 GeV/c	Proton	"	K	11.0 psia He. Below threshold
"	Pion	"	μ	θ < 5 mr
"	Electron	"	μ	θ > 5 mr

other momenta were taken with ∿15 triggers per flat top. In every case the selected particle flux exceeded 20% of the beam (S1S2S3). The only significant source of contamination may be the presence of muons among the 25 GeV/c "electrons". The marked difference observed in ionisation between pions and "electrons" shows that this contamination is not dominant. In all other cases the contamination is either very small (<5%) or of no consequence (muons amongst pions).

4. INTERCHANNEL CORRELATIONS

The presence of coupling between channels is shown in Fig. 3, where we have taken the spectra observed for 25 GeV/c electrons as an example. Fig. 3(a) shows how the energy loss observed on a channel depends on whether the

nearest-but-one neighbour was above or below average pulse height. It is seen that it does not. The same is true for protons and pions at 25 GeV/c. The very small shaded peak in the overflow region is not inconsistent with the number of δ-rays of range >3 cms expected.[5] These would give rise to such a positive crosstalk unless multiply scattered away from the parent track (i.e. outside the integration gate). The effect is not large compared with 1%. Fig. 3(b) shows the same data for nearest neighbour channels. A significant negative cross-talk is observed as expected from capacitative effects[4]. Defining the cross-talk parameter, α, in terms of the charges collected, E_i, on each channel, i, and the pulse heights observed ε_i:

$$\varepsilon_i = \alpha E_{i-1} + E_i + \alpha E_{i+1}, \qquad (1)$$

we have simulated this crosstalk in a Monte Carlo calculation using the theoretical dE/dx distribution discussed in paper I[1] and find a best value of:

$$\alpha = -0.055 \pm 0.01$$

The result is given by the smooth curve in Fig. 3(b). The same value of α provides a good fit for 25 GeV/c pions and protons, where the same phenomenon is observed. Indeed observation on an oscilloscope of a dummy (thick wire) channel without gas gain showed these small positive going pulses in coincidence with the negative pulses on the other amplifying channels. The net result of this effect is a small loss of signal amplitude and a change in the shape of the expected energy loss distribution as shown in Fig. 3(c).

A more serious problem was the effective DC level shift observed through the combined effect of all channels capacitatively coupling to the common drift electrodes. In the absence of sufficient capacity in parallel with the drift voltage supply this produced a shift of the zero proportional to the mean pulse height. Since the effect was linear it may be described by a single proportionality constant for the whole experiment, β.

488-60

TABLE III

ATOMIC CONSTANTS USED IN THEORETICAL CALCULATION

(ref. 6)

80% Argon/20% CO_2 at NTP ($\hbar\omega_p$ = 0.835 eV)

Argon	K shell	3196.0 eV	2 electrons per argon atom
	L shell	294.0	8
	M shell	39.5	8
Carbon	K shell	313.0	2 electrons per CO_2 molecule
	L shell	55.8	2
		17.7	2
Oxygen	K shell	575.0	4 electrons per CO_2 molecule
	L shell	54.4	4
		39.4	8

Note: The predictions depend only logarithmically on the energy levels assumed.

Extending equation (1) we approximate:-

$$\varepsilon_i = \alpha E_{i-1} + E_i + \alpha E_{i+1} - \beta \bar{S}$$

where $\bar{S}$ is a suitably defined mean ionisation for a particular particle velocity.

Comparing our 8 runs with theory we determined $\beta = 0.20 \pm 0.04$ or $\beta\bar{S} \sim 400 \pm 80$ eV*.

* These effects may be avoided by (1) increasing the capacity in parallel with the chamber (2) decoupling the input of the preamplifier to the cathode wires so that changes of drift field are rejected as a common mode signal (3) moving the drift electrodes farther away to reduce the capacitance.

(We have defined $\bar{S}$ as the peak of the distribution of means of the lowest 35 out of 58 signals as determined by theory. The value of $\beta\bar{S}$ is independent of this choice.)

Together with the uncertainty of its recovery characteristics this effect dominated the systematic errors in this experiment. It was probably responsible for the observation of small anomalous positive correlations between neighbouring channels at 150 GeV/c where the instantaneous particle flux was high. Data for 100 GeV/c π and 50 GeV/c protons also showed the effect. This problem was clearly instrumental since it was not observed in any of the 25 GeV/c runs which spanned the velocity range of the experiment.

5. RESULTS

We have calculated theoretical dE/dx spectra for 1.5 cms of argon/20% CO_2 at NTP according to the method described in paper I[1]. The ionisation potentials and plasma frequency used are given in Table III. These spectra have been further modified by including the 5.5% crosstalk between nearest neighbours and a resolution function with $\sigma \sim 10\%$*. The latter has a negligible effect on the broad spectra. In comparing these spectra with experiment we assume of course that an observed pulse height is directly related to the arrival of a certain number of ionisation electrons at the wire and that this in turn is proportional to the actual energy loss of the primary particle and that the proportionality is the same for the pulse height observed from the X-ray source (5.9 KeV). While this assumption is indefensible in detail it has always been found to work in practice in a statistical sense[8]. Fig. 4 shows the 8 spectra compared with the experimental data in which all 58 channels for each event are shown in the same histogram. The zeroes of the experimental spectra have been shifted as described in the previous section.

---

* This is made up of electronic noise, statistical fluctuations in the number of electrons collected for a given energy loss (Ref. 7) and fluctuations in the gas amplification process.

The value of β in equation 2 is the only free parameter in the comparison. We note that the agreement for protons, pions and electrons at 25 GeV/c is really quite good. On the other hand the comparison with the pion data at 100 GeV/c and 150 GeV/c is much weaker.

In Fig. 5 we show a superposition of the spectra for pions and protons at 25 GeV/c. This makes it clear that no useful information on particle identification is achieved by one or even a small number of measurements on each track. It also shows the long "Landau tail" which prevents the use of a simple "mean ionisation" estimator from resolving the masses. In this experiment 58 measurements are in fact available on each track. To remove the effect of the tail we may discard the largest 23 pulse heights (40%) in each case[1]. The dotted line in Fig. 5 shows the distribution of the remaining 35 pulse heights for each proton event - it has no "Landau tail". If therefore we take the mean of this set of 35 pulse heights for each beam particle we may resolve the pions and protons. Fig. 6 shows a polaroid shot of an on-line display showing the separation of pions and protons achieved in this way using raw data. The origin is some 40 bins off-scale to the left. The separation is on the order of a full width at half maximum (FWHM). Note that the distributions have gaussian shape without tails. Without the zero shift and its related noise the resolution would be much better. Since the shift is proportional to the total energy loss in 1.2 metres of gas, the Landau fluctuations (∿50%)[11] on this represent the main contribution to the loss of resolution.

We have analysed each run in terms of the mean of the lowest 35 pulse heights. The results are given in Table IV together with the equivalent Monte Carlo predictions. Fig. 7 shows the theory and data corrected for the DC shift. The difference between the theoretical and experimental widths shown in Table IV is accounted for by the Landau fluctuations on the shift (∿90 eV RMS). We quote conservative errors of 4% on the means in view of the uncertainties surrounding the shift.

Table IV

THE MEAN OF THE LOWEST 35 OUT OF 58 x 1.5 cms SAMPLES

Argon + 20% CO_2 at NTP

/mc	Run	Number of Events	Experimental Distribution Before Shift Mean	Width (RMS)	Experimental Mean After Shift ($\beta\bar{S}$)	Monte Carlo Mean	Width (RMS)
6.6	Protons at 25 GeV/c	1263	1856	168	2244 ± 90	2126	115
3.2	50 GeV/c	1521	1922	186	2324 ± 93	2319	124
06	100 GeV/c	2473	2033	180	2458 ± 98	2485	134
60	150 GeV/c	4969	2165	186	2617 ± 105	2554	134
78	Pions at 25 GeV/c	1968	2182	176	2638 ± 106	2626	138
14	100 GeV/c	2381	2173	196	2627 ± 105	2779	144
070	150 GeV/c	5568	2322	198	2809 ± 110	2798	152
9000	Electrons at 25 GeV/c	2114	2282	183	2759 ± 110	2820	158

All energies in electron volts.

Although the possibility of some muon conatmination of the 25 GeV/c electrons cannot be ruled out, the electron data are compatible with the 150 GeV/c pion data. Similarly, there is consistency between the data for 150 GeV/c protons and 25 GeV/c pions. Only the data point for 100 GeV/c pions appears significantly out of line. We note that the relativistic rise is 55 ±4% and that the Fermi plateau extends from p/mc = 500 or so upwards.

Different experimenters work with different gas mixtures, gas thicknesses and statistical methods. In spite of this in Fig. 8 we attempt to compare the ionisation data available[10-12] with the Monte Carlo prediction and curve calculated on the basis of reference 6. The latter and the data of the other experiments refer to the most probable energy loss. Further, all other data above p/mc = 150 were taken with electrons. In spite of this there is general agreement between the data points of this experiment, earlier experiments and the Monte Carlo calculation. All are in disagreement with the Sternheimer curve.

6. CONCLUSION

The results of the Monte Carlo calculation of energy loss in thin gas samples are in good agreement with the data for values of p/mc from 26 to 1000 in argon/20% CO_2 at NTP. Above 1000 the observed energy loss of pions does not differ significantly from electrons since the bremstrahlung probability in a thin gas sample is small and the electromagnetic field of the incident particle has reached its asymptotic form (Fermi plateau)[9]. The resolution of the experiment was limited by instrumental effects which can be avoided in future devices. Nontheless on-line separation of pions and protons at 25 GeV/c was obtained* and there seems to be no reason in principle why very much better separation cannot be achieved with improved systematics and more samples. Finally, we note that

---

* Separation at 9 GeV/c has been achieved previously using a 2.5 m detector (see Ref. 11).

our results are in agreement not only with our calculations by also with the size of the relativistic rise measured by others in gas samples defined by thin windows. This argues against the speculation of Garibyan and Ispiryan[13] that the disagreement with calculations is due to the effect of the windows. This experiment shows that there is no disagreement with calculation and also that the same results are obtained without windows.

ACKNOWLEDGMENTS

We would like to express our thanks for the enthusiastic cooperation and help given us by the Fermi National Accelerator Laboratory and for the support of the experiment by the Science Research Council (UK). We also thank Roger Giles, Mike Walker, Mick Flinn and the Oxford Nuclear Physics main workshop for their part in building the chamber; finally we are grateful to Peter Shield for designing and building most of the electronics.

REFERENCES

1. The ionisation loss of relativistic charged particles in thin gas samples and its use for particle identification: I, theoretical predictions. J.H. Cobb, J.N. Bunch, W.W.M. Allison (previous paper).

2. W.W.M. Allison et al, NIM 119, 499 (1974).

3. J.H. Cobb, D. Phil. thesis, University of Oxford (1975). Available from Rutherford Laboratory, HEP/T/55.

4. G. Charpak, Ann. Rev. Nucl. Sci. 20, 226, (1970).

5. J.L. Lloyd and A.W. Wolfendale, Proc. Phys. Soc. 73, 178 (1959).

6. R.M. Sternheimer and R.F. Pieirls, Phys. Rev. 88, 851 (1952) and Phys. Rev. B3, 3681 (1971).

7. See Ref. 4 page 232.

8. Methods of Experimental Physics Vol. 5A, Yuan and Wu (Eds.) Academic Press (1961) page 43.

9. O. Blunck and K. Westphal, Zeit. für Phys. 130, 641 (1951).

10. P.V. Ramana Murthy, NIM 63, 77 (1968).

11. D. Jeanne et al., NIM 111, 287 (1973); M. Aderholz et al., NIM 118 419 (1974).

12. F. Harris et al, NIM 107, 413 (1973).

13. G.M. Garibyan and K.A. Ispiryan, JETP Letters 16, 585 (1972).

FIGURES

Fig. 1

(a) Beam diagram

(b) Schematic side view of proportional chamber

(c) Top view of chamber and amplifier box

(d) View of chamber in beam direction

(e) Picture showing details of plane construction

Fig. 2

(a) Non-linearity of a typical ADC. The pedestal current was large so that only the shaded more linear region was used.

(b) A typical Fe^{55} spectrum taken during part of a run between accelerator cycles.

(c) The relative gain variation during a run as measured by Fe^{55} X-ray pulse heights plotted against the relative gain variation as measured by charged particle mean pulse heights. The line indicates the expected correlation.

(d) Linearity of amplification (gas + electronic) as shown by various X-ray sources. The dynamic range of the 8 bit ADCs were matched to the shaded region.

(e) Variation of channel gain attributable to variations in gas amplification from wire to wire (charged particle data with statistical error 2%). See table I.

(f) The gain variation along wires measured by scanning an Fe^{55} source through the operating region.

(g) The spread of test pulse response due to electronic noise on a single channel. Shaded spectrum is the same averaged over all channels.

Fig. 3

The difference in energy loss spectra due to near neighbour cross talk. The upper histogram in (a) and (b) shows the spectrum on a channel when the near neighbour pulse height is small and the shaded spectrum shows how much this changes when the near neighbour is large.

(a) For second nearest neighbours (25 GeV/c e^-).

(b) For nearest neighbours. (25 GeV/c e^-)

The smooth curve shows the expected result for $\alpha = -0.055$.

(c) Shows the effect on the theoretical dE/dx distribution of folding in crosstalk of -5.5% (for 25 GeV/c protons).

Fig. 4

The dE/dx spectra for the 8 different velocities measured, corrected to NTP and including correction for the zero shift. The theoretical curves include the effect of the 20% CO_2, the -5.5% nearest neighbour crosstalk and a small effect due to statistics of the electrons (assumed Poisson). The ordinate of the histograms is the number of samples per 100 eV energy bin. The normalisation in each case is 58 times the number of events quoted in Table IV.

Fig. 5

A superposition of the distributions of all channels for π and p at 25 GeV/c. The dashed histogram shows the effect on the proton distribution of histogramming only the smallest 35 out of 58 pulses recorded in each event.

Fig. 6

A polaroid shot showing the separation of pions and protons at 25 GeV/c achieved by the on-line PDP8 programme working with raw data. Each point in

Fig. 6 (cont.)

the two histograms refers to a single beam track with a value equal to the mean pulse height after discarding the largest 23 pulses. The origin is off scale to the left. The last column of Table IV shows that much better separation may be expected in the absence of systematic effects (see text).

Fig. 7

A comparison of the relativistic rise of the mean of the lowest 35 out of 58 x 1.5 cm samples with theory for argon/20% CO_2 at NTP.

Fig. 8

Compilation of world data on the relativistic rise in argon as measured in proportional chambers. The dashed curve refers to a calculation according to the prescription of Ref. 6. The solid curve is discussed in the text. The comparison is essentially qualitative as the various experiments and calculations relate to different quantities and different gas mixtures.

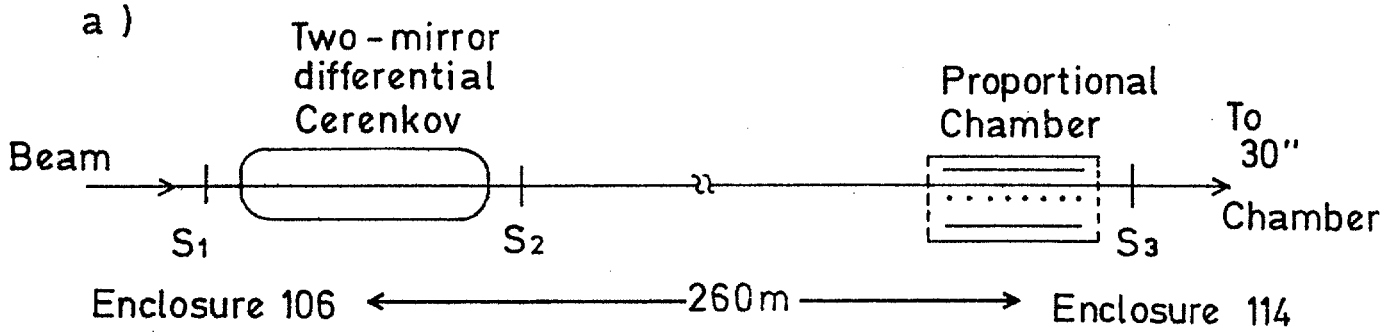

BEAM DIAGRAM

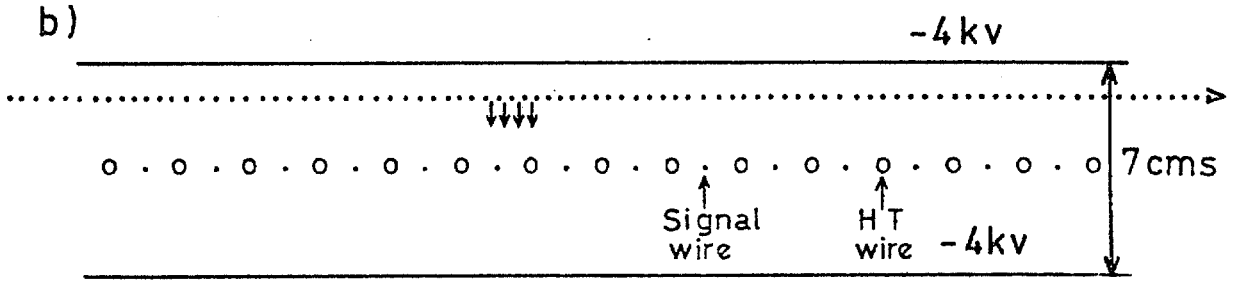

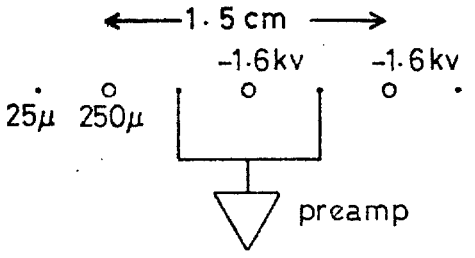

SCHEMATIC SIDE VIEW OF PROPORTIONAL CHAMBER

Fig . 1

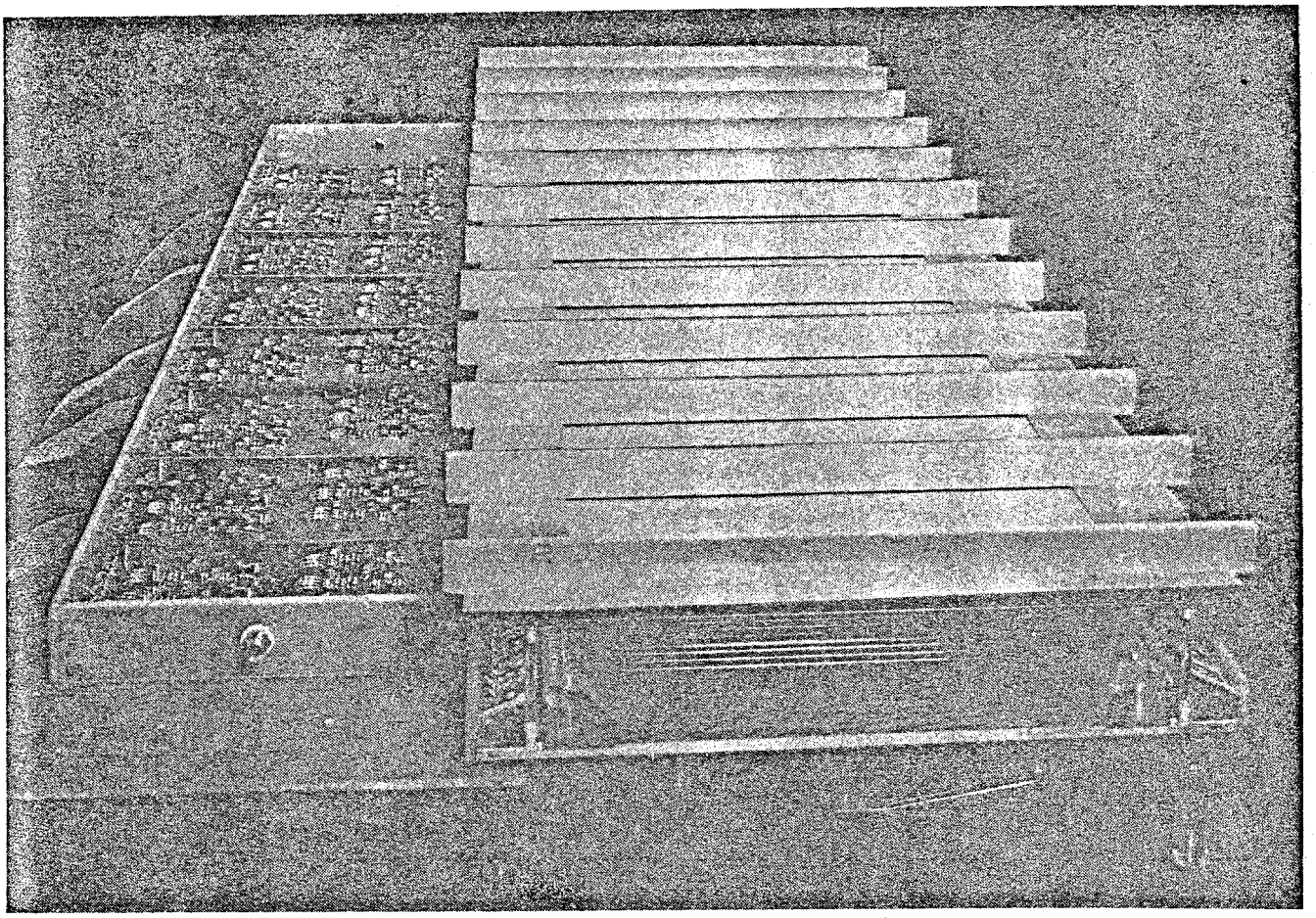

Fig. 1c

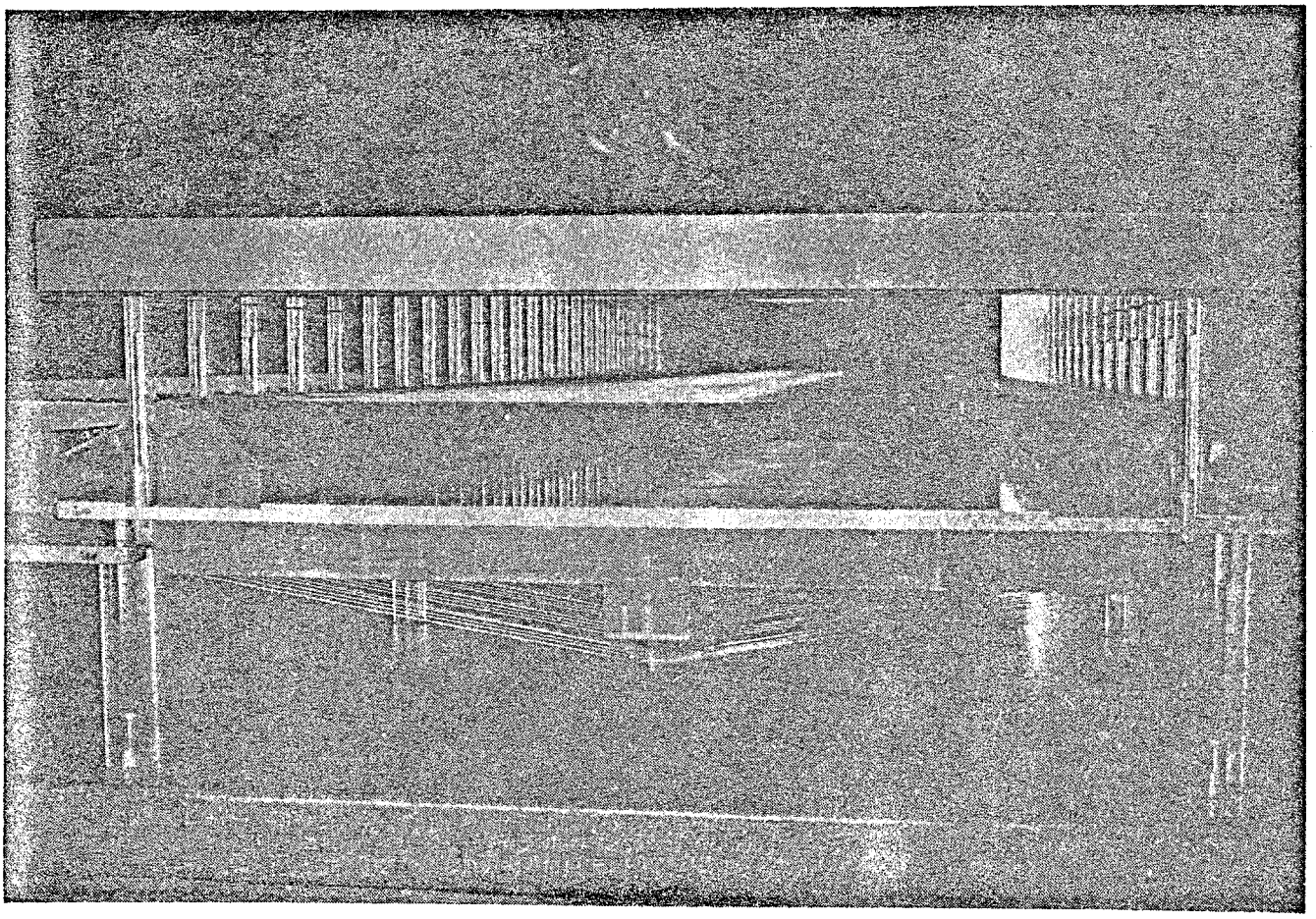

Fig. 1d

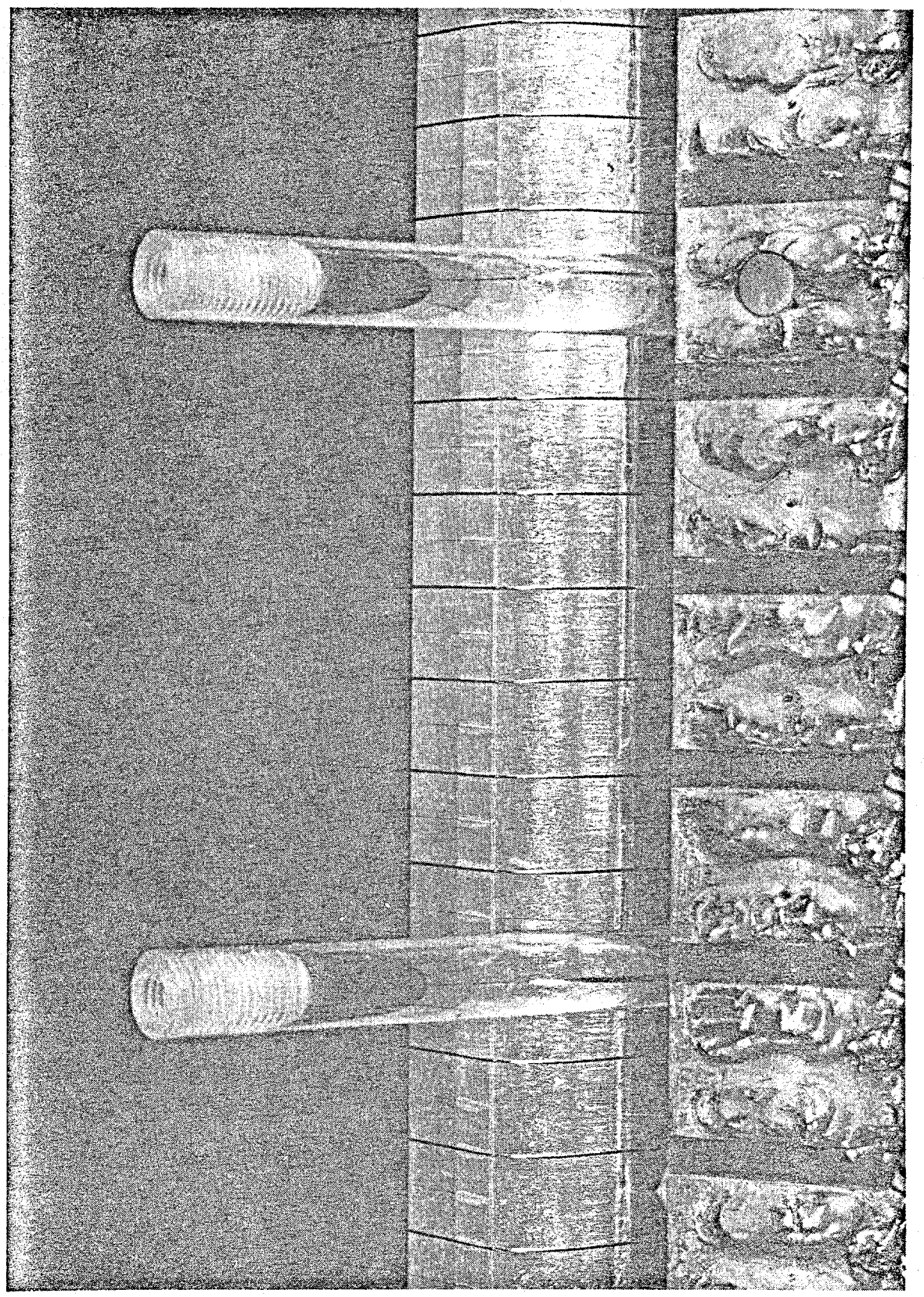

Fig. 1e

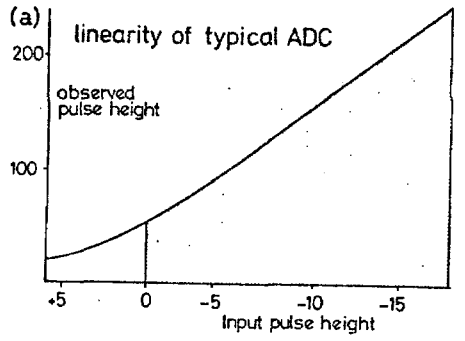
(a)
linearity of typical ADC
200
100
observed pulse height
+5
0
-5
-10
-15
Input pulse height

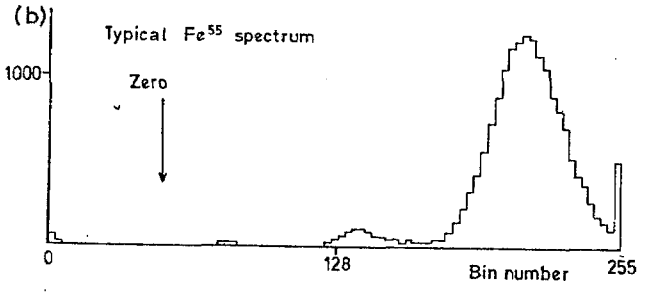
(b)
Typical Fe55 spectrum
1000
Zero
0
128
Bin number
255

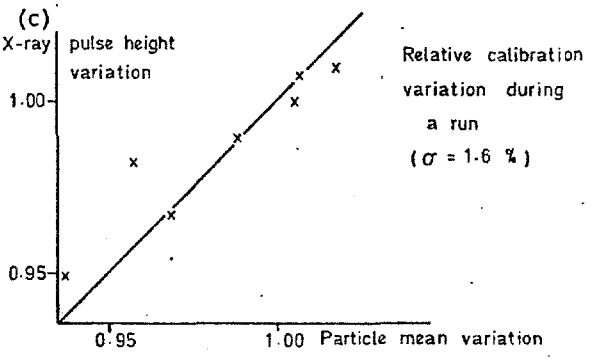
(c)
X-ray pulse height variation
1.00
0.95
Relative calibration variation during a run
(σ = 1.6 %)
0.95
1.00
Particle mean variation

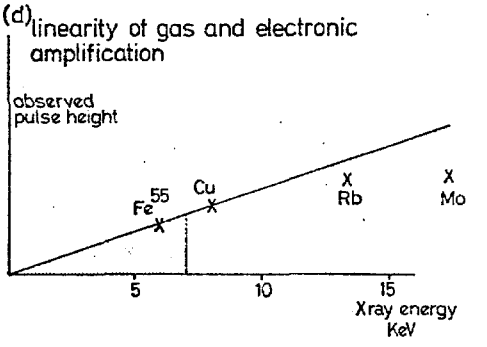
(d)
linearity of gas and electronic amplification
observed pulse height
Fe55
Cu
Rb
Mo
5
10
15
Xray energy KeV

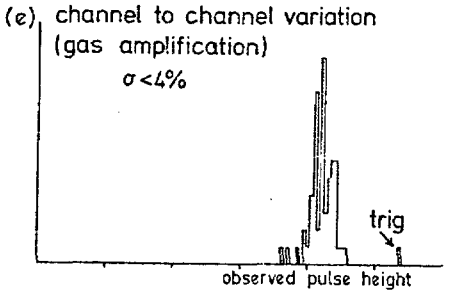
(e)
channel to channel variation
(gas amplification)
σ<4%
trig
observed pulse height

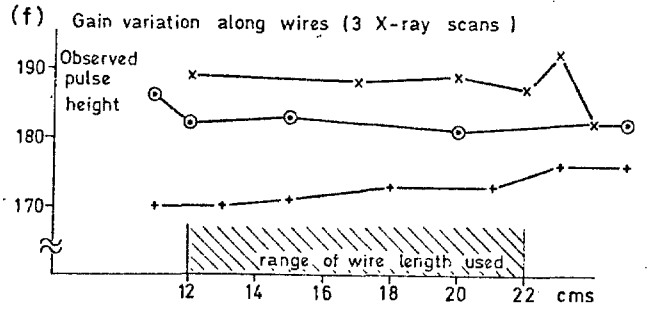
(f)
Gain variation along wires (3 X-ray scans)
Observed pulse height
190
180
170
range of wire length used
12
14
16
18
20
22
cms

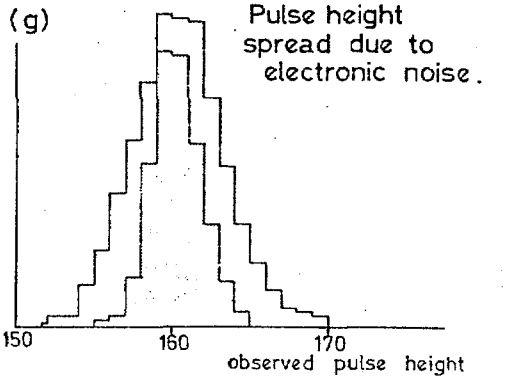
(g)
Pulse height spread due to electronic noise.
150
160
170
observed pulse height

Fig. 2

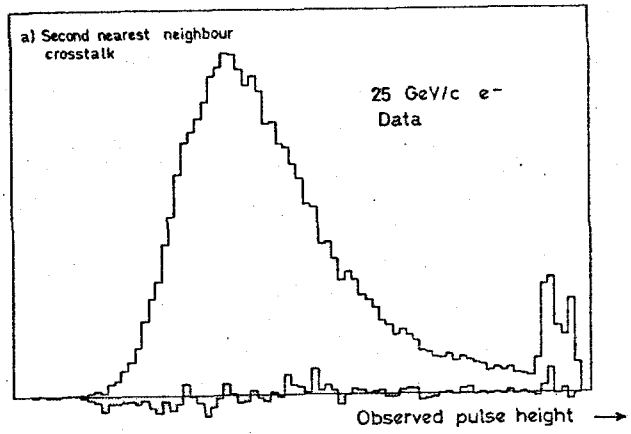

Fig. 3a

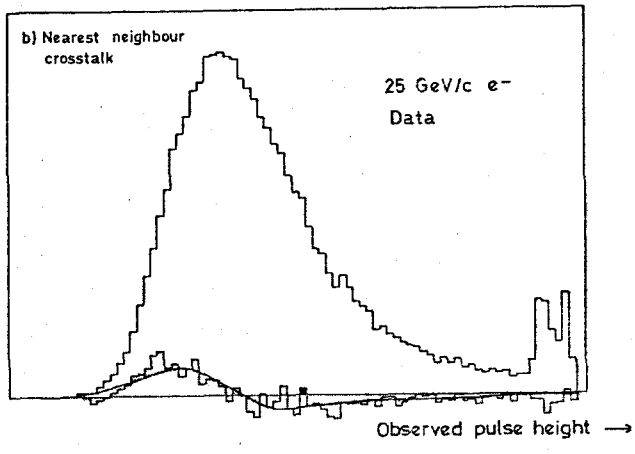

Fig. 3 b

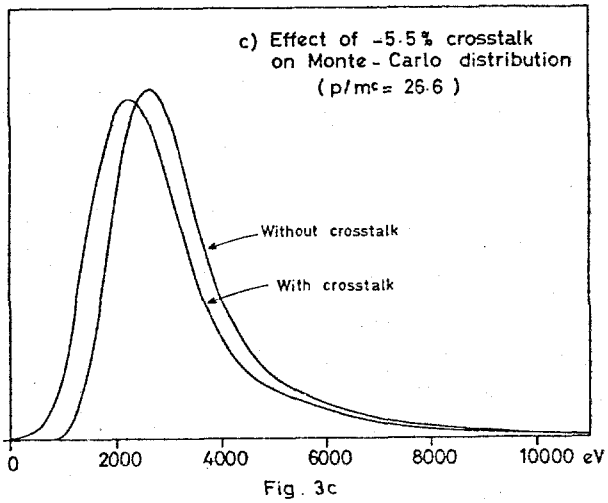

Fig. 3c

Fig. 3

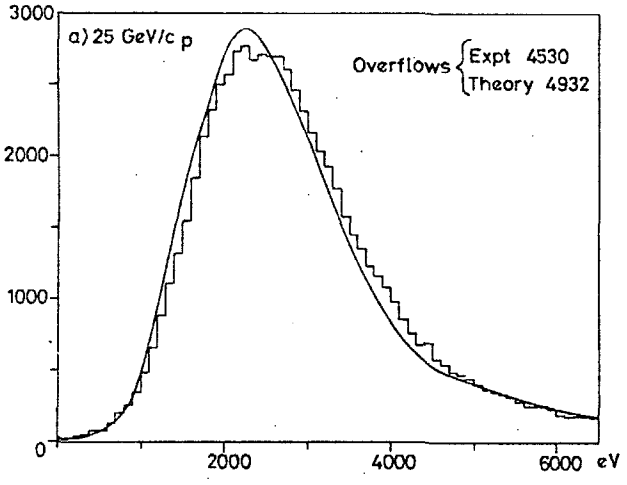
a) 25 GeV/c p
Overflows {Expt 4530
Theory 4932
3000
2000
1000
0
2000
4000
6000 eV

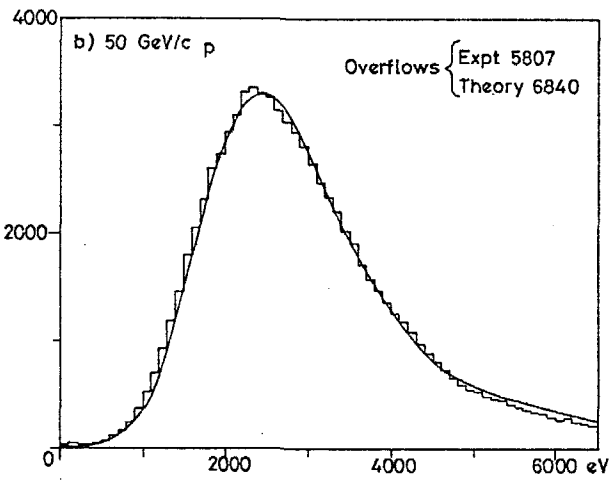
b) 50 GeV/c p
Overflows {Expt 5807
Theory 6840
4000
2000
0
2000
4000
6000 eV

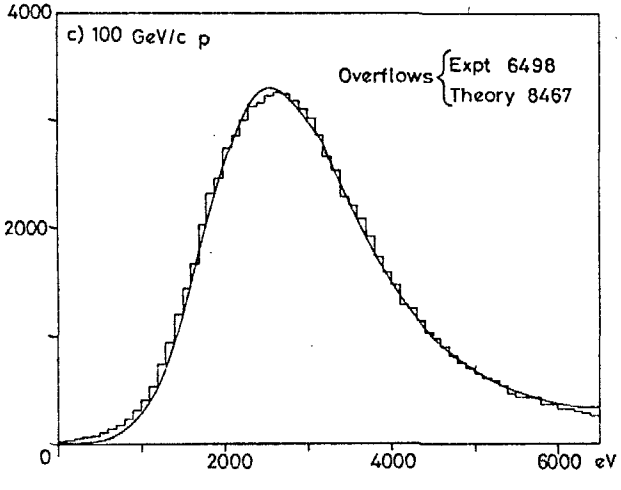
c) 100 GeV/c p
Overflows {Expt 6498
Theory 8467
4000
2000
0
2000
4000
6000 eV

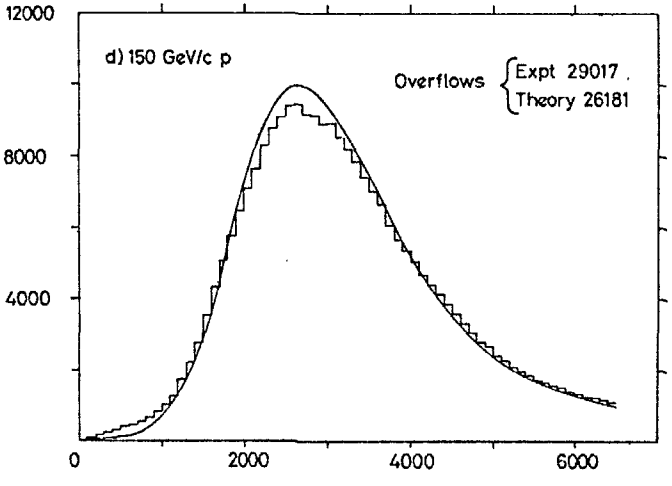
d) 150 GeV/c p
Overflows {Expt 29017
Theory 26181
12000
8000
4000
0
2000
4000
6000

Fig. 4

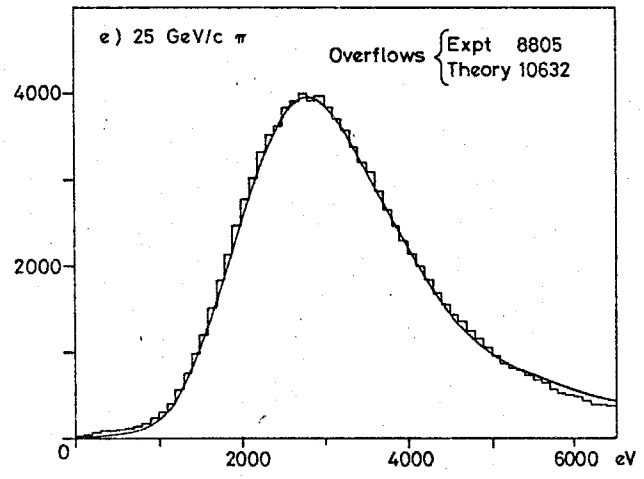
e) 25 GeV/c π
Overflows {Expt 8805
Theory 10632
4000
2000
0
2000
4000
6000 eV

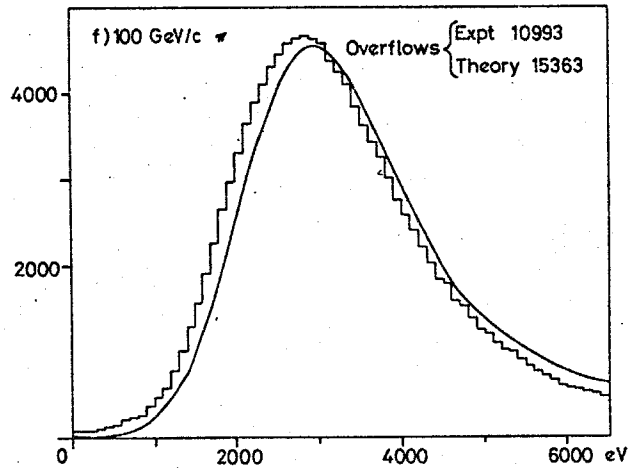
f) 100 GeV/c π
Overflows {Expt 10993
Theory 15363
4000
2000
0
2000
4000
6000 eV

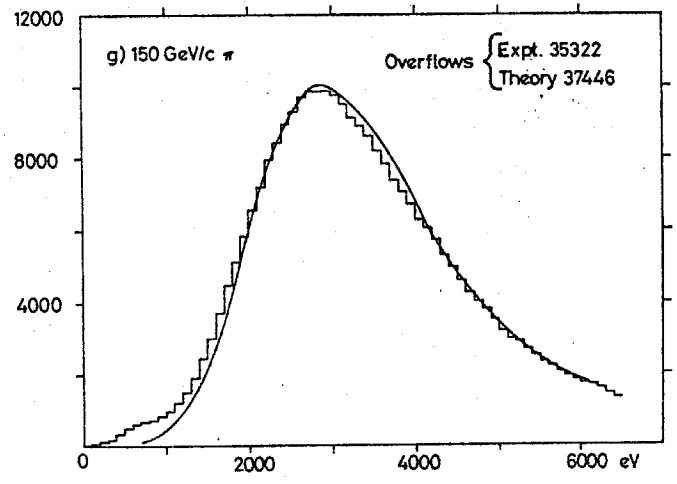
g) 150 GeV/c π
Overflows {Expt. 35322
Theory 37446
12000
8000
4000
0
2000
4000
6000 eV

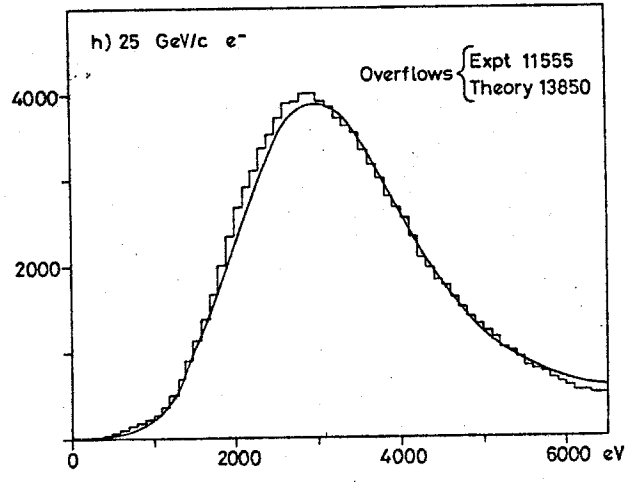
h) 25 GeV/c e⁻
Overflows {Expt 11555
Theory 13850
4000
2000
0
2000
4000
6000 eV

Fig. 4

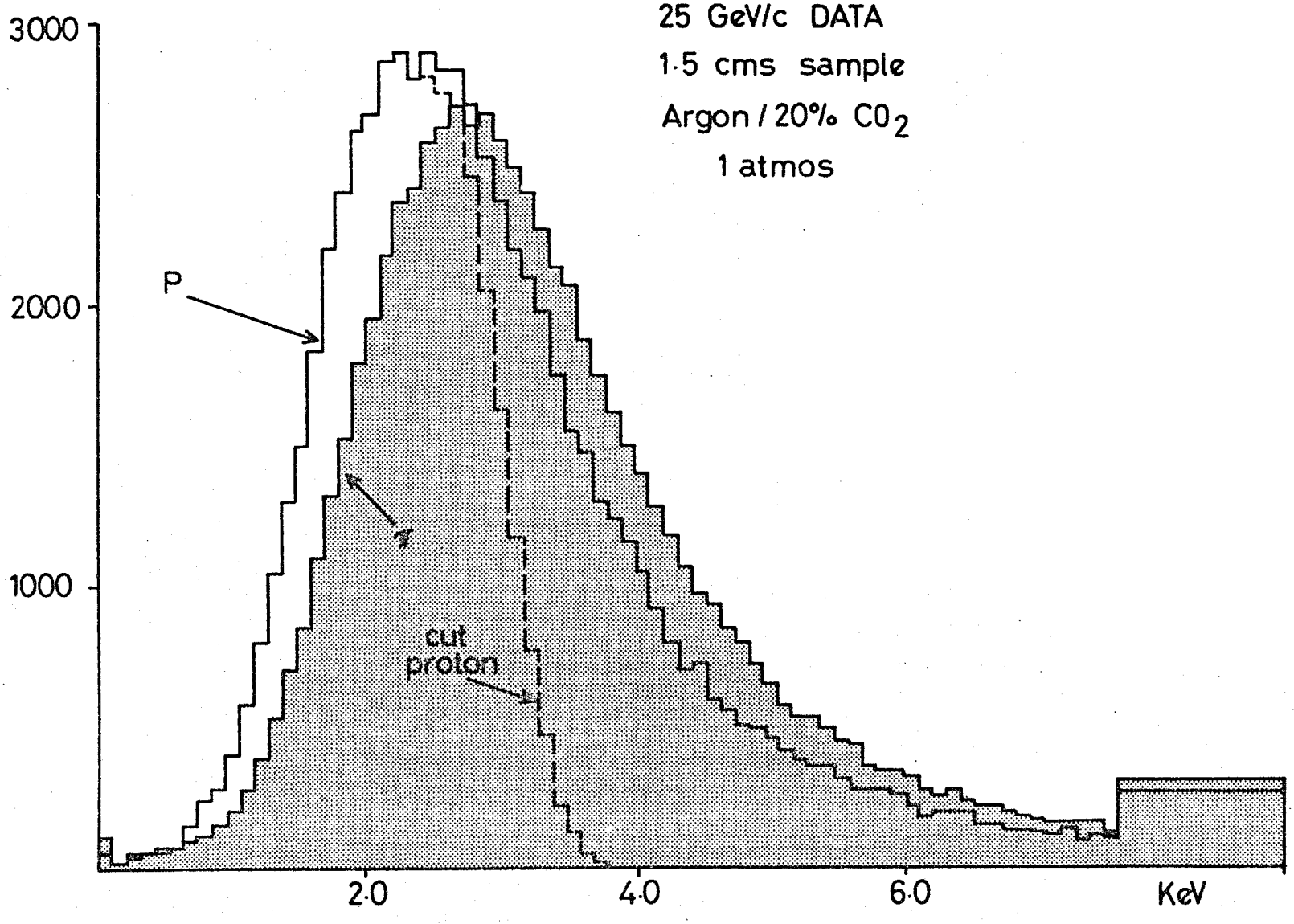
25 GeV/c DATA
1·5 cms sample
Argon / 20% CO_2
1 atmos
3000
2000
1000
P
cut
proton
2·0
4·0
6·0
KeV

Fig. 5

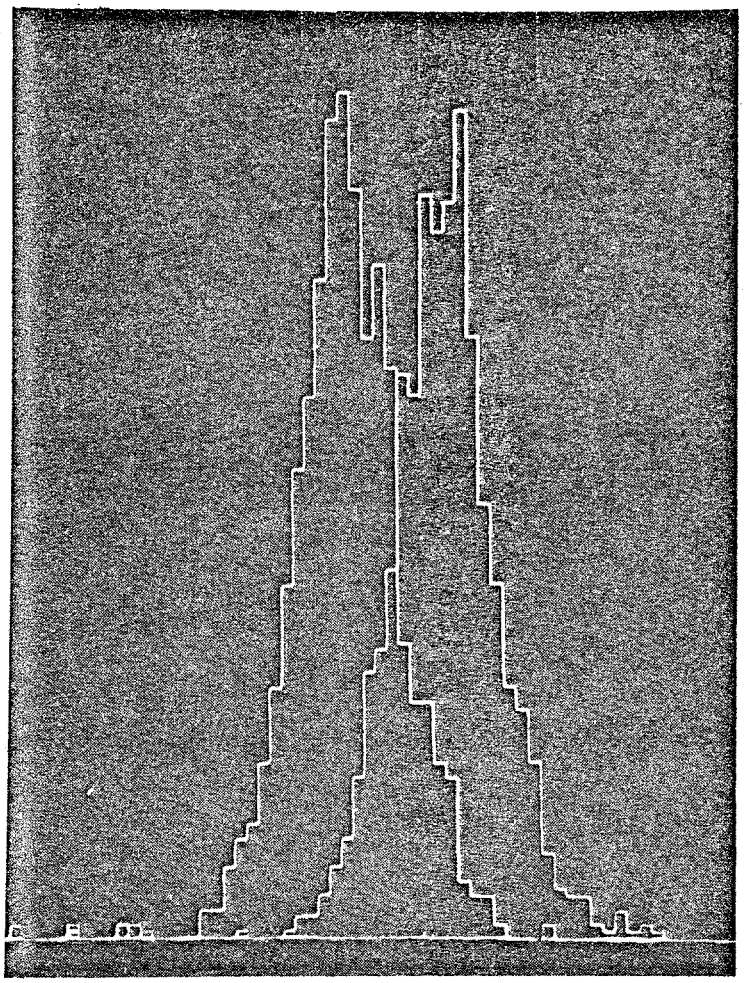

Fig. 6

Fig.7

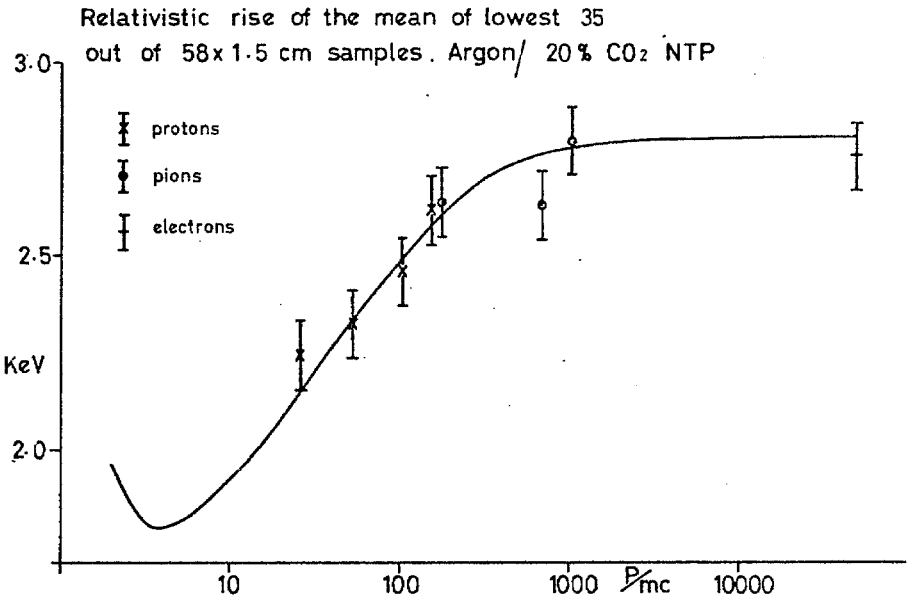
Relativistic rise of the mean of lowest 35
out of 58 x 1.5 cm samples. Argon/ 20 % CO2 NTP
protons
pions
electrons
3.0
2.5
2.0
KeV
10
100
1000
P/mc
10000

Fig.8

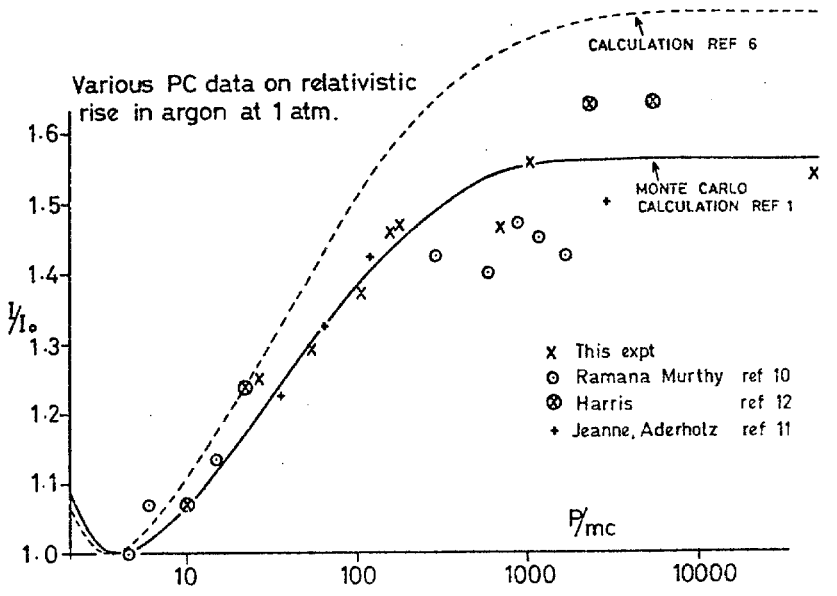
Various PC data on relativistic
rise in argon at 1 atm.
CALCULATION REF 6
MONTE CARLO
CALCULATION REF 1
This expt
Ramana Murthy ref 10
Harris ref 12
Jeanne, Aderholz ref 11
I/I0
1.6
1.5
1.4
1.3
1.2
1.1
1.0
P/mc
10
100
1000
10000

488-70

Ref. 1

Volume 61B, number 1 PHYSICS LETTERS 1 March 1976

EVIDENCE FOR CHARGED CLUSTER EMISSION IN 147 GeV/c π^-p COLLISIONS☆

D. FONG, M. HELLER, A. SHAPIRO, M. WIDGOFF
Brown University, Providence, Rhode Island 02912, USA

F. BRUYANT
CERN, Geneve 23, Switzerland

D. BOGERT, M. JOHNSON
Fermilab, Batavia, Illinois 06510, USA

R. BURNSTEIN, C. FU, D. PETERSEN, M. ROBERTSON, H. RUBIN
Illinois Institute of Technology, Chicago, Illinois 60616, USA

R. SARD, A. SNYDER, J. TORTORA
University of Illinois, Urbana, Illinois 61801, USA

D. ALYEA
Indiana University, Bloomington, Indiana 47401, USA

C-Y. CHIEN, P. LUCAS, A. PEVSNER, R. ZDANIS
Johns Hopkins University, Baltimore, Maryland 21218, USA

J. BRAU[1], J. GRUNHAUS[2], E.S. HAFEN, R.I. HULSIZER, U. KARSHON[3], V. KISTIAKOWSKY, A. LEVY[4], A. NAPIER, I.A. PLESS, P.C. TREPAGNIER, J. WOLFSON, R.K. YAMAMOTO
Massachusetts Institute of Technology, Cambridge, Massachusetts 02139, USA

H. COHN
Oak Ridge National Laboratory, Oak Ridge, Tennessee 37830, USA

T.C. OU, R. PLANO, T. WATTS
Rutgers University, New Brunswick, New Jersey 08903, USA

E. BRUCKER, E. KOLLER, P. STAMER, S. TAYLOR
Stevens Institute of Technology, Hoboken, New Jersey 07030, USA

W. BUGG, G. CONDO, T. HANDLER, E. HART
University of Tennessee, Knoxville, Tennessee 37916, USA

H. KRAYBILL, D. LJUNG, T. LUDLAM, H.D. TAFT
Yale University, New Haven, Connecticut 06520, USA

Received 17 October 1975

A study of charged particle production in 147 GeV/c π^-p collisions yields no evidence for an electrically neutral central region or corresponding rapidity plateau. The results do indicate that electric charge and transverse momentum may be locally conserved over small intervals on the rapidity axis. These results support a picture in which the observed hadrons are emitted in clusters whose quantum numbers vary as a function of rapidity and reflect the incident channel quantum numbers at the extremes of the rapidity scale.

☆ This work supported in part by the U.S. Energy Research and Development Administration and the National Science Foundation.
[1] Fannie and John Hertz Foundation Fellow.
[2] On leave of absence, Tel-Aviv University, Israel.
[3] On leave of absence, The Weizmann Institute of Science, Israel.
[4] Present address: Tel-Aviv University, Israel.

Investigations of multiparticle final states induced by proton-proton collisions at high energies have provided evidence for a "central region" on the rapidity scale in which particles, or clusters of particles, are emitted independently [e.g. 1], and for which electric charge, and perhaps other quantum numbers as well, may be locally conserved [2]. On the other hand, recently published work on high energy pion-nucleon collisions has emphasized asymmetries in the distributions of final-state particles which indicate that fragmentation-like processes play an important role even in high multiplicity events [3, 4].

In this paper we present new data from π^-p collisions at 147 GeV/c incident pion momentum. We show that while an electrically neutral central region and corresponding rapidity plateau are not seen, the expected features for particle emission in a central region are nonetheless observed. In particular, we present previously unreported evidence that electric charge and transverse momentum are locally conserved over small intervals of rapidity in π^-p collisions at Fermilab energies. These results support a picture in which the observed hadrons are emitted in clusters whose quantum numbers vary as a function of rapidity, with the incident channel quantum numbers dominating at the extremes of the rapidity scale.

The experiment consists of ~100000 exposures of the Fermilab 30-in. bubble chamber to a beam of 147 GeV/c π^- mesons, utilizing the Proportional Wire Hybrid Spectrometer [5] for accurate measurements of momenta and angles of the fast, forward-going tracks. The average charged particle multiplicity of events in this experiment is 7.4 ± 0.04 (topological cross sections and moments are discussed in ref. [6]). In order to have as complete and accurate a sample as possible for events of all multiplicities, we report here on a subsample of about 1/4 of the data (~1600 inelastic events in the fiducial volume) for which every event failing to yield a satisfactory geometric reconstruction for all tracks in the first measurement has been examined and remeasured.

The net charge distribution of final-state particles as a function of c.m. rapidity is shown in fig. 1a. Protons with lab momentum less than 1.4 GeV/c have been identified by ionization, and all other charged particles are assumed to be pions. The histogram shown is simply the difference between the inclusive differential cross sections for positively and negatively

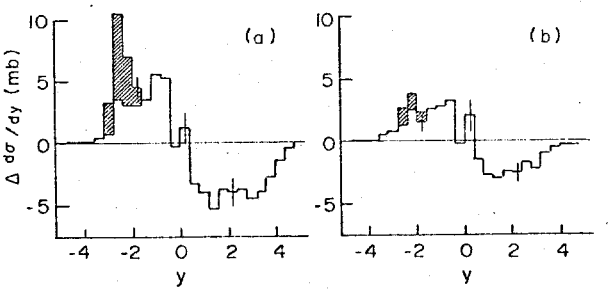

Fig. 1. (a) Net charge as a function of rapidity for all inelastic events: $\Delta d\sigma/dy = d\sigma(+)/dy - d\sigma(-)/dy$. The shaded area is the contribution from protons. (b) Same as (a), but for events with ⩾ 8 charged pions.

charged particles, with positive values indicating an excess of positive over negative particles, and vice versa. The data show a rapid change from an excess of positive particles in the backward hemisphere to an excess of negatives in the forward hemisphere, with no broad neutral interval in the central region of rapidity. The total *pion* charge excess, adding positive and negative areas under the unshaded portion of the histogram, is ~25 mb, comparable to the total cross section. This cannot be attributed to the low-multiplicity diffractive component, as the distribution for events of greater-than-average multiplicity (fig. 1b) is little different from that for the total sample.

Although the electric charge distributions do not indicate a neutral central region, the average transverse momentum of charged pions in the final state, shown in fig. 2a, is nearly independent of rapidity, over a broad interval extending approximately from $y = -2$ to $y = +3$. Again, a clear asymmetry is seen in the behavior of positive and negative charges (fig. 2b): Negative tracks have larger transverse momentum in the forward direction, while in the backward direction the average transverse momenta of positive pions systematically exceed those of negative pions. There is a rough correspondence between positive or negative charge excess and large values of the average transverse momentum. This trend apparently persists in the high-multiplicity final-states (fig. 2c). For these events the average transverse momentum for π^+ (π^-) with $-3 < y < -1$ is 343 ± 15 MeV (302 ± 16 MeV), and the corresponding values for $1 < y < 3$ are 337 ± 16 (388 ± 14).

Despite the differences between the average transverse momenta of positive and negative pions in the

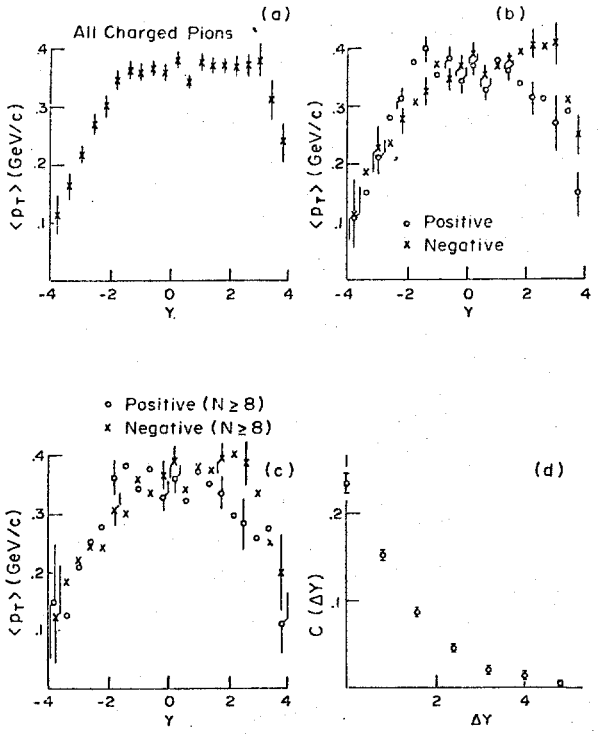

Fig. 2. (a) Average transverse momentum versus rapidity for all charged pions. (b) Average transverse momentum versus rapidity for π^+ (open circles), and π^- (X's), all inelastic events. (c) Same as (b), but for events with $\geqslant 8$ charged prongs. (d) The transverse momentum correlation function $C(\Delta y)$, as a function of the rapidity interval Δy (see text). The intervals are centered about $y = 0$.

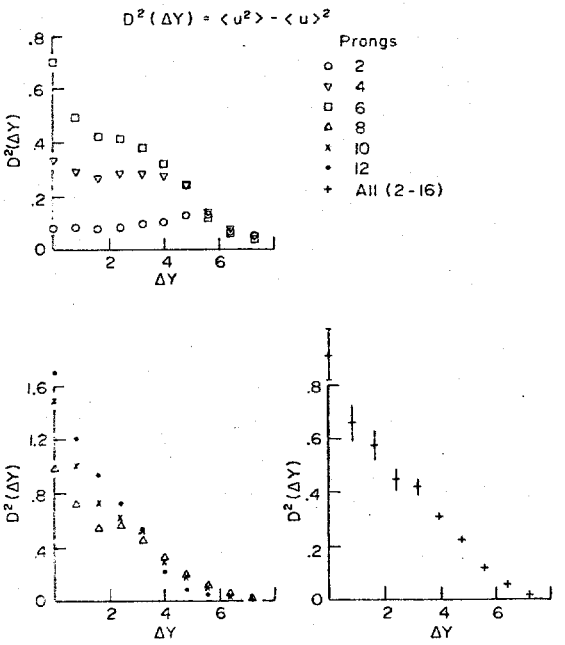

Fig. 3. The dispersion of the charge-transfer variable, $D^2(\Delta y)$, as a function of rapidity interval (see text). The intervals are centered about $y = 0$. The results labelled "all" include all inelastic events up through 16 prongs. Typical errors are displayed on the inclusive plot but have been omitted from the semi-inclusive plots for the sake of legibility.

forward and backward directions, there is a region in rapidity near $y = 0$ over which the average transverse momentum is equal for positive and negative pions, and relatively flat in rapidity for both cases. Thus we do observe a finite interval of rapidity over which the transverse momentum behavior of observed secondaries exhibits little or no dependence on either their charge or rapidity. This result is peculiar to the high energy data. In 16 GeV/c π^-p collisions [7] a rapidity-independent interval is observed for π^+ but not for π^-.

As an indication that this behavior is a consequence of local compensation of transverse momentum near $y = 0$, we show in fig. 2d the correlation function

$$C(\Delta y) = -\langle \boldsymbol{p}_{t,f} \cdot \boldsymbol{p}_{t,b} \rangle.$$

Here, for a given event, $\boldsymbol{p}_{t,f}$ is the net transverse momentum of charged secondaries for $y \geqslant +\Delta y/2$, and $\boldsymbol{p}_{t,b}$ the net observed transverse momentum for $y < -\Delta y/2$.

The average is taken over the entire inelastic event sample. The distribution in $C(\Delta y)$ falls rapidly to zero with a correlation length typical of the characteristic lengths found in the central region for 2-particle rapidity distributions ($\sim$1.5 units).

Although more definitive conclusions from this data must await similar studies at other energies, and may not be possible without direct information from neutral secondaries, it seems reasonable to draw the conclusion that transverse momentum is locally conserved over a small rapidity intervals in the central region.

We next address the question of whether electric charge is locally conserved in rapidity by studying the charge transfer variable

$$u(\Delta y) = 1/2\,(Q_f - Q_b) + 1,$$

where, for a given event, Q_f is the net charge forward of $y = +\Delta y/2$ and Q_b is the net charge backward of $y = -\Delta y/2$.

The term +1, which is not present in the usual definition for p-p collisions, accounts for the opposite charges of the incident particles. $u(0)$ is a measure of the net charge-transfer across a boundary at $y = 0$. For non-zero values of Δy, $u(\Delta y)$ measures the charge transferred across an interval of length Δy, centered at $y = 0$. Quigg [2] has discussed the interpretation of this variable in terms of a specific cluster emission model. We draw here on the qualitative aspects of such an interpretation.

For independent particle emission in the central region one expects $\langle u^2(0)\rangle$ to be independent of bombarding energy and of the incident channel quantum numbers. The value of $\langle u^2(0)\rangle$ obtained from the data of this experiment is 1.0 ± 0.1, in good agreement with the results obtained in proton-proton collisions at 105 GeV/c (0.90 ± 0.04, [9]) and 205 GeV/c (0.99 ± 0.03, Kafka et al., [1]).

In fig. 3 we show the distributions in $D^2(\Delta y) = \langle u^2\rangle - \langle u\rangle^2$. The variable D^2 measures the width of the distribution in u, or the strength of the event-to-event fluctuations in the charge transferred across the interval Δy. The data are shown as a function of Δy for various final-state topologies as well as for the total sample. For the inelastic 2-prong data, which are dominated by two-body diffractive processes, D^2 is essentially independent of the rapidity interval except for phase space effects at the kinematic limit. For the higher multiplicities, if charge is locally conserved in the central and fragmentation regions, we expect large values for $D^2(0)$ due to statistical fluctuations which decrease as Δy is increased. As Δy spans the central region and extends into the fragmentation regions, D^2 should become independent of Δy, as in in the case of the diffractive dominated 2- and 4-prong events. The essential result here is that this behavior is clearly observed in the 6-, 8- and 10-prong events: The distributions fall sharply from their values at $\Delta y = 0$, then break and level off before falling again as phase space effects take over at large intervals. This behavior is very similar to that observed in pp collisions at 205 GeV/c [10]. The width of the central region fall-off corresponds well with that observed for the transverse momentum correlations in fig. 2.

Thus, while our data have as a gross feature clear asymmetries in the forward-backward charged pion distributions for even the high multiplicity channels, there is also evidence of the short-range behavior in the central region which has motivated cluster emission models for particle production. The data support the hypothesis that charge, and perhaps transverse momentum, are locally conserved on the rapidity axis.

If the inelastic scattering process is dominated by the production of clusters of hadrons, the absence of an electrically neutral central region in π^-p collisions at Fermilab energies may result from the fact that the net charges of individual clusters vary as a function of the rapidity from target-like quantum numbers in the extreme backward direction to beam-like in the forward direction. If this were the case, a neutral central region would presumably develop at higher energies. We note, as has been pointed out before [11], that in such a picture there need be little distinction between the diffractive and high-multiplicity components of inelastic particle production: the former being simply an example of the clustering phenomenon in low-multiplicity final states.

We gratefully acknowledge the efforts on behalf of this experiment by the Fermilab Neutrino Section and 30-in. bubble chamber staffs, and the scanning and measuring personnel of the participating universities.

[1] J. Ranft and G. Ranft, Phys. Letters 49B (1974) 286; T. Kafka et al., Phys. Rev. Letters 34 (1975) 687; C. Quigg et al., Phys. Rev. Letters 34 (1975) 290; C. Bromberg et al., Phys. Rev. D12 (1975) 1224.
[2] The phenomenology of local quantum number compensation is discussed in A. Krzywicki and D. Weingarten, Phys. Letters 50B (1974) 265, and C. Quigg, Fermilab-Pub-74/104-THY (1974), Phys. Rev. D (to be published).
[3] V.P. Kenney et al., Leading particles and leading clusters in π^-p single particle inclusive reactions at 200 GeV/c, Notre Dame Preprint (1975).
[4] W.B. Fretter et al., Phys. Letters 57B (1975) 197.
[5] The proportional wire hybrid system is described in D. Fong et al., Phys. Letters 53B (1974) 290.
[6] D. Fong et al., Cross sections and multiplicity distributions for π^-p and K$^-$p interactions at 147 GeV/c, (Sept., 1975), submitted to Nuclear Physics B.
[7] P. Bosetti et al., Nucl. Phys. B54 (1973) 141.
[8] A similar correlation function is discussed by D. Weingarten, Suggestion for testing the hypothesis of local compensation of transverse momentum, (1975), University of Rochester Preprint.
[9] C.M. Bromberg et al., Phys. Rev. D9 (1974) 1864.
[10] The data to which we refer are reported by Quigg, [2].
[11] T. Ludlam et al., Phys. Letters 48B (1974) 449.

PHYSICAL REVIEW D VOLUME 12, NUMBER 3 1 AUGUST 1975

Local quantum-number compensation in multiple production

C. Quigg*

Fermi National Accelerator Laboratory,† Batavia, Illinois 60510

(Received 25 November 1974)

Experimental distributions are defined which are sensitive to the existence and nature of short-range phenomena. Clustering of produced hadrons is established directly. The possibility that clusters responsible for strange particle or baryon production differ from those responsible for pion production is entertained. Similarities and distinctions between transverse momentum and other additive quantum numbers are discussed.

I. INTRODUCTION

Short-range correlations in rapidity appear to be one of the prominent features of multiple production at high energies. It is also generally accepted that long-range correlations arise from interference between diffractive and nondiffractive components of the production cross section.[1] Whether intrinsic long-range correlations are present within the nondiffractive component is uncertain. However, whatever other effects might be present, considerable indirect evidence does exist for the dominance of short-range phenomena in the nondiffractive component. This paper deals with the existence and the origins of such phenomena.

It is now widely held that a useful, if somewhat ingenuous, description of the origin of short-range correlations is provided by cluster emission models.[2,3] Despite successes of cluster models and the circumstantial evidence for clustering, some efforts persist to show, by means of Monte Carlo simulations, that experimental features adduced in support of the short-range correlation hypothesis do not depend upon short-range correlation dynamics. In my opinion, these efforts need not be taken seriously in themselves,[4] but they raise a valid challenge which should be met: to provide unambiguous evidence for short-range phenomena. I see, therefore, two immediate objectives in the study of nondiffractive multiple production. First, it is important to verify the existence of short-range phenomena and to quantify their properties. It will then be obligatory to ask whether the cluster description of the short-range correlation dynamics is a necessity of merely a useful fiction.[5] In other words, it will be necessary to find the clusters.

In this paper two topics are studied in pursuit of these objectives. In Sec. II I discuss tests of the hypothesis that internal quantum numbers are conserved locally in rapidity. This hypothesis follows naturally from any (factorizable) t-channel exchange picture, and is an immediate corollary of cluster or short-range correlation dynamics. Data are presented which give a direct demonstration of the local compensation of electric charge, and the extension to other internal quantum numbers is treated. In Sec. III I investigate the consequences of local compensation of transverse momentum. The information contained in a number of new experimental distributions is developed in detail. If the transverse momenta of all secondaries (including neutrals) can be measured, a technique exists for probing the transverse momentum distribution of clusters. A summary is given in Sec. IV.

II. LOCAL COMPENSATION OF INTERNAL QUANTUM NUMBERS

In this section I shall develop direct experimental evidence for the local compensation of electric charge and provide a direct measure of the mobility[6] of electric charge. My immediate interest is to deduce characteristics of multiple production and to integrate them with existing information. However, as a number of authors have emphasized recently,[7] the unitarity equation connects the locality of quantum-number compensation with the energy dependence of two-body to two-body quantum-number exchange reactions. An accurate determination of, for example, charge mobility in collisions at different primary energies bears not only on the tenability of the cluster description, but also on the origin of the energy dependence of charge exchange cross sections.[8]

A. Local charge compensation

The analysis of charge transfer observables[9] has verified in detail[10] the predictions of the independent cluster emission picture.[11-14] This success was a psychological prerequisite for the present investigation, in which I rely upon a specific, idealized short-range-order model to anticipate the data. It will, however, soon become apparent

that the qualitative theoretical expectations do not rest on details of the model. The basic assumption to be tested is that charge compensation is a short-range phenomenon. In the specific language of cluster models, the corresponding assumption is that observed hadrons emanate from independently emitted clusters, are characterized by a mobility in rapidity from their parent cluster, and experience no final-state interactions. In this picture all short-range correlations are intracluster effects. I shall use a simplified one-dimensional model to explore the consequences of this assumption.[15] In the model neutral three-pion clusters ($\pi^+\pi^-\pi^0$) have an equal chance to be produced anywhere in the available rapidity interval $[-Y/2, Y/2]$. A cluster produced at rapidity $\hat{y}$ will yield pions at rapidities $\hat{y}-\Delta$, $\hat{y}$, and $\hat{y}+\Delta$, where Δ will be called the mobility. The transfer of charge from one c.m. hemisphere to the other is therefore a consequence of decays of clusters in the active region $(-\Delta, \Delta)$. For every cluster the correspondence between rapidities $(\hat{y}-\Delta, \hat{y}, \hat{y}+\Delta)$ and pion charges $(-1, 0, +1)$ can be made in six equally probable ways. Each cluster in the active region has a $\frac{1}{3}$ probability to contribute $(-1, 0, +1)$ to the *net charge transfer*,

$u = \frac{1}{2}$ (total charge in the forward hemisphere minus beam charge)

$-\frac{1}{2}$ (total charge in the backward hemisphere minus target charge),

independent of the behavior of other clusters.

The consequences of this model in the usual experimental situation were dealt with in Ref. 11. Let us now turn our attention to charge transfer across a gap centered at zero c.m. rapidity. Clearly, when the gap width exceeds the cluster mobility, no charge is actually exchanged between the forward and backward regions. The tedious calculations to be described lead to the following important qualitative result. As the gap width G is increased from 0 to 2Δ, the mean-squared charge fluctuation at fixed topology, $\langle u^2\rangle_n$, decreases. For $G > 2\Delta$, $\langle u^2\rangle_n$ remains constant, independent of G, until forced by kinematical end effects to decrease to zero. The experimental observation of this behavior provides direct evidence for a short-range, or clustering, effect and yields a direct measure of the mobility Δ.

It is convenient to employ the generating function technique introduced in Ref. 11. Let us define

$$p \equiv 2\Delta/Y, \qquad (1)$$
$$g \equiv G/Y,$$

and construct the generating function $P_N(x)$ corresponding to the emission of N clusters, in terms of which[16]

$$\langle u^k\rangle_N = (\tfrac{1}{2}x\partial_x)^k P_N(1). \qquad (2)$$

Three cases must be distinguished: (i) $G<\Delta$; (ii) $\Delta<G<2\Delta$; (iii) $G>2\Delta$. In each case, pions which are products of clusters emitted in certain intervals may go unobserved in the gap. The various possibilities are identified in Fig. 1. It is then a straightforward counting exercise to determine, for each interval marked in Fig. 1, the probability that a specific charge transfer will occur and so to construct the appropriate generating function. The results are

$$P_N(x) = \left[(1-p-g) + \frac{p-2g}{3}(x^2+1+x^{-2}) + \frac{g}{6}(x^2+2x+2/x+x^{-2}) + \frac{2g}{3}(x+1+1/x)\right]^N, \qquad (3)$$

$$\langle u^2\rangle_N = N\left[\frac{2p}{3} - \frac{g}{2}\right], \qquad (4)$$

if $0<G<\Delta$;

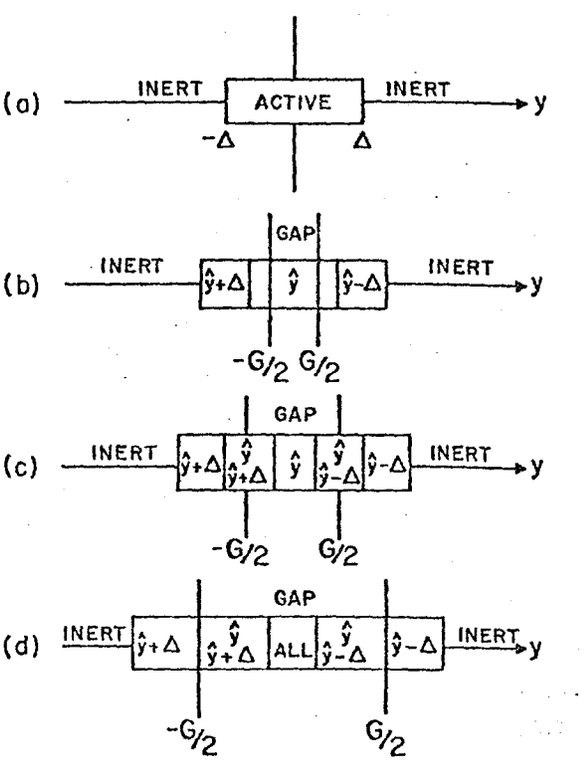

FIG. 1. Partitions used in the discussion of quantum-number transfer across a gap. The abscissa is c.m. rapidity. Notations (e.g., $\hat{y}+\Delta$) in an indicated region specify the lost pions originating from clusters in that region. (a) No gap; (b) $G<\Delta$; (c) $\Delta<G<2\Delta$; (d) $G>2\Delta$.

$$P_N(x)=\left[(1-p-g)+\frac{2g}{3}(x+1+1/x)+\frac{p-g}{6}(x^2+2x+2/x+x^{-2})\right]^N, \quad (5)$$

$$\langle u^2\rangle_N = N\left[\frac{p}{2}-\frac{g}{6}\right], \quad (6)$$

if $\Delta < G < 2\Delta$; and

$$P_N(x)=\left[(1-2p)+\frac{2p}{3}(x+1+1/x)\right]^N, \quad (7)$$

$$\langle u^2\rangle_N = Np/3, \quad (8)$$

if $G > 2\Delta$.

The expected gap dependence of the charge transfer fluctuation is sketched in Fig. 2. This prediction is to be compared with the experimental results[17] from the Fermilab 205-GeV/c bubble-chamber exposure, which are shown in Fig. 3. The two-prong and four-prong events are largely quasi-two-body in character, so they should not display the features expected in the cluster picture. Indeed, they do not. For the 6-, 8-, and 10-prongs, there is clear evidence of a rapid decrease in the charge transfer fluctuation as G increases from 0 to 1.5, followed by an interval in which $\langle u^2\rangle_N$ is essentially independent of G. The absence of any plateau in the 12-prongs is consistent with the observed shape of $d\sigma_{12}/dy$. For such a high multiplicity, the region (in G) in which $\langle u^2\rangle_N$ decreases because of local charge compensation overlaps with the region in which the kinematically imposed decrease occurs. To emphasize the importance of these results, I remark that if individual pions were independently emitted, $\langle u^2\rangle_N = (N/4)(1-G/Y)$, so no plateau would be seen.

Several important conclusions may be drawn from these data.[18]

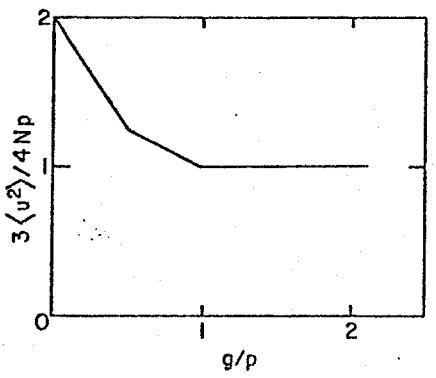

FIG. 2. Prediction of Eqs. (4), (6), and (8) for the fluctuation in charge transferred across a gap in events of fixed topology.

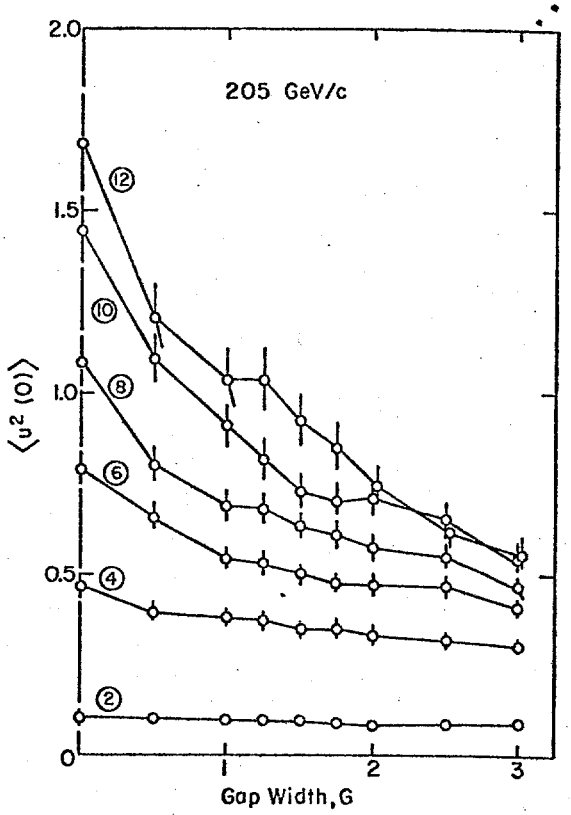

FIG. 3. Fluctuations in charge transfer across a gap in fixed-topology events in 205-GeV/c pp collisions (from Ref. 18).

(1) Charge is compensated locally in rapidity in multiparticle production. For this to be so in the sense of Refs. 7, it must further be shown that the mobility of charge is independent of energy.

(2) The mobility of electric charge, which is $\Delta \approx 0.75$ in 205-GeV/c pp collisions, appears not to depend strongly on event topology.

(3) The measured charge mobility is quite consistent with the expectations of the isotropic cluster decay model and with the range parameter deduced from fits to the two-particle correlation function in the central region.[19] It also agrees with the value inferred from data on forward-backward multiplicity correlations across a gap at this energy.[2,17]

It is of great interest to compare these results with measurements of charge mobility at other energies, and in collisions initiated by other beams. Unfortunately the existing statistics at 102 and 405 GeV/c are inadequate for this purpose.[20]

B. Other internal quantum numbers

In the context of explicit exchange models it is natural to suppose that rare quantum numbers

such as strangeness and baryon number might be conserved more locally than charge, because the corresponding Regge trajectories are lower-lying than those which carry charge. Equivalently, arguments based on Q values of known resonances[21] (e.g., $\phi, A_2 - K\bar{K}$ *versus* $\rho, f - \pi\pi$) lead to the same expectations. According to the Mueller-Regge analysis of two-particle correlations in the central region, for $K\bar{K}$ correlations there will be a correlation length = 1 term arising from ϕ and f^* exchange, in addition to the usual correlation length = 2 term. The same considerations applied to the $N\bar{N}$ case are less enlightening.[22] It is highly desirable to subject these preconceptions to experimental tests. Given the difficulty of identifying particles in a large-acceptance detector, the task is not an easy one, but in the following discussion I will assume that all such technical difficulties can be overcome.

The transfer of any additive quantum number across a gap in rapidity can be treated in the same manner as electric charge, so that the results of Sec. II A are immediately applicable. A closely related distribution also is useful for studying the mobility of quantum numbers explicitly absent from the initial state (e.g., strangeness in pp collisions). Consider a bin of extent B in rapidity which lies fully within the central region. The dependence upon bin size of the mean-squared fluctuation in the amount of an additive quantum number confined within the bin is governed by the locality of compensation of that quantum number. To be specific, let us consider strangeness compensation in a model with "ϕ" $- K\bar{K}$ clusters. A cluster produced at $\hat{y}$ gives rise to kaons at $\hat{y} \pm \Delta$. By performing the same kind of counting as occurred in the charge transfer example, we can construct a generating function $R_N(x)$ appropriate for the emission of N "ϕ" clusters, in terms of which

$$\langle S^2 \rangle_N = (x\partial_x)^2 R_N(1), \tag{9}$$

where S represents the total strangeness contained in the bin.

For $B < 2\Delta$, the generating function is

$$R_N(x) = [(1-2b) + b(x + 1/x)]^N, \tag{10}$$

where $b \equiv B/Y$, and

$$\langle S^2 \rangle_N = 2Nb = 2NB/Y. \tag{11}$$

For $B > 2\Delta$, the corresponding results are

$$R_N(x) = [(1-2p) + p(x + 1/x)]^N \tag{12}$$

and

$$\langle S^2 \rangle_N = 2Np = 4N\Delta/Y. \tag{13}$$

The average over cluster multiplicities yields

$$\langle\langle S^2 \rangle\rangle = \begin{cases} 2\langle N \rangle B/Y, & B < 2\Delta \\ 4\langle N \rangle \Delta/Y, & B > 2\Delta. \end{cases} \tag{14}$$

The strangeness fluctuation increases with bin size, attaining a saturation value at $B = 2\Delta$, the point at which entire clusters may be confined within the bin. This behavior is sketched in Fig. 4.[23] It is completely analogous to the case of quantum-number transfer across a gap sketched in Fig. 2. The onset of B independence both establishes the locality of strangeness compensation and measures the mobility of strangeness. Evidently the same expectations apply to any additive quantum number.

III. LOCAL COMPENSATION OF TRANSVERSE MOMENTUM

Knowledge of the mobility of transverse momentum will be especially useful for making inferences about the underlying (exchange?) mechanism of particle production. In many respects, transverse momentum is simply another additive quantum number[24] (although a continuous, rather than a discrete one), and can be treated on the same footing as the others. The important practical distinction is that, unlike visible charge, the visible transverse momentum is not balanced event-by-event in bubble-chamber pictures. If all produced particles including neutrals could be measured, the techniques of Sec. II would be useful for measuring transverse momentum mobility as well. If neutrals go undetected, the theoretical expectations are modified to the extent that no effects as striking as those already discussed will appear.

A very simple model suffices to explore the possibilities. I assume that transverse momenta $\gamma, 0, -\gamma$ are carried by the pion products of an "ω" cluster. For each cluster, the correspondence between rapidities $(\hat{y} - \Delta, \hat{y}, \hat{y} + \Delta)$, pion charges $(-1, 0, 1)$, and transverse momenta $(-\gamma, 0, \gamma)$ can be made in 36 equally probable ways. It is

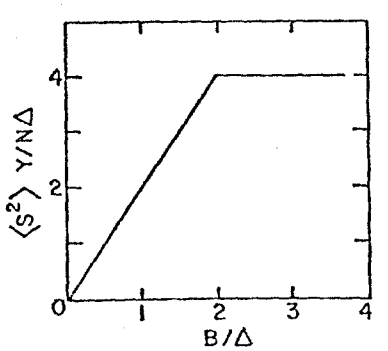

FIG. 4. Prediction for quantum-number deposit in a bin.

convenient to define, in analogy with charge transfer, the net transverse momentum transfer

$$v \equiv \tfrac{1}{2}\,(\text{visible transverse momentum in the forward hemisphere}) - \tfrac{1}{2}\,(\text{visible transverse momentum in the backward hemisphere}). \quad (15)$$

Because neutrals go undetected, each inactive cluster will make a contribution to v of $(-\gamma/2, 0, \gamma/2)$ with equal probability. Each cluster in the active region will contribute $(-\gamma, -\gamma/2, 0, \gamma/2, \gamma)$ with probability $(\frac{1}{9}, \frac{1}{3}, \frac{1}{9}, \frac{1}{3}, \frac{1}{9})$. Hence

$$T_N(x) = \left[\frac{(1-p)}{3}(x+1+1/x) + \frac{p}{9}(x^2+3x+1+3/x+x^{-2})\right]^N$$

is a generating function in terms of which

$$\langle v^k \rangle_N = (\tfrac{1}{2}\gamma x \partial_x)^k T_N(1). \quad (17)$$

The mean-squared fluctuation of $p_\perp$ transfer in N-cluster events is

$$\langle v^2 \rangle_N = \frac{4\Delta\gamma^2}{9}\frac{N}{Y} + \frac{\gamma^2 N}{6}, \quad (18)$$

which should be compared with the charge transfer fluctuation

$$\langle u^2 \rangle_N = \frac{4\Delta}{3}\frac{N}{Y}. \quad (19)$$

The first term in (18) has the expected form for the fluctuation of $p_\perp$ transfer arising from the decay of active clusters. The second term, which is proportional to the number of clusters instead of the cluster density, represents the event-to-event imbalance in visible transverse momentum. The origin of this term in the nonobservation of neutrals is made more explicit if N is replaced by the associated multiplicity of neutrals, so that

$$\langle v^2 \rangle_N = \frac{4\Delta\gamma^2}{9}\frac{N}{Y} + \frac{\gamma^2}{6}\langle n_0(N) \rangle. \quad (20)$$

The quantity N/Y represents the mean density of clusters in the active region, $\langle dN(\bar{y})/dy \rangle$, where the brackets imply an average over the region $(\bar{y}-\Delta, \bar{y}+\Delta)$. This in turn is related to the observed density of charged pions by

$$\left\langle \frac{dN}{dy}(\bar{y}) \right\rangle \simeq \frac{1}{2}\left\langle \frac{1}{\sigma_n}\frac{d\sigma_n}{dy}(\bar{y}) \right\rangle, \quad (21)$$

where the factor $\frac{1}{2}$ occurs because each cluster produces two charged particles, and $n = 2N+2$ in pp collisions. Therefore, the fluctuation in charge transferred across an arbitrary boundary at $\bar{y}$ in n-prong events will be

$$[D_n^{(\text{charge})}(\bar{y})]^2 \simeq \frac{2\Delta}{3\sigma_n}\left\langle \frac{d\sigma_n}{dy}(\bar{y}) \right\rangle, \quad (22)$$

whereas the corresponding fluctuation in $p_\perp$ transfer will be

$$[D_n^{(p_\perp)}(\bar{y})]^2 \simeq \frac{2\Delta\gamma^2}{9\sigma_n}\left\langle \frac{d\sigma_n}{dy}(\bar{y}) \right\rangle + \frac{\gamma^2}{6}\langle n_0(n) \rangle. \quad (23)$$

The structure of Eqs. (22) and (23) is characteristic of the cluster picture, but the numerical factors depend on the explicit parameters of the model. The forms of both (22) and (23) have been verified in the 205-GeV/c data,[25] for events with at least six charged prongs. However, the extraction of charge mobility or transverse momentum mobility from these distributions would be rather model-dependent.

The transfer of transverse momentum across a gap can be studied in the same fashion as that of other additive quantum numbers. Without neutral detection, it is not possible to give direct evidence for short-range effects. The remaining results, therefore, are presented not because they are intrinsically interesting, but to indicate how much experiments are compromised by the inability to measure neutrals. What follows may be regarded as case for highly efficient detection of *all* produced particles. The results are

$$T_N(x) = \left[\frac{1-p-g}{3}(x+1+1/x) + \frac{p-2g}{9}(x^2+3x+1+3/x+x^{-2}) + \frac{g}{18}(x^2+6x+4+6/x+x^{-2})\right]^N, \quad (24)$$

$$\langle v^2 \rangle_N = \frac{N\gamma^2}{18}[3+4p-6g], \quad (25)$$

if $0 < G < \Delta$;

$$T_N(x) = \left[\frac{1-g}{3}(x+1+1/x) + \frac{p-g}{18}(x^2+6x+4+6/x+x^{-2}) + \frac{2g-p}{9}(2x+5+2/x)\right]^N, \quad (26)$$

$$\langle v^2 \rangle_N = \frac{N\gamma^2}{18}[3+3p-4g], \quad (27)$$

if $\Delta < G < 2\Delta$;

$$T_N(x) = \left[(g-p) + \frac{1-g}{3}(x+1+1/x) + \frac{p}{9}(2x+5+2/x)\right]^N, \quad (28)$$

$$\langle v^2 \rangle_N = \frac{N\gamma^2}{18}[3+2p-3g], \quad (29)$$

if $G > 2\Delta$ (but $G+2\Delta < Y$). The dependence of $\langle v^2 \rangle_N$ upon the gap size is sketched in Fig. 5. In contrast to the behavior indicated in Fig. 2, which would apply to $p_\perp$ if neutrals were also observed,

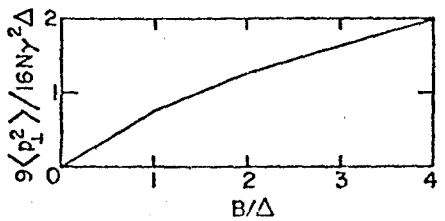

FIG. 5. Prediction of Eqs. (25), (27), and (29) for the fluctuation in transverse momentum transferred across a gap if neutrals are not observed.

there is no striking change in the behavior of $\langle v^2\rangle_N$ at the point in $G=2\Delta$. Basically this is because the larger the gap, the smaller are the event-to-event fluctuations in visible transverse momentum transfer.

The same shortcoming applies to the dependence upon bin size of the mean-squared transverse momentum confined in a bin within the central region. In the schematic model considered here, one expects

$$\langle p_\perp^2\rangle_N = \frac{4\gamma^2\Delta}{9}\frac{N}{Y}\times\begin{cases} 3B/\Delta, & 0\leq B<\Delta \\ 1+2B/\Delta, & \Delta\leq B<2\Delta \\ 2+3B/2\Delta, & B\geq 2\Delta. \end{cases} \quad (30)$$

This behavior, which is sketched in Fig. 6, is to be contrasted with what would be found if neutrals were measured also. The latter situation corresponds to Fig. 4.

IV. SUMMARY

Charge is balanced locally in rapidity, as expected in short-range correlation models. In such models it is required that the mobility of charge be independent of the incident beam energy. This prediction has not been tested. The measured

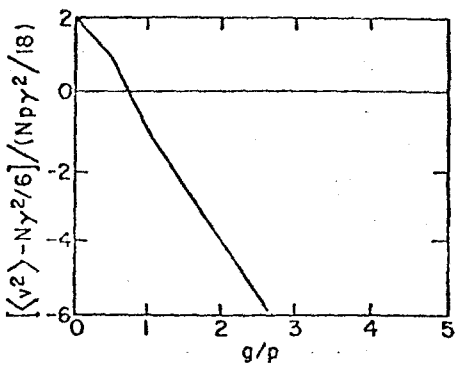

FIG. 6. Prediction for transverse momentum deposit in a bin if neutrals are not observed.

mobility of charge is compatible with the observed range of two-particle rapidity correlations. Measurement of the mobility of other internal quantum numbers will provide important insights into the nature of the particle production mechanism. Although it is attractive to suppose that transverse momentum is balanced locally, and existing experimental results are consistent with this hypothesis, no direct proof is possible unless the momenta of all produced particles can be measured. Verification of local transverse momentum compensation is an important goal.

ACKNOWLEDGMENTS

This work was begun at the State University of New York at Stony Brook. It is a pleasure to thank my former colleagues, R. Engelmann, T. Kafka, and M. Pratap, for their stimulating cooperation, and for permission to cite their unpublished data. I also appreciate the interest of C. Bromberg and T. Ferbel.

---

*Alfred P. Sloan Foundation Fellow. Also at Enrico Fermi Institute, University of Chicago, Chicago, Illinois 60637.

†Operated by Universities Research Association Inc. under contract with the United States Atomic Energy Commission.

[1]C. Quigg, in *Proceedings of the Canadian Institute of Particle Physics Summer School, McGill University, 1973*, edited by R. Henzi and B. Margolis (Institute of Particle Physics, Montreal, 1974), p. 517; H. Harari, in *Phenomenology of Particles at High Energies*, edited by R. L. Crawford and R. Jennings (Academic, New York, 1974), p. 297. These lecture notes provide extensive references to the primary literature.

[2]A. W. Chao and C. Quigg, Phys. Rev. D 9, 2016 (1973); S. Pokorski and L. Van Hove, Acta. Phys. Polon. B5, 229 (1974).

[3]The most extensive development since the summaries contained in the introductory sections of Refs. 2 has been in the area of semi-inclusive correlations. See, for example, E. L. Berger, Phys. Lett. 49B, 369 (1974); Nucl. Phys. B85, 61 (1975); J. Ranft and G. Ranft, Phys. Lett. 49B, 286 (1974); A. Morel and G. Plaut, Nucl. Phys. B78, 541 (1974); R. Arnold and G. H. Thomas, Phys. Rev. D 9, 3121 (1974); F. Hayot and M. Le Bellac, Nucl. Phys. B86, 333 (1975).

[4]When such programs succeed, it invariably develops that dynamics have been imposed, either implicitly or unwittingly.

[5]For some recent evidence in favor of the cluster interpretation, see C. Quigg, P. Pirilä, and G. H. Thomas, Phys. Rev. Lett. 34, 290 (1975).

[6]Although I shall consistently use this nomenclature, the reader who is more comfortable with terms such as

range, correlation length, cluster mass, Q value, etc. is welcome to substitute them at this point.

[7]Chan Hong-Mo and J. E. Paton, Phys. Letters 46B, 228 (1973); A. Krzywicki and D. Weingarten, *ibid.* 50B, 265 (1974); P. Grassberger, C. Michael, and H. I. Miettinen, *ibid.* 52B, 60 (1974); A. Krzywicki, Nucl. Phys. B86, 296 (1975); D. Weingarten, Phys. Rev. D11, 1924 (1974).

[8]In exchange models these questions are not separate; charge mobility and charge-exchange energy dependence both are prescribed by (or prescribe) the hadron spectrum. If the only theoretical constraint imposed is unitarity (which is the spirit of Refs. 7), it is not disingenuous to seek an explanation of the one in terms of the other.

[9]T. T. Chou and C. N. Yang, Phys. Rev. D 7, 1425 (1973).

[10]U. Idschok *et al.* (Bonn-Hamburg-Munich Collaboration), Nucl. Phys. B67, 93 (1973); T. Ferbel, in *Particles and Fields—1973,* proceedings of the Conference on Particles and Fields, Berkeley, California, 1973, edited by H. H. Bingham, M. Davier, and G. Lynch (A.I.P., New York, 1973), p. 400; J. Whitmore, in *Experiments on High Energy Particle Collisions—1973,* proceedings of the International Conference on New Results from Experiments on High Energy Particle Collisions, Vanderbilt University, 1973, edited by Robert S. Panvini (A.I.P., New York, 1973), p. 14; T. Kafka *et al.*, Phys. Rev. Lett. 34, 687 (1975); C. Bromberg *et al.*, Rochester Report No. UR-522 (unpublished); E. Malamud *et al.*, Bull. Am. Phys. Soc. 20, 591 (1975).

[11]C. Quigg and G. H. Thomas, Phys. Rev. D 7, 2752 (1973).

[12]A. Białas, in *Proceedings of the IVth International Symposium on Multiparticle Hadrodynamics, Pavia, Italy, 1973,* edited by F. Duimio, A. Giovannini, and S. Ratti (Instituto Nazionale di Fisica Nucleare, Pavia, 1974), p. 93.

[13]P. Bosetti *et al.* (Aachen-Berlin-CERN-London-Vienna Collaboration), Nucl. Phys. B62, 46 (1973); Argonne–Fermilab–Stony Brook Collaboration, quoted by Chao and Quigg, Ref. 2.

[14]A. Białas, K. Fiałkowski, M. Jezabek, and M. Zieliński, Acta Phys. Polon. B6, 59 (1975).

[15]It will be obvious, and has also been shown explicitly in Ref. 14, that no important features of the cluster picture are compromised by the idealization, for the observables discussed here.

[16]That is, the coefficient of x^{2q} in a power-series expansion of $P_N(x)$ is the probability that an N-cluster event will lead to charge transfer q.

[17]ANL–Fermilab–Stony Brook Collaboration (unpublished).

[18]The presence of intrinsic (but limited) charge exchange between clusters would not affect these conclusions. Whether clusters are neutral or only nearly neutral (carrying limited charge) is immaterial except for numerical details I shall not discuss.

[19]For a review, see G. H. Thomas, in *Proceedings of the XVII International Conference on High Energy Physics,* edited by J. R. Smith (Rutherford Laboratory, Chilton, Didcot, Berkshire, England, 1974), p. I-83.

[20]I thank C. Bromberg and T. Ferbel for sending me the Michigan-Rochester data at these energies.

[21]From all indications, clusters closely resemble the prominent resonances. See Ref. 5, and P. Pirilä, G. H. Thomas, and C. Quigg, Phys. Rev. D 12, 92 (1975).

[22]I suspect this is because of the familiar problems of duality diagrams for two-body $N\bar{N}$ scattering.

[23]Although the boundaries of the allowed phase space have been excluded from my considerations, it is obvious that as $b \to 1$ (so that all produced particles are contained in the bin) the fluctuations $\langle\langle S^2\rangle\rangle \to 0$.

[24]A. Białas emphasized this similarity in a parallel session of the XVII International Conference on High Energy Physics, London, 1974. His remark stimulated the investigation summarized here, in which I have tried to specify what is to be learned from a study of $p_\perp$ transfer. Since this paper was submitted for publication, A. Białas *et al.*, Nucl. Phys. B86, 365 (1975), have reported a study of $p_\perp$ transfer in fitted events in 12- and 24-GeV/c pp collisions. More recently, Krzywicki, Ref. 7, has attempted to use local $p_\perp$ compensation as a starting point for overlap function calculations.

[25]T. Kafka (private communication).

found. The existence of gaugelike invariance for the equation satisfied by (u, ζ) makes it possible to find a self-Bäcklund transformation for q and q'. These Bäcklund transformations can be divided into classes. Equations in the same class have an identical spatial part of their Bäcklund transformations. Their solutions therefore satisfy the same superposition formula. For example the mKdV and sine-Gordon equations have the same superposition formula,

$$\tan\frac{w_3-w_0}{2}=\frac{k_1+k_2}{k_1-k_2}\tan\frac{w_1-w_2}{2}.$$

This formula renders it possible to construct N-soliton solutions by algebraic manipulations only.

Further generalizations to higher-order inverse problems of what has been done above is possible. I will report some examples in another paper.

The author wishes to thank Professor C. S. Liu for helpful discussions.

*Research sponsored by the U. S. Atomic Energy Commission under Grant No. AT(11-1)-3237.

[1]M. J. Ablowitz, P. J. Kaup, A. C. Newell, and H. Segur, Phys. Rev. Lett. 31, 125 (1973).

[2]C. S. Gardner, J. M. Green, M. D. Kruskal, and R. M. Miura, Phys. Rev. Lett. 19, 1095 (1969).

[3]M. Wadati, J. Phys. Soc. Jpn. 34, 1289 (1973).

[4]M. J. Ablowitz, D. J. Kaup, A. C. Newell, and H. Segur, Phys. Rev. Lett. 30, 1262 (1973).

[5]V. E. Zakharov and A. B. Shabat, Zh. Eksp. Teor. Fiz. 61, 118 (1971) [Sov. Phys. JETP 34, 62 (1972)].

[6]G. L. Lamb, Jr., Rev. Mod. Phys. 43, 99 (1971).

[7]H. D. Wahlquist and F. B. Estabrook, Phys. Rev. Lett. 31, 1386 (1973).

[8]R. Hirota, J. Math. Phys. (N.Y.) 14, 805 (1973).

Total Cross Sections of p and $\bar{p}$ on Protons and Deuterons between 50 and 200 GeV/c*

A. S. Carroll, I-H. Chiang, T. F. Kycia, K. K. Li, P. O. Mazur, P. Mockett,† D. C. Rahm, and R. Rubinstein‡
Brookhaven National Laboratory, Upton, New York 11973

and

W. F. Baker, D. P. Eartly, G. Giacomelli,§ P. F. M. Koehler, K. P. Pretzl,‖ and A. A. Wehmann
Fermi National Accelerator Laboratory, Batavia, Illinois 60510

and

R. L. Cool and O. Fackler
Rockerfeller University, New York, New York 10021

(Received 15 July 1974)

Proton and antiproton total cross sections on protons and deuterons have been measured at 50, 100, 150, and 200 GeV/c. The proton cross sections rise with increasing momentum. Antiproton cross sections fall with increasing momentum, but the rate of fall decreases between 50 and 150 GeV/c, and from 150 to 200 GeV/c there is little change in cross section.

We have measured p and $\bar{p}$ total cross sections on protons and deuterons in 50-GeV/c steps between 50 and 200 GeV/c. The experiment, which was carried out in the $M1$ beam[1,2] at the Fermi National Accelerator Laboratory, used a "good geometry" transmission technique.

Incident particles were defined by scintillation counters and identified by two differential gas Cherenkov counters,[3] allowing cross sections of two different particles to be measured simultaneously; in addition, a threshold gas Cherenkov counter[4] could be used in anticoincidence when required. Contamination of unwanted particles in the selected p and $\bar{p}$ beams was always below 0.1%.

The 3-m-long liquid hydrogen and deuterium targets and an identical evacuated target were surrounded by a common outer jacket of liquid hydrogen for temperature stability.[5] By continuously monitoring the vapor pressure in the oute jacket, the target temperature and therefore the hydrogen and deuterium densities were determined[6]; density variations were less than 0.07% throughout the experiment. Target lengths were

TABLE I. Results of this experiment: Cross sections in millibarns.

	Momentum (GeV/c)				
	50	100	150	200	Momentum-independent scale uncertainty
σ_{pp}	38.14 ± 0.07	38.39 ± 0.06	38.62 ± 0.06	38.90 ± 0.06	±0.5%
σ_{pd}	72.98 ± 0.13	73.12 ± 0.11	73.46 ± 0.11	73.84 ± 0.11	±0.6%
$\sigma_{\bar{p}p}$	43.86 ± 0.11	42.04 ± 0.09	41.72 ± 0.18	41.54 ± 0.29	±0.5%
$\sigma_{\bar{p}d}$	82.21 ± 0.24	79.32 ± 0.19	78.24 ± 0.35	78.77 ± 0.57	±0.6%
σ_{pn}	38.86 ± 0.16	38.85 ± 0.14	39.02 ± 0.14	39.18 ± 0.14	±1.5%
$\sigma_{\bar{p}n}$	43.69 ± 0.30	42.22 ± 0.23	41.32 ± 0.44	42.09 ± 0.71	±1.5%
$\sigma_{\bar{p}p} - \sigma_{pp}$	5.72 ± 0.13	3.65 ± 0.11	3.10 ± 0.19	2.64 ± 0.30	
$\sigma_{\bar{p}d} - \sigma_{pd}$	9.23 ± 0.28	6.20 ± 0.22	4.78 ± 0.37	4.92 ± 0.58	
$\sigma_{\bar{p}n} - \sigma_{pn}$	4.83 ± 0.34	3.37 ± 0.27	2.30 ± 0.46	2.91 ± 0.72	

asured under operating conditions to ±0.03%. he transmission through the targets was mea- ed by twelve scintillation counters of differ- diameters, with eleven independent channels ng formed by coincidences between pairs of acent counters to minimize accidental counts tube noise. These counters were mounted ether, smallest upstream, on a movable cart were positioned such that for each momentum counters accepted the same range of $|t|$, ex- ding up to 0.008 (GeV/c)^2 for the smallest nnel and up to 0.08 (GeV/c)^2 for the largest. efficiencies of the transmission counters e measured at frequent intervals throughout experiment using two small counters placed ind them. Such efficiencies were constant and ays >99.8%

or each momentum, the beam was tuned to a final focus at the transmission counters. sets of proportional wire chambers were in incident beam, each set giving two coordin- s, and a matrix coincidence was set up be- en appropriate wires to ensure that each in- ent particle trajectory would pass through a m square at the transmission counters.[7] This nique eliminates systematic effects in the ex- olation procedure from beam halo and pos- e beam instability. In addition, the electronic c for these chambers required that one and one particle register in each chamber. This, ther with large veto counters around the m, eliminated possible fluctuations due to ac- ntals. Cross sections were found to be stable etter than 0.2% for variations in beam flux of ctor of 3 around the value (2×10^5 per pulse) hich data were normally taken.

he data were corrected[8] for single Coulomb scattering (<0.1%) and Coulomb-nuclear interference (<0.3%). For the latter, the ratio ρ of real to imaginary parts of the forward scattering amplitude was obtained from Bartenev *et al.*[9] for pp and the predictions of Cheng *et al.*[10] for $\bar{p}p$. The value of ρ for neutrons was assumed to be the same as for protons.

The extrapolation to $t=0$ of the partial cross sections was carried out using the expression

$$\sigma_i = \sigma_T \exp(At_i + Bt_i^2 + Ct_i^3),$$

where σ_i is the partial cross section measured by the ith transmission counter combination subtending a maximum $|t_i|$, and σ_T is the total cross section. For all of the four cross sections measured here, the Bt_i^2 term was necessary, as determined by a substantial reduction in the χ^2 of the fit when it was added. For cross sections on protons, there was no change in the total cross section when the Ct_i^3 term was added, nor was there any change in χ^2, and so C was set equal to zero; for deuteron cross sections, the Ct_i^3 term was found to improve the fit substantially. The extrapolations were carried out using the third through the tenth transmission counter combinations, covering $0.016 \leq |t_i| \leq 0.062$ (GeV/c)^2. Using fewer counters changed the results by less than 0.1%, indicating negligible multiple Coulomb scattering and beam size effects in the counters used for the extrapolation. This method, of course, cannot take into account a rapid change in slope below 0.016 (GeV/c)^2.

From the reproducibility of our data we quote a momentum-dependent uncertainty in the results for a particular incident particle of ±0.15% for those cross sections where the statistical error was smaller than this. The momentum-indepen-

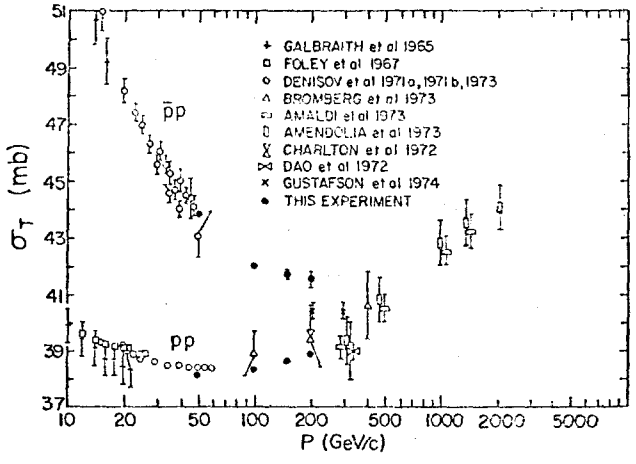

FIG. 1. Total cross sections for pp and $\bar{p}p$. Momentum-dependent errors only are shown. Data of other experiments are from Refs. 11-21.

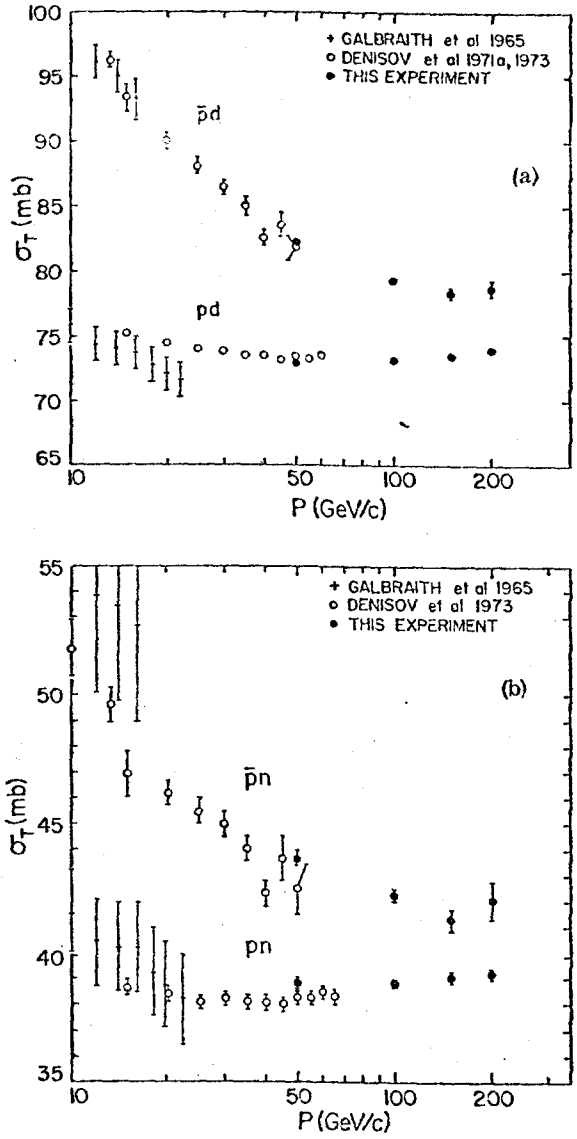

FIG. 2. Total cross sections for (a) pd and $\bar{p}d$, and (b) pn and $\bar{p}n$. Momentum-dependent errors only are shown. References as for Fig. 1.

dent scale uncertainty for the absolute magnitude of the cross section, caused by uncertainties in the form of the extrapolation and in the hydrogen and deuterium densities and contaminations, is estimated to be ±0.5% for protons and ±0.6% for deuterons.

The results are listed in Table I and shown in Figs. 1 and 2, together with previous data.[11-21] Agreement with other experiments in the same momentum range is within the quoted scale errors, except for that of Gustafson *et al.*[21]

As the incident momentum increases from 50 to 200 GeV/c the pp total cross section rises by 2%. The rise is consistent with the rise observed at the CERN intersecting storage rings.[17,18] The $\bar{p}p$ cross sections continue to fall with increasing momentum, but the rate decreases markedly, and above 150 GeV/c there is very little variation.

Cross sections of p and $\bar{p}$ on deuterons show a momentum dependence similar to those on protons. The $\bar{p}d$ cross section is also nearly constant above 150 GeV/c.

The antiparticle-particle differences $\sigma_{\bar{p}p} - \sigma_{pp}$ and $\sigma_{\bar{p}d} - \sigma_{pd}$ are shown in Fig. 3. These differences are becoming smaller with increasing momentum, and can be fitted by the form $As^{\alpha-1}$. Using only data from this experiment gives $\alpha = 0.39 \pm 0.04$ for $\sigma_{\bar{p}p} - \sigma_{pp}$ and $\alpha = 0.43 \pm 0.05$ for $\sigma_{\bar{p}d} - \sigma_{pd}$. If this form for $\sigma_{\bar{p}p} - \sigma_{pp}$ is extrapolated to higher momentum, together with the known σ_{pp}, an estimate of $\sigma_{\bar{p}p}$ at higher momenta can be obtained. This procedure predicts a minimum in the antiproton-proton cross section at about 200 GeV/c.

The purpose of measuring deuteron cross sections is to extract cross sections on neutrons. We have done this to within the accuracy of the Glauber-Wilkin formula,[22,23] which takes into account the shadowing in the deuteron. A parameter $\langle r^{-2} \rangle$ is used in the formula, and we have derived it from our pion data[24]; it is consistent with being momentum independent and averages 0.039 mb^{-1}. There has been recent discussion to whether this parameter is dependent upon the incident particle, or whether a more complex formula should be used.[25-28] Using the work of Gorin *et al.*[28] our measured value of $\langle r^{-2} \rangle$ would

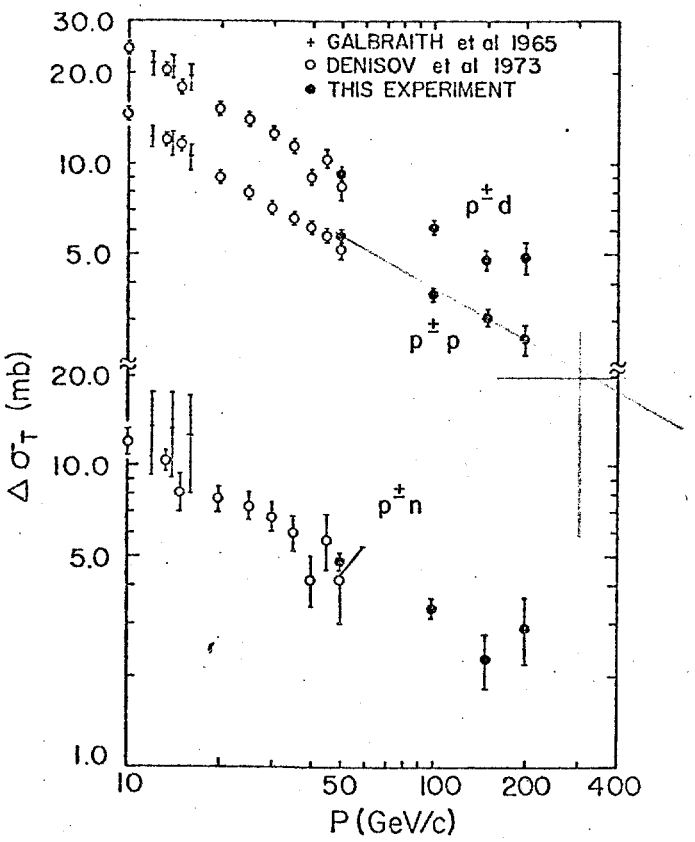

FIG. 3. Values of total-cross-section differences $\sigma_{\bar{p}d}-\sigma_{pd}$, $\sigma_{\bar{p}p}-\sigma_{pp}$, and $\sigma_{\bar{p}n}-\sigma_{pn}$. References as for Fig. 1.

be scaled to 0.031 mb^{-1} for incident protons. In view of the uncertainties in the method, we have used a value of 0.035 mb^{-1} with a systematic uncertainty of ± 0.004 mb^{-1} in extracting pn and $\bar{p}n$ cross sections. We note that this systematic uncertainty causes a $\pm 1.5\%$ scale uncertainty in the neutron cross sections, but does not affect the momentum dependence. We note further that the cross sections on neutrons shown in Fig. 1(b) have a behavior with momentum similar to those on protons. The difference $\sigma_{\bar{p}n}-\sigma_{pn}$, which is only slightly affected by the values of $\langle r^{-2}\rangle$, is shown in Fig. 3, and also shows the same behavior as on protons.

*Work supported by the U. S. Atomic Energy Commission.

†Present address: Physics Department, University of Washington, Seattle, Wash. 98195.

‡Present address: Fermi National Accelerator Laboratory, P. O. Box 500, Batavia, Ill. 60510.

§Visitor from Istituto di Fisica, University of Padova, and Istituto Nazionale di Fisica Nucleare, Sezione di Padova, Padova, Italy.

¶Present address: Max Planck Institute for Physics and Astrophysics, Munich, Germany.

[1]J. R. Orr and A. L. Read, NAL Meson Laboratory Preliminary Design Report, 1971 (unpublished).

[2]W. F. Baker *et al.*, NAL Report No. NAL-Pub.-74/13-EXP (unpublished), and to be published.

[3]T. F. Kycia, to be published.

[4]S. M. Pruss, NAL Report No. TM-470 (unpublished) and to be published.

[5]Targets of similar construction have been described by R. L. Cool *et al.*, Phys. Rev. D 1, 1887 (1970), and W. Galbraith *et al.*, Phys. Rev. 138, B913 (1965).

[6]R. J. Tapper, Rutherford Laboratory Report No. NIRL/R/95, 1965 (unpublished).

[7]A. S. Carroll *et al.*, to be published.

[8]Cool *et al.*, Ref. 5.

[9]V. Bartenev *et al.*, Phys. Rev. Lett. 31, 1367 (1973).

[10]H. Cheng *et al.*, Phys. Lett. 44B, 283 (1973).

[11]Galbraith *et al.*, Ref. 5.

[12]K. J. Foley *et al.*, Phys. Rev. Lett. 19, 857 (1967).

[13]S. P. Denisov *et al.*, Phys. Lett. 36B, 415 (1971).

[14]S. P. Denisov *et al.*, Phys. Lett. 36B, 528 (1971).

[15]S. P. Denisov *et al.*, Nucl. Phys. B65, 1 (1973).

[16]C. Bromberg *et al.*, Phys. Rev. Lett. 31, 1563 (1973).

[17]U. Amaldi *et al.*, Phys. Lett. 44B, 112 (1973).

[18]S. R. Amendolia *et al.*, Phys. Lett. 44B, 119 (1973).

[19]G. Charlton *et al.*, Phys. Rev. Lett. 29, 515 (1972).

[20]F. T. Dao *et al.*, Phys. Rev. Lett. 29, 1627 (1972).

[21]H. R. Gustafson *et al.*, Phys. Rev. Lett. 32, 441 (1974).

[22]R. J. Glauber, Phys. Rev. 100, 242 (1955).

[23]C. Wilkin, Phys. Rev. Lett. 17, 561 (1966).

[24]A. S. Carroll *et al.*, following Letter [Phys. Rev. Lett. 33, 932 (1974)].

[25]J. Pumplin and M. Ross, Phys. Rev. Lett. 21, 1778 (1968).

[26]V. V. Anisovich *et al.*, Phys. Lett. 42B, 224 (1972).

[27]D. Sidhu and C. Quigg, Phys. Rev. D 7, 755 (1973); C. Quigg and L. L. Wang, Phys. Lett. 43B, 314 (1973).

[28]Yu. P. Gorin *et al.*, Yad. Fiz. 15, 953 (1972) [Sov. J. Nucl. Phys. 15, 530 (1972)].